International Journal of Modern Physics C, Vol. 12, No. 7 (2001) 911–1009

MONTE CARLO STUDIES OF THE THREE-DIMENSIONAL ISING MODEL IN EQUILIBRIUM*

MARTIN HASENBUSCH

NIC/DESY Zeuthen Platanenalle 6, D-15738 Zeuthen, Germany

Received 25 May 2001
Revised 17 July 2001

We review Monte Carlo simulations of the Ising model and similar models in three dimensions that were performed in the last decade. Only recently, Monte Carlo simulations provide more accurate results for critical exponents than field theoretic methods, such as the ϵ-expansion. These results were obtained with finite size scaling and "improved actions". In addition, we summarize Monte Carlo results for universal amplitude ratios, the interface tension, and the dimensional crossover from three to two dimensions.

Keywords: Monte Carlo; Ising Model; Critical Phenomena; Three-Dimensions.

Contents

1. Introduction 912
2. The Models 917
   2.1. Observables 919
3. Finite Size Scaling 920
   3.1. Real space renormalization group 923
   3.2. Transformation of observables 927
   3.3. Derivation of finite-size scaling 928
   3.4. The critical temperature of the spin-1/2 Ising model 930
   3.5. Elimination of leading corrections to scaling 931
      3.5.1. R_1^* and R_2^* are known 932
      3.5.2. R_1^* and R_2^* are not known 933
   3.6. Computing critical exponents 936
      3.6.1. The exponent ν 936
      3.6.2. The exponent η 938
      3.6.3. Averaged results for ν and η: Ising universality class 939
   3.7. Comparison with the literature 939
      3.7.1. Other Monte Carlo studies 939
      3.7.2. Field theoretic methods 940
      3.7.3. High temperature expansions 941
      3.7.4. Other theoretical methods 942

*This review is based on the author's "Habilitationsschrift" at the Humboldt-Universität zu Berlin, Germany, 2000.

3.7.5. Experimental results . . . 943
4. The Mass Spectrum and the Correlation Length . . . 945
4.1. The transfer matrix . . . 945
4.2. Correlation length from Monte Carlo simulation . . . 947
4.2.1. Second moment correlation length . . . 948
4.2.2. The $\xi/\xi_{2\mathrm{nd}}$ ratio . . . 949
4.2.3. Variational analysis . . . 950
4.2.4. The operator basis . . . 950
4.3. The spectrum of the three-dimensional Ising model . . . 954
4.3.1. Monte Carlo results for the Z_2 gauge theory . . . 954
4.3.2. Monte Carlo results for the Ising spin model and the ϕ^4 model 956
4.3.3. The ratio $\xi/\xi_{2\mathrm{nd}}$ . . . 957
4.3.4. Comparison with low temperature series expansions . . . 958
5. Universal Amplitude Ratios . . . 959
5.1. Monte Carlo results . . . 960
5.2. Analysis of the data . . . 963
5.3. Comparison with other theoretical and experimental results . . . 968
6. Interfaces . . . 970
6.1. The interface tension and the RG . . . 972
6.2. Finite size effects . . . 973
6.2.1. Effects of a finite L_3 . . . 973
6.2.2. Capillary wave model: Effects of a finite interface area $L_1 \times L_2$ 975
6.3. Numerical methods to study the interface tension . . . 977
6.3.1. The boundary flip . . . 977
6.3.2. The tunneling correlation length . . . 978
6.3.3. Integration of the interface energy . . . 978
6.3.4. Histogram method . . . 979
6.4. Numerical results . . . 980
6.5. Results from field theory . . . 982
6.6. Experimental results . . . 983
6.7. Magnetization profile and width of the interface . . . 983
7. Dimensional Crossover . . . 986
8. Conclusions and Outlook . . . 989
Appendix A. Monte Carlo Simulations . . . 990
A.1. The Metropolis algorithm . . . 991
A.2. Demons . . . 992
A.3. Cluster algorithms . . . 994
A.3.1. Boundary flip algorithm . . . 996
A.3.2. The Brower–Tamayo method . . . 997
A.4. Random numbers . . . 998
Appendix B. Free Field Theory on the Lattice . . . 999
Acknowledgments . . . 1002
References . . . 1002

1. Introduction

Phase transitions are fascinating phenomena. Substances change their appearance fundamentally when a certain temperature, the transition temperature, is crossed: solids melt to liquids, liquids evaporate to gas, magnets loose the magnetization, mixtures of fluids separate, crystals change their structure, smooth surfaces become rough. This is by far not a complete list. For example, phase transitions also

play a fundamental role in cosmology. In the present universe, the electro-weak SU(2) × U(1) symmetry is spontaneously broken. One believes that in the early universe, before the so-called electro-weak phase transition, this symmetry was restored. Before the deconfinement transition, quarks were free particles, while under present conditions, free quarks cannot be observed.

Most of the transitions mentioned above are first order, i.e., for temperature-driven transitions, there exists a finite latent heat at the phase transition. Here, we will be focused on continuous (second order) phase transitions. The behavior of systems at a continuous phase transition is generally referred to as "critical phenomena". The temperature at which phase transition occurs is called the critical temperature T_c. At continuous phase transitions, various thermodynamic quantities diverge in a characteristic way. For example, for a magnetic system, we have for vanishing external field,

$$M \simeq Bt^{\beta} \quad \text{for } t < 0\,, \quad C \simeq A_{\pm}|t|^{-\alpha}\,, \quad \chi \simeq C_{\pm}|t|^{-\gamma}\,, \quad \xi \simeq f_{\pm}|t|^{-\nu}\,, \tag{1}$$

where $t = (T - T_c)/T_c$ is the reduced temperature, M is the magnetization, C is the specific heat, χ the magnetic susceptibility and the correlation length ξ is a measure of the range of correlations. The index $\pm$ indicates $t > 0$ or $t < 0$. Here, $\simeq$ means equal to, up to a factor that goes to 1 as $t \to 0$. At the critical temperature, the magnetization behaves as $M \sim |h|^{1/\delta}$, where h is the external field. $\sim$ means proportional, up to a factor that goes to a constant as $h \to 0$. The exponents β, α, γ, δ and ν are called critical exponents. The critical exponent η is defined by the behavior of the connected two-point correlation function $G(r)$ at T_c: $G(r) \sim 1/r^{d-2+\eta}$, where r is the distance of the points and d the dimension of the system.

The magnetization is the "order parameter" of the phase transition. In the high temperature phase, the magnetization vanishes for a vanishing external field, while it takes a finite value in the low temperature phase. The fact that at continuous phase transitions, the correlation length ξ becomes infinite, makes them hard to deal with. On the other hand, the diverging correlation length is the origin of "universality". Systems that undergo a continuous phase transition can be grouped into "universality classes". Systems within one universality class have exactly the same critical exponents. This is, however, not the only consequence of universality. For example, the "amplitude ratios" A_+/A_-, C_+/C_- and f_+/f_- are also universal, while B, A_+, A_-, C_+, C_-, f_+ and f_- depend on the details of the system that is considered.

The Landau theory[1] was the first systematic approach to critical phenomena. It explains the existence of phase transitions and power laws. However, it fails to predict the correct critical exponents for two and three-dimensional systems.

The "renormalization group" (RG) was developed around 1970 and is now the basis of our understanding of critical phenomena. The RG explains the origin of power laws, it allows to deduce all the exponents defined above from just two independent exponents! Universality classes are related to fixed points of "RG-flows". They are characterized by the spatial dimension of the system, the symmetry

of the order parameter and the range of the interactions.[2] The renormalization group is also the basis of quantitative methods such as the "ϵ-expansion".[3]

For an introduction to critical phenomena, see for example the textbooks.[4–12] For a recent review article, see, e.g., Ref. 13.

An important theoretical tool for the study of phase transitions are the so-called lattice models. A lattice model can be thought of as an idealization of a crystal. On the sites of the lattice lives a field variable that describes some simple property of the atom at the site. All other features of the atom are ignored.

The first lattice model of a magnetic system is the Ising model.[a] It was proposed by Lenz and solved by his student Ising[14] on the one-dimensional lattice. At the microscopic level, the Ising model describes a magnet very crudely. On each site of the lattice lives an elementary magnet that can point either up or down. Mathematically this means that the spin (or field variable) s takes either the value 1 or -1. The energy (classical Hamiltonian) of the Ising model is given by:

$$H = -J \sum_{\langle xy \rangle} s_x s_y - \tilde{h} \sum_x s_x \,. \tag{2}$$

$\langle xy \rangle$ denotes pairs of nearest neighbor sites on the lattice. J is the coupling strength and $\tilde{h}$ is an external field. For positive J, the configuration of minimal energy is given by $s_x = \mathrm{sign}(\tilde{h})$ for all sites x. Mostly, the canonical ensemble is considered. The partition function is given by:

$$Z = \sum_{\mathrm{conf}} \exp(-\beta H) \,, \tag{3}$$

where the sum is taken over all possible configurations of the spins. $\beta = 1/k_B T$ is the inverse temperature.

In one dimension, there is no phase transition. The magnetization is vanishing for all temperatures when no external field is applied. Peierls[15] has shown in 1936 that for dimensions $d \geq 2$ for sufficiently large β, there exists a spontaneous magnetization. Using the duality transformation, Kramers and Wannier[16] obtained the inverse transition temperature $J\beta_c = (1/2)\ln(1+\sqrt{2}\,)$ of the two-dimensional Ising model on the square lattice. In 1944, Onsager[17] solved the two-dimensional Ising model for a vanishing external field. Since then many papers have appeared, which re-derived Onsagers results in alternative (simpler) ways and computed further quantities. For a review, see the book of Mc Coy and T. T. Wu.[18] The exact result shows that the phase transition is continuous and the values for the critical exponents are $\nu = 1$, $\gamma = 7/4$, $\beta = 1/8$, $\alpha = 0$, $\delta = 15$ and $\eta = 1/4$. Further two-dimensional lattice models have been exactly solved up to now (see for example Ref. 19).

Conformal field theory considerably extended our understanding of critical phenomena in two dimensions. Seminal work was done in 1984 by Belavin, Polyakov and

[a]The Ising model can also serve as model for other systems, e.g., binary mixtures.

Zamolodchikov.[20] For a recent introduction to conformal field theory, see Ref. 21. By perturbing the conformal field theory, Zamolodchikov[22] obtained the mass spectrum of the two-dimensional Ising universality class in an external field.

However, in three dimensions, exact solutions for nontrivial models are missing. In particular, there is no exact solution of the three-dimensional Ising model! We have to rely on approximations or numerical methods to study lattice models in three dimensions.

The simplest approximation is the so-called mean-field approximation. The mean-field approximation, in fact, predicts a phase transition for the Ising model, even in one dimension. However, it predicts (as the Landau theory) values for the critical exponents $\nu = 1/2$, $\gamma = 1$, $\beta = 1/2$, $\alpha = 0$, $\delta = 3$ and $\eta = 0$ that are independent of the dimension of the system. These values do not coincide with the exact results for two dimensions and with experimental results for three-dimensional systems. It turns out that only for dimensions $d \geq 4$ the mean field exponents are correct.

The analysis of high temperature series expansions of lattice models was the first theoretical tool that gave results for the critical exponents of three-dimensional systems that were consistent with experiments. For a historical account, see Ref. 12. Still, the analysis of series expansions provides the most accurate estimates for universal quantities.[23]

For textbooks on lattice models, see Refs. 24–27.

In this review, we will focus on the study of three-dimensional lattice models by Monte Carlo simulations.

Early Monte Carlo simulations go back to the 1950s, when the first computers became available. For a pioneering application to a statistical system, see Metropolis *et al.*[28] For a short discussion of simulation techniques, see Appendix A.

In order to obtain accurate and reliable results from Monte Carlo simulations, clear physical concepts have to be the basis of the numerical study. The so-called Monte Carlo Renormalization Group (MCRG) implements rather directly the concepts of the real space renormalization group in the numerical study. For seminal work, see Refs. 29–31.

Here, we will mainly concentrate on the so-called "finite-size scaling" (FSS) method. FSS extends scaling to the situation of finite system sizes. For reviews, see Refs. 32 and 33. The study of critical phenomena using Monte Carlo simulations and FSS was pioneered by Binder[34] in the early 1970s. Note in particular his method of the cumulant crossing to locate the transition point.[35]

However, only recently Monte Carlo results for critical exponents of the three-dimensional Ising model became more accurate than those of field theoretic methods. This progress has been achieved by several means. Computers become faster and cheaper very rapidly. Nowadays, a desktop PC at the cost of about 1000 Euro is more powerful than a supercomputer a decade ago. Very efficient algorithms became available. The cluster algorithm of Swendsen and Wang in 1987[36] was a great

breakthrough. A number of improvements in the implementation of the algorithms and the analysis of the data have been accumulated over the years.

Recently, "improved actions" have been used in the Monte Carlo study of the Ising universality class in three dimensions.[37–39] Such actions have been already studied in the eighties with high temperature series expansions.[40,41] The aim of using improved actions is to reduce corrections to scaling and to finite-size scaling. In Monte Carlo simulations, this allows to extract accurate results for critical exponents from relatively small lattices. Improved actions have also been studied for the XY,[42–44] the Heisenberg and the O(4)-invariant[45] universality classes. For a review, see Ref. 46.

In Sec. 3, we will discuss Monte Carlo FSS studies of the phase transition in detail. In particular, Refs. 38, 39 and 47 will be reviewed.

The remainder of the review is devoted to the study of universal properties of the high and in particular the low temperature phase of the Ising model.

Above, we have already mentioned the amplitude ratios. In order to obtain these ratios, we have to study the power laws, Eq. (1), which are valid in the thermodynamic limit. We have computed several amplitude ratios in Refs. 48 and 49 (see Sec. 5).

The low temperature phase of the three-dimensional Ising model is related by duality[16] with the confining phase of Z_2 gauge theory in three dimensions,[50] which is the most simple lattice gauge theory[51] in $2+1$ dimensions. The notation $2+1$ reminds us that the model describes a quantum system with two spatial directions. An important theoretical prediction of lattice gauge theory is the existence of glueballs. The Z_2 gauge theory in $2+1$ dimensions allows for a very precise numerical determination of the glueball spectrum.[52] These results can be used as check of phenomenological glueball models. The mass spectrum of the Z_2 gauge theory can be recovered in the three-dimensional Ising spin model.[53,54] It turns out that the spectrum is more complicated than one would expect from naive perturbation theory. These results will be discussed in Sec. 4.

In the low temperature phase, one can study interfaces between regions of positive and negative magnetization. These interfaces can be forced into the system by appropriate boundary conditions (e.g., anti-periodic boundary conditions). One can study macroscopic properties of these interfaces, such as the interface tension or the interface stiffness. For reviews, see Refs. 55–57. In Sec. 6, we will summarize the results of Refs. 58–62.

Finally, we will discuss the cross-over from three to two dimensions. This means that systems are considered where the extension in one direction is much smaller that in the other two directions. In the context of field theory, this situation corresponds to a finite temperature of the quantum system. In Sec. 7, we will discuss the results of Ref. 63.

In the present review, the selection of topics is strongly biased by the author's own work. For a complement, the reader is referred to the recent review of Binder and Luijten.[64]

2. The Models

In this section, we fix our notation and introduce further variants of the Ising model. For a more comprehensive collection of lattice models, see, e.g., Ref. 65 or the textbooks.[24–27]

In the following, we will always consider square lattices in two dimensions or simple cubic lattices in three dimensions. Other lattice structures, like triangular or honeycomb in two dimensions, and body-centered or face-centered cubic lattices in three dimensions, are also discussed in the literature.

It is a standard convention in the study of lattice models to set the lattice spacing to one: $a = 1$. On the computer, we can only simulate a finite lattice. We consider lattices of the extension $L_1 \times \cdots \times L_d$, where d is the dimension of the lattice. The sites of the lattice are labeled by $x = (x_1, \ldots, x_d)$, where x_i runs from 1 to L_i. Mostly, periodic boundary conditions are applied. This means that the site $(1, x_2, \ldots, x_d)$ is the neighbor of $(L_1, x_2, \ldots, x_d)$ and analogously for the remaining $d - 1$ directions.

In the following, we will adopt the language of Euclidean field theory and use the action instead of the Hamiltonian: $S = \beta H$. The action of the (standard, spin-1/2) Ising model, that we have discussed already in the introduction, becomes

$$S = -\beta \sum_{\langle xy \rangle} s_x s_y - h \sum_x s_x \,, \tag{4}$$

with $J = 1$ and $h = \beta\tilde{h}$. The field variable (or spin) takes the values $s_x \in \{-1, 1\}$. $\langle xy \rangle$ denotes pairs of nearest neighbor sites on the lattice.

The action is invariant under global Z_2 transformations (i.e., all spins are multiplied by -1) for vanishing field $h = 0$.

In the following, we will always consider the canonical ensemble. The partition function is given as the sum of the Boltzmann factor over all configurations

$$Z = \sum_{s_{(1,\ldots,1)}=\pm 1} \cdots \sum_{s_{(L_1,\ldots,L_d)}=\pm 1} \exp(-S) \,. \tag{5}$$

In the literature, link dependent coupling constants $J_{\langle xy \rangle}$ and site dependent external fields h_x are also discussed. An important example are spin glasses, see, e.g., Ref. 66 for a book on this subject.

A generalization of the standard Ising model, discussed, e.g., in Ref. 67, is given by:

$$S = -\beta_1 \sum_{\langle xy \rangle} s_x s_y - \beta_2 \sum_{[xy]} s_x s_y \,. \tag{6}$$

Here, the field variable takes the values $s_x \in \{-1, 1\}$ as in the standard Ising model. However, in addition to the nearest neighbor interaction, there is an interaction of spins with distance $\sqrt{3}$ ($[x, y]$). Following Ref. 67, we will denote this model by "NNN" (next to next nearest neighbor) Ising model.

We also consider the so-called spin-1 Ising model defined by the action

$$S = -\beta \sum_{\langle xy \rangle} s_x s_y + D \sum_x s_x^2 \,, \tag{7}$$

where the field variable takes the values $s_x \in \{-1, 0, 1\}$. It was studied by Blume[68] and Capel[69] in the mean-field approximation. See also Ref. 70. M. Blume, V. J. Emery and R. B. Griffiths[71] employed it as a simple model of mixtures of ^{3}He and ^{4}He in the neighborhood of the λ transition.[b]

In the limit $D \to -\infty$, the "state" $s = 0$ is completely suppressed, compared with $s = \pm 1$, and the standard Ising model is recovered. In $d \geq 2$ dimensions, the model undergoes a continuous phase transition for $-\infty \leq D < D_{\rm tri}$ at a β_c that depends on D. For $D > D_{\rm tri}$, the model undergoes a first order phase transition.

References 72 and 73 give for the three-dimensional simple cubic lattice $D_{\rm tri} = 2.84479(30)/1.4182(55) \approx 2.006$ and $D_{\rm tri} \approx 2.05$, respectively.

The Landau–Ginzburg model or ϕ^4 theory on the lattice is defined by the action

$$S = \sum_x \left\{ -\beta \sum_\mu \phi_x \phi_{x+\hat{\mu}} + \phi_x^2 + \lambda(\phi_x^2 - 1)^2 - h\phi_x \right\}, \tag{8}$$

where the field variable ϕ_x is a real number and x labels the lattice sites. μ labels the directions and $\hat{\mu}$ is an unit-vector in μ-direction (note that we could also write $\sum_{\langle xy \rangle}$ instead of $\sum_x \sum_\mu$).

The Landau–Ginzburg model on the lattice can either be viewed as a generalization of the Ising model (the $\lambda \to \infty$ limit of the ϕ^4 theory on the lattice is the Ising model) or as discretization of the continuum action of the ϕ^4 theory:

$$S = \int d^d x \left[\frac{1}{2} (\nabla \varphi)^2 + \frac{1}{2} m^2 \varphi^2 + \frac{g}{4!} \varphi^4 - h\varphi \right]. \tag{9}$$

For $\lambda = 0\, (g = 0)$, we obtain the exactly solvable Gaussian model that belongs to the universality class of Bose–Einstein condensation in the ideal Bose gas. The Gaussian model is the starting point for an expansion in λ (an introduction to perturbation theory can be found in textbooks on field theory, e.g., Refs. 74–76.)

In contrast to the models discussed above, the field variable of the Landau–Ginzburg model is continuous. Therefore, the sum over all configurations is replaced by a multi-dimensional integral.

The partition function of the ϕ^4 theory on the lattice is given by:

$$Z = \int D[\phi] \exp(-S(\phi)) \,, \tag{10}$$

[b]Up to 67% of ^{3}He, the mixture undergoes a continuous phase transition (λ-transition), while for a larger percentage, there is a first order transition. The atoms of ^{3}He are identified with $s = 0$ and the atoms of ^{4}He with ± 1. The basic idea is that ^{4}He carries the order parameter, while ^{3}He just dilutes the system. Note that the order parameter of the λ-transition has $U(1)$ symmetry, while the spin-1 Ising model has just Z_2 symmetry.

and the expectation value of an observable A is given by:

$$\langle A\rangle = \frac{1}{Z}\int D[\phi]\exp(-S(\phi))A(\phi)\,, \tag{11}$$

with

$$\int D[\phi] := \int_{-\infty}^{\infty} d\phi_{(1,\ldots,1)}\cdots\int_{-\infty}^{\infty} d\phi_{(L_1,\ldots,L_d)}\,. \tag{12}$$

The field variables ("gauge fields") of a lattice gauge theory (for an introduction to lattice gauge theories, see, e.g., Refs. 76 and 77) live on the links of the lattice. In the case of the Z_2 gauge theory (which was first discussed by Wegner[50]), the gauge fields are elements of Z_2: $\sigma_{x,\mu}\in\{-1,1\}$. Note that a link is characterized by the site x it is attached to and its direction μ. The action of the Z_2 gauge theory is given by:

$$S = -\beta_{\text{gauge}}\sum_x\sum_{\mu<\nu} p_{x,\mu\nu}\,, \tag{13}$$

where the "plaquette" is given by:

$$p_{x,\mu\nu} = \sigma_{x,\mu}\sigma_{x+\hat{\mu},\nu}\sigma_{x+\hat{\nu},\mu}\sigma_{x,\nu}\,. \tag{14}$$

The Z_2 gauge theory in three dimensions is related with the standard Ising (spin) model by duality.[16] The partition function of the gauge model at β_{gauge} is proportional to the partition function of the spin model at β_{spin}, where β_{gauge} and β_{spin} are related by:

$$\sinh(2\beta_{\text{spin}})\sinh(2\beta_{\text{gauge}}) = 1\,. \tag{15}$$

Interesting observables in the gauge theory are the "Wilson-loops". They are products of gauge fields along closed loops of links.

2.1. *Observables*

Let us briefly discuss the basic observables that are studied. Below, we use the notation of the Ising model. For the ϕ^4 theory, s has to be replaced by ϕ.

The magnetization of a configuration is defined by:

$$m = \frac{1}{V}\sum_x s_x\,. \tag{16}$$

On a finite lattice, the naive expectation value of m, for a vanishing external field $h=0$, is always zero (a configuration and the configuration with all spins flipped (multiplied by -1) have the same Boltzmann weight).

In analytic work, one therefore breaks the symmetry for finite lattices by an external field. First, the thermodynamic limit $L\to\infty$ is taken and finally the limit $h\searrow 0$.

$$\langle m\rangle(\infty,0) := \lim_{h\searrow 0}\lim_{L\to\infty}\langle m\rangle(L,h)\,. \tag{17}$$

For Monte Carlo simulations, it is too cumbersome to mimic this definition. Binder and Rauch[78] suggested to measure $\sqrt{\langle m^2 \rangle}$ for $h = 0$ instead. It turns out that $\langle |m| \rangle$ has a faster convergence to the thermodynamic limit.

The magnetic susceptibility is defined as the derivative of the magnetization with respect to the external field h. One easily finds

$$\chi = V(\langle m^2 \rangle - \langle m \rangle^2) \,. \tag{18}$$

Again, care has to be taken for $h = 0$ in low temperature phase:

$$\chi|_{h=0,\, T<T_c} := \lim_{L\to\infty} V(\langle m^2 \rangle - \langle |m| \rangle^2) \,. \tag{19}$$

(Note that in the following, m is used for the expectation value of the magnetization as well as for the magnetization of a single configuration. The meaning should always be clear from the context).

The reduced free energy density (a factor of $k_B T$ is omitted) is the logarithm of the partition function

$$f = -\frac{1}{V} \ln Z \,. \tag{20}$$

In general, it is hard to access the partition function directly in Monte Carlo simulations. Therefore, it is also difficult, in general, to obtain the free energy density.

Our definition of the energy density at vanishing external field is:

$$E = \frac{1}{V} \left\langle \sum_{\langle xy \rangle} s_x s_y \right\rangle . \tag{21}$$

With this definition, $E = -\partial f / \partial \beta$. The energy density can be very easily obtained in Monte Carlo simulation. Therefore, one way to obtain the free energy density is to numerically integrate the energy density over T or β.

The specific heat is the derivative of the energy with respect to the inverse temperature β. For vanishing external field, we get

$$C = \frac{1}{V} \left(\left\langle \left(\sum_{\langle xy \rangle} s_x s_y \right)^2 \right\rangle - \left\langle \sum_{\langle xy \rangle} s_x s_y \right\rangle^2 \right) . \tag{22}$$

The correlation length ξ gives the range of correlations. A precise definition will be given in Sec. 4. In Sec. 6, we will discuss the interface tension.

3. Finite Size Scaling

As explained in the introduction, critical exponents appear in power laws like $\xi \sim t^{-\nu}$ or $\chi \sim t^{-\gamma}$, where ξ and χ are the correlation length and the magnetic susceptibility. $t = (T - T_c)/T_c$ is the reduced temperature. These power laws apply to quantities in the thermodynamic limit. For Monte Carlo simulations, this means that the quantities have to be computed on lattices of size $L \gg \xi$.

In order to study the immediate vicinity of the phase transition, one has to take into account the finite lattice size L. This can be achieved by the so-called finite-size scaling (FSS) Ansätze. For example

$$\chi(L,\beta) \simeq L^{\gamma/\nu} f_{\pm}\left(\frac{L}{\xi}\right), \tag{23}$$

where $\pm$ indicates $t > 0$ or $t < 0$. The idea of such finite size scaling Ansätze is that in the neighborhood of the transition, only the lattice size and the correlation length are important length scales. The scale of the lattice spacing becomes less and less important as the critical point is approached. The theory of finite-size scaling goes back to Refs. 79 and 80. Review articles can be found in Refs. 32 and 33. There, one can find discussions of various systems with all kinds of boundary conditions. In the following, we will always assume periodic (or anti-periodic) boundary conditions. The use of finite size scaling in Monte Carlo simulations was pioneered by Binder.[34]

Dimensionless ratios are particularly useful in the study of critical phenomena. They show a very simple finite size scaling behavior:

$$R(L,\beta) \simeq f_{\pm}\left(\frac{L}{\xi}\right). \tag{24}$$

At the critical point, the correlation length becomes infinite. Therefore, $R(L,\beta_c)$ does not depend on the lattice size. This is the basis of the so-called crossing method to locate the phase transition. The intersection of $R(L_1,\beta)$ and $R(L_2,\beta)$, with $L_1 \neq L_2$, gives an estimate for β_c.

Using $\xi \sim t^{-\nu}$, one derives from Eq. (24)

$$R(L,\beta) \simeq g(L^{1/\nu} t)\,. \tag{25}$$

Therefore,

$$\left.\frac{\partial R(L,\beta)}{\partial \beta}\right|_{\beta_c} \sim L^{1/\nu}\,, \tag{26}$$

which allows to extract ν from simulations at β_c.

The idea of the "phenomenological renormalization group" goes back to Nightingale.[81] He proposed to study the ratio

$$R = \frac{\xi_L}{L}\,, \tag{27}$$

where ξ_L is the correlation length on a system of the size $L^{d-1} \times \infty$. He studied this ratio at the example of two-dimensional Ising model. There, one can use the exact result for the correlation length on a strip of width L.

Later, Binder[35] proposed to study the so-called fourth order cumulant (or Binder cumulant):

$$U = \frac{\langle m^4 \rangle}{\langle m^2 \rangle^2}\,. \tag{28}$$

(He uses the convention $U = 1 - (1/3)\langle m^4\rangle/\langle m^2\rangle^2$). The Binder cumulant is easier to access in Monte Carlo simulations than the quantity of Nightingale. For temperatures much larger than the transition temperature, the magnetization is fluctuating around 0 with a Gaussian distribution. Therefore, the Binder cumulant assumes the value 3. On the other hand, at low temperatures, the modulus of the magnetization assumes an almost constant finite value. Therefore, the Binder cumulant takes the value 1.

In Fig. 1, we demonstrate the power of the crossing method to locate the phase transition of the standard Ising model in three dimensions. The Binder cumulant is shown for a 2^3 and a 3^3 lattice with periodic boundary conditions. For these small lattices, we can easily generate all configurations and compute the quantities without a Monte Carlo simulation. The two curves cross at $\beta \approx 0.231$. The most accurate estimate of the inverse critical temperature is $\beta_c = 0.22165459(10)$.[82] The accuracy obtained from the crossing of $L = 2$ and $L = 3$ can be compared with the mean-field result $\beta_{c,\,\mathrm{MF}} = 1/6 = 0.16\ldots$.

In Ref. 47, we proposed to study the ratio Z_a/Z_p of the partition function with anti-periodic boundary conditions Z_a and the partition function with periodic boundary conditions Z_p. We have demonstrated that Z_a/Z_p can be used analogously to the Binder cumulant. However, corrections to finite-size scaling are smaller for Z_a/Z_p than for the Binder cumulant.

Another dimensionless ratio that is used quite frequently in Monte Carlo simulations is $\xi_{2\mathrm{nd}}/L$. This ratio is very similar to Nightingales original proposal. Only the correlation length on the $L^{d-1} \times \infty$ lattice is replaced by the so-called "second moment correlation length" on a L^d lattice. The second moment correlation length

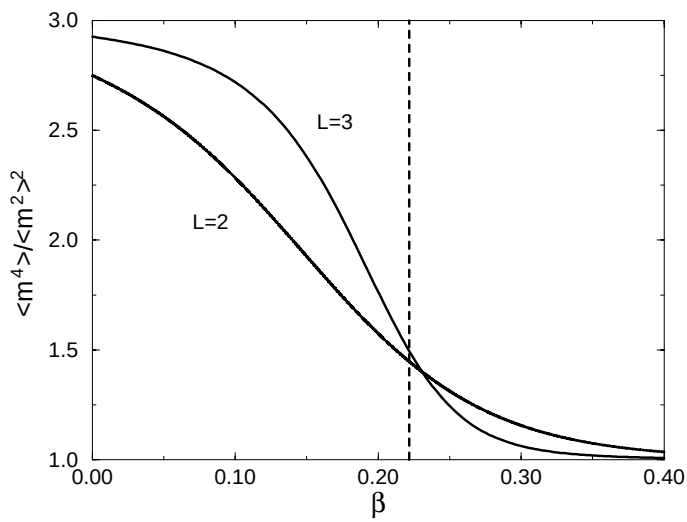

Fig. 1. The Binder cumulant for $L = 2$ and $L = 3$ for the three-dimensional Ising model. For comparison, the dashed line gives the best Monte Carlo estimate of β_c that is available today.

is defined by:

$$\xi_{\rm 2nd} = \left(\frac{\chi/F - 1}{4\sin^2(\pi/L)} \right)^{1/2} , \tag{29}$$

where the magnetic susceptibility is given by:

$$\chi = V\langle m^2 \rangle \quad \text{and} \quad F = \frac{1}{V} \left\langle \left| \sum_x \exp\left(i \frac{2\pi x_1}{L} \right) \phi_x \right|^2 \right\rangle . \tag{30}$$

In addition to the dimensionless ratios discussed above (and used in practice), there are infinitely many other choices (e.g., $\langle m^{2n} \rangle / \langle m^2 \rangle^n$ for arbitrary $n > 2$), see also Ref. 83.

3.1. *Real space renormalization group*

In the following, we derive finite-size scaling in the framework of the real-space renormalization group (RG). For an introduction to the real-space RG, see Ref. 2 or for example the books.[8–12] For the convenience of the reader and to introduce the notation, we give a short introduction to the real-space RG on the next few pages.

The basic idea of the RG is to reduce the number of degrees of freedom of the system by integrating out fluctuations that reside on a short range. In real space RG, this is implemented by so-called block spin transformations. The idea goes back to the work of Kadanoff.[84] In the block transformation, a block of b^d sites on the original lattice is identified with one site of the blocked lattice. The lattice constant of the blocked lattice is rescaled by b^{-1} to 1. For an illustration, see Fig. 2. A block field (or block spin in the case of the Ising model) is then constructed from the fields (spins) of the original lattice. One possible rule for this construction, in the case of the Ising model, is the so-called majority rule. The block spin takes the sign of the sum of the spins in the block as value. If the sum of the spins in a block is zero, then the block spin takes with probability 0.5 either the value -1 or $+1$. In the literature, we can find many more transformation rules. See for example Ref. 85.

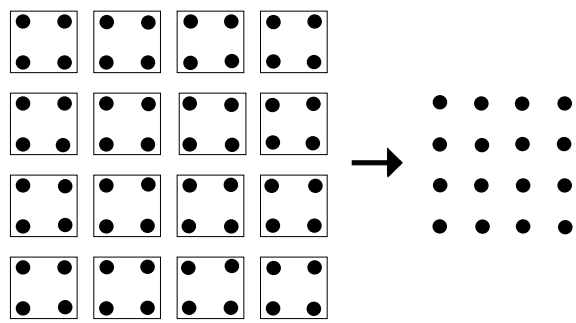

Fig. 2. Sketch of a real-space blocking. An 8×8 lattice (the lattice sites are displayed as circles) is blocked by the scaling factor of two to a 4×4 lattice.

Let us now discuss the RG-transformation more formally at the example of the ϕ^4 theory. The assignment of a block field Φ to the field ϕ on the original lattice is expressed by the transformation kernel $T(\Phi, \phi)$. The transformation kernel satisfies the following conditions:

$$T(\Phi, \phi) \geq 0\,, \tag{31}$$

for all configurations Φ and ϕ, and

$$\int D[\Phi] T(\Phi, \phi) = 1\,, \tag{32}$$

for all field-configurations ϕ on the original lattice. This means that $T(\Phi, \phi)$ can be interpreted as the probability to assign the block configuration Φ to the field-configuration ϕ on the original lattices.

A "decent" transformation kernel should also respect the internal symmetries of the model. In the case of Z_2 symmetry for example, we should have $T(\Phi, \phi) = T(-\Phi, -\phi)$. In addition, the transformation kernel should be local, i.e., it should only relate the field Φ_X at the block site X with fields ϕ_x in the neighborhood of X.

The action of the blocked system is defined by:

$$\exp(-S'(\Phi)) := \int D[\phi] T(\Phi, \phi) \exp(-S(\phi))\,. \tag{33}$$

Note that this definition applies in the given form only to finite lattices. Using Eq. (32), we see immediately that the partition function is invariant under the block spin transformation $Z' = Z$.

As an example for a block spin transformation, we consider the so-called linear blocking. The block field of the block site X is the average of the fields within the associated block:

$$T_X(\Phi, \phi) = \delta\left(\Phi_X, \frac{1}{b^{d-d_\phi}} \sum_{x \in X} \phi_x\right). \tag{34}$$

Note that the exponent d_ϕ takes a nontrivial value. Its meaning will be explained below. The transformation kernel $T(\Phi, \phi)$ is then given as the product over all block sites X:

$$T(\Phi, \phi) = \prod_X T_X(\Phi, \phi)\,. \tag{35}$$

For generalizations of this rule, see, e.g., Ref. 86.

In order to analyze the RG transformations, one introduces a coordinate system in the space of actions. The action is parametrized by:

$$S(\phi) = \sum_\alpha K_\alpha S_\alpha(\phi)\,, \tag{36}$$

where S_α are translational invariant functions of the field ϕ. Now, the action is characterized by the values of the "couplings" K_α.

An example of such a parametrization for the ϕ^4 theory on the lattice is:

$$S^{(n)}_{r_2,r_3,\ldots,r_n} = -\sum_x \phi_x \phi_{x+r_2} \cdots \phi_{x+r_N} \,, \tag{37}$$

where r_i give the distance from the point x. In this basis, the terms of the action, Eq. (8), can be written as:

$$\sum_x \phi_x^2 = S^{(2)}_{(0,0,0)} \,, \tag{38}$$

$$\sum_x \phi_x^4 = S^{(4)}_{(0,0,0),(0,0,0),(0,0,0)} \,, \tag{39}$$

and

$$\sum_x \phi_x \phi_{x+\hat{\mu}} = S^{(2)}_{\hat{\mu}} \,. \tag{40}$$

Still this labeling is ambiguous. For example $S^{(2)}_{r_2} = S^{(2)}_{-r_2}$. In the following, we assume that by some appropriate rule, the labeling is made unique.

Given such a parametrization of actions, the RG-transformation, Eq. (33), induces a mapping of the couplings

$$K \to K' = R(K) \,. \tag{41}$$

Even on the finite lattice, the number of possible terms of the action is infinite. In general, an RG-transformation produces an infinite number of couplings with finite values. However, a major assumption of the real space RG is that one can find finite truncations of the terms such that the physics (i.e., the value of observables) is almost unchanged compared with the full action. In the case of the parametrization explicitly discussed above, this means that the importance of the terms decreases with the number n of fields and the value of the couplings K_α decay exponentially with the distances $r_2, \ldots, r_n$. The decay constant of the couplings is small (a few lattice spacings).

The main argument that supports this hypothesis is that the block field acts like a magnetic field on the original field. Therefore, the constraint system with the weights $T(\Phi, \phi) \exp(-S(\phi))$ for fixed Φ becomes noncritical, even if the original system is critical.

This hypothesis is also confirmed by an exact calculation for free field theory (Gaussian model)[86] and by approximate calculations for the two-dimensional Ising model.[85]

For a more mathematical discussion of this hypothesis, see, e.g., Ref. 87.

Once the RG-transformation is written in terms of a mapping of coupling constants and the above hypothesis is fulfilled, the thermodynamic limit can be taken. Also in the thermodynamic limit, the RG-mapping, Eq. (41), of the coupling constants is an analytic function.

In the RG-framework, the nonanalytic behavior of thermodynamic quantities at the continuous phase transition arises from an infinite iteration of RG-transformations. Continuous phase transitions are associated with nontrivial fixed points of the RG-transformation. The critical exponents of a system are determined by the flow in the neighborhood of the nontrivial fixed point $R(K^*) = K^*$. This is the origin of universality. All systems that share the same nontrivial fixed point belong to the same universality class. The critical behavior can be understood from linearized RG-transformations in the neighborhood of the fixed point. The linearized transformation at the fixed point can be represented by a matrix

$$T_{\alpha\beta} = \left.\frac{\partial K'_\alpha}{\partial K_\beta}\right|_{K=K^*} . \tag{42}$$

One introduces "scaling fields" by:

$$u_i = \sum_\alpha \varphi_{i,\alpha}(K_\alpha - K^*_\alpha) , \tag{43}$$

where φ_i denotes the ith (left) eigenvector of the matrix T,

$$\sum_\alpha \varphi_{i,\alpha} T_{\alpha\beta} = \lambda_i \varphi_{i,\beta} .$$

The u_i transform under RG transformations like

$$u_i \to \lambda_i u_i .$$

The scaling field u_i is classified as relevant if $\lambda_i > 1$, marginal if $\lambda_i = 1$, and irrelevant if $\lambda_i < 1$. In order to remove the b dependence, one introduces so-called RG-exponents y_i by:

$$\lambda_i = b^{y_i} . \tag{44}$$

The above classification becomes:

$$\begin{aligned} \text{relevant} \quad & y_i > 0 , \\ \text{marginal} \quad & y_i = 0 , \\ \text{irrelevant} \quad & y_i < 0 . \end{aligned} \tag{45}$$

In Ising-like systems, the terms of the action can be classified with respect to their behavior under global Z_2 transformations (i.e., all fields are multiplied by -1). In the basis given in Eq. (37), all terms with even n are invariant under a global Z_2 transformation. They form the even sector of the theory. On the other hand, terms with odd n change sign under a global Z_2 transformation. They form the odd sector. By construction, the RG-transformation commutes with a global Z_2 transformation. Therefore, the eigenvectors of T are either even or odd. The RG-mapping of coupling constants $R(K)$ obviously depends on the precise form of the transformation kernel that has been chosen. For the RG-exponents, this means that in addition to the physical exponents there are so-called "redundant" exponents that are mere artifacts of the RG-transformation. While the value of the

redundant RG-exponents depends on the particular form of the RG-transformation, the value of the physical RG-exponents does not.

"Dangerous" irrelevant scaling fields are characterized by the fact that observables have a singular dependence on these scaling fields.

From actual calculations, one knows that three-dimensional Ising type systems have two relevant scaling-fields: u_t in the even (or temperature-like) sector and u_h in the odd (or external field-like) sector. Their exponents are denoted by $y_1 = y_t$ and $y_2 = y_h$. There is no marginal scaling field. The exponent of the most important irrelevant scaling field in the even sector is denoted by $y_3 = -\omega$. One has to expect an infinite sequence of higher corrections with $y_i < y_3$. However, there is little quantitative knowledge about these correction exponents.

For the derivation of power laws and finite-size scaling Ansätze, in the following section, we need only the qualitative knowledge that there is one relevant scaling field u_t in the even and one relevant scaling field u_h in the odd sector. Below, we will see how the RG-exponents y_t and y_h are related to the phenomenologically defined critical exponents ν, γ, β, α, η and δ that have been introduced before.

3.2. *Transformation of observables*

In order to derive power laws and finite-size scaling Ansätze, we also have to know how the quantities of interest transform under RG transformations. In this section, we discuss the lattice size L, the free energy density f, the magnetization and its moments, the correlation length and the dimensionless ratios $\langle m^4\rangle/\langle m^2\rangle^2$, Z_a/Z_p and $\xi_{2\mathrm{nd}}/L$.

The lattice size L transforms trivially as $L' = L/b$.

We have learned already that partition functions do not change under RG-transformations. Therefore, the ratio of partition functions Z_a/Z_p is RG-invariant (we assume that anti-periodic boundary conditions remain anti-periodic boundary conditions under RG-transformations).

Since the partition function is RG-invariant, the free energy is also RG-invariant. The free energy density transforms as:

$$f' = b^d f\,, \tag{46}$$

where d is the dimension of the system. In the literature, we find a splitting of the free energy into a nonsingular and a singular part

$$f = f_{ns} + f_s\,. \tag{47}$$

The critical behavior of thermodynamic quantities is then derived from the singular part. Also, the singular part of the free energy density transforms as:

$$f'_s = b^d f_s\,. \tag{48}$$

On a lattice of size L^d, the magnetization is given by:

$$m = \frac{1}{L^d}\sum_x \phi_x\,. \tag{49}$$

With the linear transformation, Eq. (34), we get

$$m' = \frac{1}{L'^d} \sum_X \Phi_X = \frac{b^d}{L^d} b^{-d+d_\phi} \sum_x \phi_x = b^{d_\phi} m \,. \tag{50}$$

Hence, we obtain for the expectation values of the moments of the magnetization

$$\langle m^n \rangle' = b^{n d_\phi} \langle m^n \rangle \,. \tag{51}$$

It follows that the Binder cumulant is invariant under the linear blocking, since the factors b^{4d_ϕ} in numerator and denominator cancel.

The correlation length ξ transforms as $\xi' = \xi/b$ since the block correlation function is proportional to the original correlation function. Only the rescaling of the lattice spacing has to be taken into account

$$G'(x) \sim G\left(\frac{x}{b}\right) . \tag{52}$$

$\xi'_{2\mathrm{nd}} = \xi_{2\mathrm{nd}}/b$ holds (up to L^{-2} corrections) also for the second moment correlation length. Therefore, the ratio $\xi_{2\mathrm{nd}}/L$ is RG-invariant.

3.3. *Derivation of finite-size scaling*

All quantities that we have discussed above transform like

$$A' = b^x A \,. \tag{53}$$

We assume that sufficiently many RG-transformations have been performed such that only u_t, u_h and u_3 remain significant. In addition, we assume that we have started sufficiently close to the transition temperature to ensure that the linearization of the RG-flow is valid. We can write the observables as functions of these scaling fields and of the finite lattice size L. Combining the transformation of the observable, Eq. (53) and the transformation of the scaling fields, we get

$$A(u_t, u_h, u_3, L) = b^x A(b^{y_t} u_t, b^{y_h} u_h, b^{y_3} u_3, b^{-1} L) \,. \tag{54}$$

Now, we iterate the RG-transformation until a fixed size $L' \gg 1$ is reached. The number n of blocking steps is given by $L' = b^{-n} L$. Hence, we obtain

$$\begin{aligned} A(u_t, u_h, u_3, L) &= b^{-nx} A(b^{n y_t} u_t, b^{n y_h} u_h, b^{n y_3} u_3, b^{-n} L) \\ &= \left(\frac{L}{L'}\right)^x A\left(\left(\frac{L}{L'}\right)^{y_t} u_t \,, \left(\frac{L}{L'}\right)^{y_h} u_h \,, \left(\frac{L}{L'}\right)^{y_3} u_3 \,, L'\right) . \end{aligned} \tag{55}$$

Since the RG-transformation is analytic, the scaling fields u_t, u_h and u_3 are analytic functions of the parameters t and h of the original model. Hence, we can write the scaling fields as:

$$u_t = \frac{t}{t_0} + O(t^2, h^2) \,, \tag{56}$$

and

$$u_h = \frac{h}{h_0} + O(th)\,. \tag{57}$$

The absence of $O(h)$ and $O(th)$ corrections in u_t and $O(t)$, $O(t^2)$ and $O(h^2)$ corrections in u_h is due to the Z_2 symmetry. By construction, L' is a constant. Hence, A does not depend on it. Inserting Eqs. (56) and (57) into Eq. (55), we arrive at the finite-size scaling Ansatz:

$$A(t,h,L) = L^x \Phi_A \left(\frac{t}{t_0} L^{y_t}, \frac{h}{h_0} L^{y_h}, cL^{y_3} \right), \tag{58}$$

where Φ is a universal scaling function. The constants t_0, h_0 and c depend on the microscopic details on the model. In the case of the ϕ^4 theory, for instance, they are functions of the coupling λ. Note, however, that t_0, h_0 and c do not depend on the quantity A that is considered.

Equation (58) is appropriate for the physical situation of a finite lattice. In the thermodynamic limit, we expect that quantity A converges to a finite value. Therefore, the divergence of L^x has to be compensated by Φ_A:

$$A(t,h) = \left| \frac{t}{t_0} \right|^{-x/y_t} \tilde{\Phi}_{A,\pm} \left(\left| \frac{t}{t_0} \right|^{-y_h/y_t} \frac{h}{h_0}, \left| \frac{t}{t_0} \right|^{-y_3/y_t} c \right). \tag{59}$$

With the results of the previous sub-section, we get, e.g., for the correlation length

$$\xi \sim |t|^{-1/y_t}\,. \tag{60}$$

Hence, $\nu = 1/y_t$.

In a similar fashion, all critical exponents that have been introduced phenomenologically can be expressed in terms of the RG-exponents y_t and y_h:

$$\begin{aligned} &\alpha = 2 - \frac{d}{y_t}\,, \qquad \eta = d + 2 - 2y_h\,, \quad \beta = \frac{d - y_h}{y_t}\,, \\ &\gamma = \frac{2y_h - d}{y_t}\,, \quad \delta = \frac{y_h}{d - y_h}\,, \end{aligned} \tag{61}$$

where d is the dimension of the system. In these equations, we can easily eliminate the RG-exponents to obtain equations among the phenomenological exponents. These equations are called "scaling relations". "Hyperscaling" relations are those scaling relations that relate the singular behavior of the specific heat with the behavior of the correlation length. Hyperscaling relations may fail when a dangerously irrelevant scaling field influences the scaling form of the free energy. This happens above the upper critical dimension (which is $d = 4$ for the systems that we discuss in this review). In the following, we will always assume that hyperscaling relations are valid.

For corrections to scaling, the exponents ω and θ are related to RG-exponents by:

$$\omega = -y_3\,, \quad \theta = \nu\omega = -\frac{y_3}{y_t}\,. \tag{62}$$

3.4. *The critical temperature of the spin-1/2 Ising model*

The critical temperature of the standard (spin-1/2) Ising model on simple cubic lattice is no universal quantity. Nevertheless, it is important for various reasons: it serves as a consistency check among different studies. It is used as input in the analysis of high and low temperature series and the analysis of Monte Carlo data for $\beta \neq \beta_c$. Finally, one might check the conjecture of Rosengren[88] for the exact value of β_c:

$$\tanh(\beta_c) = (\sqrt{5}-2)\cos\left(\frac{\pi}{8}\right), \quad \text{i.e., } \beta_c = 0.22165863\ldots. \tag{63}$$

For theoretical objections against this conjecture, see Ref. 89.

The most accurate Monte Carlo estimates of β_c are obtained with the cumulant crossing method (or refinements of it) that we have illustrated in Fig. 1. For a dimensionless ratio R, the exponent in Eq. (53) is $x = 0$. Hence, Eq. (58) becomes (for the special case $h = 0$):

$$R(\beta, L) = \Phi_R\left(\frac{t}{t_0} L^{y_t}, \tilde{c} L^{y_3}\right). \tag{64}$$

Taylor-expansion around zero arguments gives:

$$R(\beta, L) = R^* + a(\beta - \beta_c) L^{y_t} + c L^{y_3} + \cdots. \tag{65}$$

One easily derives that:

$$\beta_{\text{cross}} = \beta_c + \text{const}\, L^{-y_t + y_3} + \cdots, \tag{66}$$

where β_{cross} is the location of the intersection of the Binder cumulant (or any other dimensionless ratio) for L and $L' = bL$ with b fixed. Since $y_t - y_3 = 1/\nu + \omega \approx 2.4$, the convergence of β_{cross} to β_c is rather fast.

Table 1. The inverse critical temperature β_c of the 3D spin 1/2 Ising model on the simple cubic lattice obtained from Monte Carlo simulations. These results were obtained either with finite-size scaling (FSS) or the Monte Carlo renormalization group (MCRG) method.

Ref.	Year	Method	β_c
82	1999	FSS	0.22165459(10)
38	1999	FSS	0.2216543(2)(2)
91	1999	FSS	0.22165456(15)(5)
92	1996	FSS	0.2216544(6)
93	1996	MCRG	0.221655(1)(1)
67	1995	FSS	0.2216546(10)
94	1994	FSS	0.2216576(22)
95	1992	MCRG	0.221652(3)
96	1991	FSS	0.221657(3)
97	1991	FSS	0.2216595(26)
98	1991	FSS	0.2216544(10)

In Table 1, we have summarized the results that were obtained in the last decade. The most accurate and also most recent estimate is given in Ref. 82. In this study, a special purpose computer was used for a single cluster[90] simulation. Note that all previous estimates that we have listed are consistent with the result of Ref. 82, except for Ref. 97, which is by two standard deviation too large.

At least the four most recent estimates[38,82,91,92] of β_c clearly exclude the conjectured value of β_c.[88]

The critical temperature can also be extracted from the analysis of a high temperature series. For this purpose, the magnetic susceptibility is mostly considered. Here, we quote only the most recent results for comparison. Butera and Comi[99] find $\beta_c = 0.221654(1)$ from the series up to the order β^{23}. Before, the same authors[100] extracted $\beta_c = 0.221663(9)$ and $\beta_c = 0.2216544(3)$ from the series up to the order β^{21}. The second, more accurate value stems from a so-called "θ-biased" analysis. Salman and Adler[101] have reanalyzed the series of Ref. 100. They find $\beta_c = 0.221659^{+0.000002}_{-0.000005}$. We note that all of these values are consistent with the recent Monte Carlo results. However, it seems that the quoted error-bars are rather subjective.

3.5. *Elimination of leading corrections to scaling*

When computing critical exponents (or other universal quantities) in Monte Carlo simulations, we have to take into account corrections to scaling. Either the lattice size L (for finite-size) or the correlation length ξ (thermodynamic limit) has to be sufficiently large such that corrections can be ignored, or, alternatively, corrections to scaling have to be included in the fit ansatz. It is well known that the statistical error of the results increases, when the number of free parameters in the fit is increased. Hence, both ways to deal with the problem increase the CPU time that is needed to reach a given accuracy of the result.

Hence, it is desirable to eliminate corrections to scaling. The most radical approach would be to simulate good approximations of the fixed point action. Then, one could obtain accurate results from lattices that are just a little larger than the interaction-range of the action. For an application of this strategy to asymptotically free models, see the work on "perfect actions".[102]

Here, we restrict ourselves to the elimination of leading corrections to scaling. Eliminating leading corrections to scaling means, in the language of the renormalization group, that at the critical point (the thermal scaling field $u_t = 0$ is vanishing), the scaling field of the leading correction is vanishing: $u_3 = 0$ (note that the magnetic scaling field is vanishing $u_h = 0$ for vanishing external field $h = 0$). The scaling fields are analytic functions of the parameters of the model that is studied. Hence, we need, in the general case, a model with two parameters to be able to remove leading order corrections to scaling at the critical point.

In Refs. 40 and 41, it was suggested that for models that interpolate between the Gaussian and the Ising model, there exists one value of the interpolation parameter

at which leading corrections to scaling vanish. These models were studied with high temperature series expansions.

Below, we discuss finite-size scaling methods[37–39] that allow to determine the parameter of the action at which leading corrections to scaling vanish. These methods were used in simulations of the spin-1 Ising model,[38] the NNN Ising model[38] and the ϕ^4 theory[37–39] on the three-dimensional simple cubic lattice.

The crossing method with dimensionless ratios has proven to be very efficient in locating the critical temperature. The method to be described below can be seen as a generalization of the crossing method. Since we search for $u_3 = 0$, in addition to $u_t = 0$, two dimensionless ratios are advantagous. Let us denote them by R_1 and R_2.

Their finite size behavior is given by Eq. (65). Writing explicitly the dependence on λ (for the ϕ^4-theory) and add a term due to subleading corrections, we get

$$R_i(\lambda, \beta, L) = R_i^* + a_i(\lambda)(\beta - \beta_c)L^{y_t} + c_i(\lambda)L^{y_3} + d_i(\lambda)L^{y_4} \dots , \tag{67}$$

where i labels the dimensionless ratio that is considered. Eliminating leading corrections means to find the zero of the correction amplitude: $c_i(\lambda_{\rm opt}) = 0$. Below, we discuss two numerical strategies to locate $\lambda_{\rm opt}$.

3.5.1. *R_1^* and R_2^* are known*

If good estimates for R_1^* and R_2^* are known from previous studies, we require, for a given lattice size L, that R_1 and R_2 assume the values R_1^* and R_2^*. Equation (67) becomes

$$0 = a_i(\lambda)(\beta - \beta_c(\lambda))L^{y_t} + c_i(\lambda)L^{y_3} + d_i(\lambda)L^{y_4} + \cdots , \tag{68}$$

for $i = 1, 2$. The solution of these two equations is given by:

$$\lambda = \lambda_{\rm opt} + {\rm const}\, L^{-y_3+y_4} + \cdots , \tag{69}$$

and

$$\beta = \beta_c(\lambda) + {\rm const}' L^{-y_t+y_4} + \cdots . \tag{70}$$

The critical line is approached very rapidly, while $\lambda_{\rm opt}$ is approached much slower.

In Ref. 38, we applied this method to three different models. The ϕ^4 theory, Eq. (8), the spin-1 Ising model, Eq. (7), and the NNN Ising model, Eq. (6).

The parameters of these models are (β, λ), (β, D) and (β, β_2), respectively.

As input, we used[c]

$$U^* = \frac{1}{0.6240(10)} , \tag{71}$$

and

$$\frac{Z_a}{Z_p^*} = 0.5425(10) , \tag{72}$$

[c]At present, the most accurate estimate is $U^* = 1/0.62358(15)$.[82]

which were obtained with the standard Ising action on lattices of a size up to $L = 128$.

On lattices of size up to $L = 9$, $L = 10$ and $L = 13$ for the three models, respectively, we found, $\lambda_{\rm opt} \approx 1.145$ with $\beta_c(\lambda) \approx 0.3728$ for the ϕ^4 theory and $D_{\rm opt} \approx 0.6241$ with $\beta_c \approx 0.3832$ for the spin-1 Ising model. In the case of the NNN Ising model, we did not quote a final result.

3.5.2. *R_1^* and R_2^* are not known*

In the above approach, the accuracy in the determination of $\lambda_{\rm opt}$ is limited by the accuracy of the estimates of R_1^* and R_2^*. Therefore, we will discuss below how $\lambda_{\rm opt}$ can be obtained without the previous knowledge of R_1^* and R_2^*.

In order to fix β, we require that the first dimensionless ratio takes a fixed value $R_{1,f}$:

$$R_1(\lambda, \beta_f, L) = R_{1,f}\,. \tag{73}$$

With Eq. (67), we get

$$\beta_f = \beta_c + \frac{R_{1,f} - R_1^*}{a_1(\lambda)} L^{-y_t} + \frac{c_1(\lambda)}{a_1(\lambda)} L^{-y_t+y_3} + \cdots\,. \tag{74}$$

β_f is converging to β_c as L increases. However, the convergence is slower than for $\beta_{\rm cross}$.

Then, we compute the second dimensionless ratio R_2 at β_f:

$$\bar{R}(\lambda, L) := R_2(\lambda, \beta_f, L)\,. \tag{75}$$

In the following, we will frequently refer to $\bar{R}$ as "R_2 at $R_{1,f}$". Inserting this definition in Eq. (67) yields

$$\bar{R}(\lambda) = \bar{R}^* + \bar{c}(\lambda) L^{y_3} + \bar{d}(\lambda) L^{y_4} + \cdots\,, \tag{76}$$

with

$$\bar{R}^* = R_2^* - \frac{a_2(\lambda)}{a_1(\lambda)} (R_1^* - R_{1,f})\,, \tag{77}$$

$$\bar{c}(\lambda) = c_2(\lambda) - \frac{a_2(\lambda)}{a_1(\lambda)} c_1(\lambda)\,, \tag{78}$$

and

$$\bar{d}(\lambda) = d_2(\lambda) - \frac{a_2(\lambda)}{a_1(\lambda)} d_1(\lambda)\,. \tag{79}$$

Note that the ratio $a_2(\lambda)/a_1(\lambda)$ does not depend on λ. In order to find the null of $\bar{c}(\lambda)$, one has to simulate for various values of λ and lattice sizes L. Then, $\bar{c}(\lambda)$ is computed for these λ-values by fitting the numerical results for $\bar{R}$ with Eq. (76). The null is then found by some standard null-search method.

This method was used in Ref. 39 to improve the estimate of $\lambda_{\rm opt}$ for the ϕ^4 model. As $\bar{R}$, we had taken U at $Z_a/Z_p = 0.5425$. We simulated for a large number

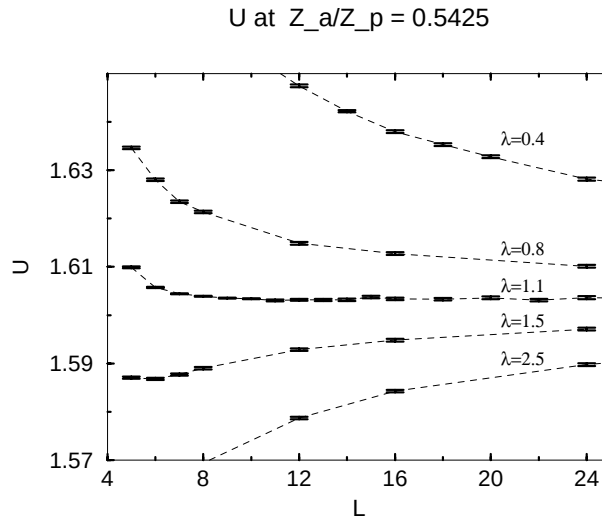

Fig. 3. The Binder cumulant U at $Z_a/Z_p = 0.5425$ as a function of the lattice size L for $\lambda = 0.4$, 0.8, 1.1, 1.5 and 2.5. The dashed line is used to guide the eye. It connects data points of the same λ.

of λ-values (0.1, 0.2, 0.4, 0.7, 0.8, 0.9, 1.1, 1.145, 1.3, 1.4, 1.5, 2.5) and lattice sizes up to $L = 96$. For the illustration of the method, we give a subset of the data in Fig. 3 (the figure is taken from Ref. 39).

For $\lambda = 0.4$ and 0.8, the value of $\bar{R}$ is decreasing with increasing lattice size, while for $\lambda = 1.5$ and 2.5, it is increasing with increasing lattice size. For $\lambda = 1.1$, starting from $L = 9$, the value of $\bar{R}$ is constant within the numerical precision. Hence, we expect that $\lambda_{\rm opt}$ is close to 1.1. The deviations for smaller lattice sizes are due to sub-leading corrections.

In order to demonstrate the close connection with the cumulant crossing method, we have plotted in Fig. 4, $\bar{R}$ as a function of λ for $L = 8$, 12, 16 and 24. Note that here, since $y_3 = -\omega < 0$, the slope of the curves becomes smaller as L increases. The curves intersect close to $\lambda = 1.1$.

In order to obtain a final result for $\lambda_{\rm opt}$, we fitted all our data with an ansatz that includes leading corrections

$$\bar{R} = \bar{R}^* + \bar{c}(\lambda) L^{-\omega} \,, \tag{80}$$

as well as corrections that are quadratic in the leading order corrections

$$\bar{R} = \bar{R}^* + \bar{c}(\lambda) L^{-\omega} + \bar{c}_2 \bar{c}^2(\lambda) L^{-2\omega} \,. \tag{81}$$

Fitting with Eq. (81) yields

$$\lambda_{\rm opt} = 1.095(12) \,, \tag{82}$$

where only lattices with $L \geq 16$ were taken into account. We also obtain $\omega = 0.845(10)$. For details of the fit-procedure, see Ref. 39.

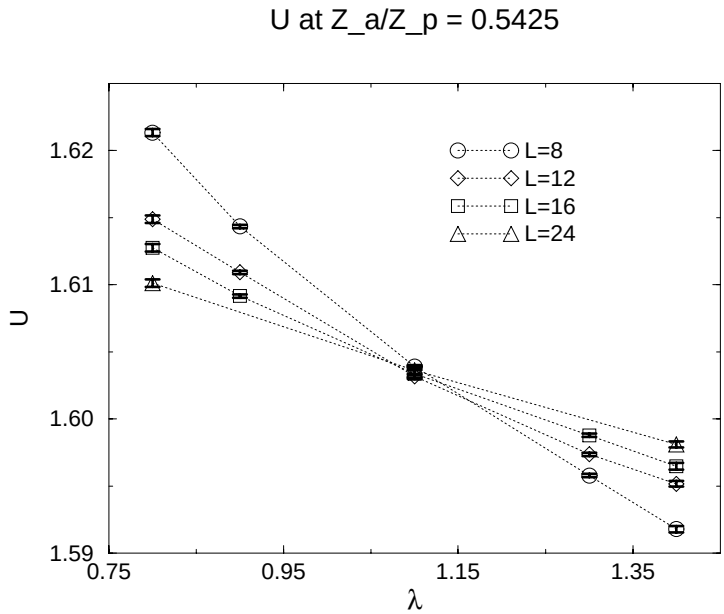

Fig. 4. The Binder cumulant U at $Z_a/Z_p = 0.5425$ as a function of λ for the lattice sizes $L = 8$, 12, 16 and 24. The dashed line is used to guide the eye. It connects data points of the same L. Note that here the slope of the curve becomes smaller as L increases.

We also fitted the difference of $\bar{R}$, for the two values of the coupling, $\lambda_1 = 0.9$ and $\lambda_1 = 1.3$, with the ansatz

$$\Delta\bar{R}(L, \lambda_1, \lambda_2) = [\bar{c}(\lambda_1) - \bar{c}(\lambda_2)]L^{-\omega}\,. \tag{83}$$

The interesting observation was that, already starting from $L_{\min} = 4$, the data are well fitted by this simple ansatz. This means that sub-leading corrections depend very little on λ and are, to a large extent, cancelled in $\Delta\bar{R}$.

We also analyzed the data of Ref. 38 for $Q = 1/U$ at $Z_a/Z_p = 0.5425$ for the spin-1 Ising model with this method.

The analysis of larger lattices, with high statistics, in Sec. III of Ref. 38 shows that the value $D_{\rm opt} \approx 0.6241$ has to be revised. Fitting the data at $D = 0.624235$ with Eq. (25) of Ref. 38

$$\bar{R} = \bar{R}^* + \bar{c}(D)L^{-\omega} \tag{84}$$

gives $\bar{c} = 0.0036(16)$ for $L_{\min} = 12$. Hence, we still see a small signal of corrections to scaling. In order to correct the value of $D_{\rm opt}$, we need to know the derivative $d\bar{c}(D)/dD$.

The analysis of the Monte Carlo data in Ref. 39 with the fit ansatz, Eq. (20), reveals that this derivative can be obtained accurately from the study of small lattices. Therefore, we simulated lattice sizes $L = 8$, 9 and 10 for $D = 0.6421$ and

Table 2. Spin-1 Ising model: The Binder Cumulant $U = \langle m^4 \rangle / \langle m^2 \rangle^2$ at $Z_a/Z_p = 0.5425$ fixed.

L	$D = 0.6421$	$D = 0.6931$
8	1.60195(19)	1.60718(18)
9	1.60202(19)	1.60659(19)
10	1.60184(19)	1.60577(19)

Table 3. Spin-1 Ising model: $\Delta\bar{c}(D)/\Delta D$ from Eq. (85) and the numbers given in Table 2.

L	$\Delta r(D)/\Delta D$
8	−0.23(1)
9	−0.22(1)
10	−0.21(1)

$D = 0.6931$. In Table 2, we give the results from runs with 10.000.000 measurements each.

Next, we computed estimates for $\Delta\bar{c}$ for each lattice size

$$\Delta\bar{c} := \left(\bar{R}(L, 0.6931) - \bar{R}(L, 0.6421)\right) L^{\omega} , \tag{85}$$

with $\omega = 0.845$. The results for $\Delta\bar{c}(D)/\Delta D$ are given in Table 3.

Using linear extrapolation, we arrive (using $\Delta\bar{c}(D)/\Delta D = -0.21(1)$ and $\bar{c}(0.624235) = 0.0036(16)$ from $L_{\min} = 12$) at the revised value for the optimal coupling

$$D_{\rm opt} = 0.641(8) . \tag{86}$$

Here, we made no attempt to estimate systematical errors caused by higher order corrections.

One can also compute the location of vanishing leading correction by using just one dimensionless ratio. However, as we can easily see from Eq. (67), at least three different lattice sizes are needed to obtain an estimate. This way, one can extract the optimal ratio β_2/β_1 of the NNN Ising model from Table 7 of Ref. 82. By linear interpolation of the results for the correction amplitude of $1/U$ at $\beta_2/\beta_1 = 0.2$ and $\beta_2/\beta_1 = 0.3$, one obtains

$$\left(\frac{\beta_2}{\beta_1}\right)_{\rm opt} = 0.247(8) . \tag{87}$$

3.6. *Computing critical exponents*

3.6.1. *The exponent ν*

The experience shows that it is most efficient to compute ν from the slope of the Binder cumulant or another dimensionless ratio at β_c:

$$\left.\frac{dU}{d\beta}\right|_{\beta_c} = aL^{1/\nu}(1 + cL^{-\omega} + \cdots) . \tag{88}$$

Also, it can be advantageous to compute the slope at β_f instead of β_c. In particular, the propagation of the error of β_f is simpler than for β_c, since β_f is obtained from only one lattice size. We define

$$\overline{\frac{dU}{d\beta}} := \left.\frac{dU}{d\beta}\right|_{\beta_f} , \tag{89}$$

where β_f is, as before, the inverse temperature, where $R = R_f$. Let us start from the leading order Taylor-expansion of the slope of the Binder cumulant at β_c:

$$\frac{dU}{d\beta} = \left.\frac{dU}{d\beta}\right|_{\beta_c} + \left.\frac{d^2U}{d\beta^2}\right|_{\beta_c} (\beta - \beta_c) + \cdots , \tag{90}$$

with

$$\left.\frac{d^2U}{d\beta^2}\right|_{\beta_c} \sim L^{2/\nu} . \tag{91}$$

Inserting

$$\beta_f = \beta_c + \frac{R_f - R^*}{a_R} L^{-1/\nu} + \cdots , \tag{92}$$

yields

$$\overline{\frac{dU}{d\beta}} = \bar{a} L^{1/\nu} (1 + \bar{c} L^{-\omega} + \cdots) . \tag{93}$$

In Ref. 38, we have computed ν from the standard Ising model as well as from the spin-1 Ising model with $D = 0.624235$.

From the standard Ising model on lattices in the range from $L = 12$ up to 128, we have obtained, with the ansatz

$$\left.\frac{dU}{d\beta}\right|_{\beta_c} = a L^{1/\nu} (1 + c L^{-\omega}) , \tag{94}$$

the result

$$\nu = 0.62973(43)\{46\}\langle 14\rangle . \tag{95}$$

In the ansatz (94), we have fixed $\omega = 0.81$, taken from the literature, and $\beta_c = 0.22165431$ from the analysis of the crossings of Z_a/Z_p. The quoted errors have different sources: the statistical error is given in the round brackets ( ); an estimate of systematical errors due to higher order corrections is given in curly brackets { } and in the spiky brackets $\langle\ \rangle$, we give the error caused by the uncertainty of the value of ω.

For fits without correction term, one has to go to larger lattice sizes. Fitting the slope of Z_a/Z_p for lattice sizes from $L = 40$ up to $L = 128$ yields

$$\nu = 0.63014(54)[55] . \tag{96}$$

Again, we give the statistical error in round brackets. The systematical error that is introduced by neglecting corrections is given in square brackets.

From fits of the slope of the Binder cumulant of the spin-1 Ising model at $D = 0.624235$, we get from lattices of size $L = 10$ up to $L = 56$

$$\nu = 0.62982(22)[16]\{15\} . \tag{97}$$

The statistical error is given in round brackets. The systematical error caused by sub-leading corrections is given in square brackets. In curly brackets, we give an

estimate of the error caused by the deviation of $D = 0.624235$ from the true value of $D_{\rm opt}$. For details of the numerical analysis, see Ref. 38.

In Ref. 39, we have analyzed the slope of the Binder cumulant of the ϕ^4 model at $\lambda = 1.1$. Fitting the slope of the Binder cumulant at $Z_a/Z_{p_f} = 0.5425$, for lattice sizes of $L = 12$ up to $L = 96$, yields

$$\nu = 0.6296(3)[4]\,. \tag{98}$$

The number in the round brackets gives the statistical error. In the square brackets, we give the sum of systematical errors caused by sub-leading corrections and the possible error of $\lambda_{\rm opt}$.

3.6.2. *The exponent η*

The exponent η can be obtained from the finite-size behavior of the magnetic susceptibility:

$$\chi|_{\beta_c} = b + L^{2-\eta}(a + cL^{-\omega} + \cdots)\,. \tag{99}$$

In the case of the magnetic susceptibility, it turns out to be necessary to include the analytic correction b into the fit-ansatz to obtain good fits from relatively small lattice sizes.

Also, it is advantageous to compute the magnetic susceptibility at β_f (remember that $R(\beta_f) = R_f$) instead of β_c. We get for $\bar\chi := \chi(\beta_f)$:

$$\bar\chi = \bar b + L^{2-\eta}(\bar a + \bar c L^{-\omega} + \cdots)\,. \tag{100}$$

In Ref. 38, we obtain from a fit with the ansatz (100) for the standard Ising model, from lattices in the range of $L = 10$ up to $L = 128$, the result

$$\eta = 0.0366(8)\{9\}\,. \tag{101}$$

We have fixed $\omega = 0.81$ in this fit. In the round brackets, we give the statistical error. In the curly brackets, the systematical error is given.

In the analysis of the improved models, we have skipped the term $\bar c L^{-\omega}$ of the ansatz (100). From the spin-1 model, we obtain in Ref. 38, from lattices of $L = 8$ up to $L = 56$, the result

$$\eta = 0.0366(6)[2]\,. \tag{102}$$

From the ϕ^4 theory, we get in Ref. 39, from lattices of $L = 12$ up to $L = 96$, the result

$$\eta = 0.0358(4)[5]\,. \tag{103}$$

In both cases, the round brackets contain the statistical error, while in the square brackets, the systematical errors are summarized. The systematical errors are caused by sub-leading corrections to scaling and by the numerical uncertainty of $D_{\rm opt}$ and $\lambda_{\rm opt}$, respectively.

The results obtained for η with three different models (standard Ising, spin-1 Ising and ϕ^4) nicely agree. On the one hand, this is again a nice confirmation of the universality hypothesis. On the other hand, it indicates that systematical errors are well under control. The error of the result from the standard Ising model is about twice as large as that obtained from the improved models.

3.6.3. *Averaged results for ν and η: Ising universality class*

For the convenience of the reader, we merge the results for ν and η from the spin-1 Ising model and the ϕ^4 theory. The quoted errors are the sum of statistical and systematical errors. Since the systematical errors are of the same nature for both models, we quote the error of a single model as the final error:

$$\nu = 0.6297(5)\,, \quad \eta = 0.0362(8)\,. \tag{104}$$

From this result, we directly obtain the RG-exponents (Eq. (44)):

$$y_t = 1.5881(13)\,, \quad y_h = 2.4819(4)\,. \tag{105}$$

In order to make comparisons with the literature easier, we compute the remaining exponents using the scaling relations:

$$\alpha = 0.1109(15)\,, \quad \gamma = 1.2366(15)\,, \quad \beta = 0.3262(4)\,, \quad \delta = 4.790(5)\,. \tag{106}$$

3.7. *Comparison with the literature*

There exist exhaustive compilations of results for critical exponents in the literature, see for example Refs. 67 and 103. In the following, we do not intend to give a complete overview of the literature, but rather try to select some typical work.

3.7.1. *Other Monte Carlo studies*

In Table 4, we have listed results for the critical exponents ν, η and ω for the 3D Ising universality class obtained from Monte Carlo simulations. All authors simulate the standard Ising model on the simple cubic lattice. In Ref. 67, in addition, the spin-1 Ising model at $D = \ln 2$ and the NNN Ising model were simulated. In the recent study,[82] the standard Ising model was simulated on a special purpose computer. In addition, the NNN Ising model was simulated on PCs and workstations.

The studies that we have listed use either finite-size scaling (FSS) or MCRG. As algorithm, either a cluster algorithm or the Metropolis algorithm in multi-spin coding implementation was used.

The results for the exponent ν are all in good agreement with our result, except for Refs. 93 and 95. The situation is quite different in the case of the exponent η. Here, the values obtained in Refs. 93, 95, 97 and 107 are too small. Very likely this deviation is due to leading corrections to scaling that were not dealt with appropriately in the analysis of the Monte Carlo data. The values quoted for the correction exponents ω are more or less all consistent with our result. Our result for ω is, however, considerably more accurate than that of previous studies.

Table 4. Results for critical exponents of the 3D Ising universality class obtained from Monte Carlo simulations. These results were obtained either with finite-size scaling (FSS) or the Monte Carlo renormalization group (MCRG) method. In the second row, we give the combined results of Refs. 38 and 39 for comparison. For a discussion, see the text.

Ref.	Year	Method	ν	η	ω
38, 39	1999	FSS	0.6297(5)	0.0362(8)	0.845(10)
82	1999	FSS	0.6303(6)	0.0372(10)	0.82(3)
91	1999	FSS	0.6294(5)(5)	0.0374(6)(6)	0.87(9)
67	1995	FSS	0.6301(8)	0.037(3)	0.82(6)
104	1993	FSS			0.85(4)
58	1993	FSS	0.630(2)		
97	1991	FSS	0.6289(8)	0.0172(57)	
105	1990	FSS	0.6303(14)		
93	1996	MCRG	0.625(1)	0.025(6)	≈ 0.7
106	1996	MCRG	0.6309(12)	0.038(2)	
95	1992	MCRG	0.624(1)(2)	0.0262(2)(30)	0.80–0.85
107	1989	MCRG	0.629(3)	0.027(5)	0.92(8)
31	1984	MCRG	0.629(4)	0.031(5)	1.0(1)

3.7.2. *Field theoretic methods*

The ϵ-expansion was invented by Wilson and Fisher.[3] The expansion parameter is the deviation from four dimensions: $d = 4 - \epsilon$. As an example, for recent results from the ϵ-expansion, we give in Table 5 the numbers of Ref. 103. The series has been computed up to $O(\epsilon^5)$ in Ref. 108.

The results for ν and η obtained from the ϵ-expansion are in perfect agreement with our results. However, the error-bars are considerably larger than those obtained now from Monte Carlo. The result for ω is smaller than ours, but still consistent within error-bars.

Parisi[109] proposed to perform perturbative expansions directly in three-dimensions (3D PT). In this approach, the exponents are expanded in the four-point coupling g (for a precise definition, see textbooks, e.g., Refs. 6, 74 and 75).

Table 5. Results for critical exponents of the Ising universality class from perturbation theory in three-dimensions (3D PT) and the ϵ-expansion. bc means that the exact result in two-dimensions is used as boundary condition. For a discussion, see the text.

Ref.	Method	ν	η	ω
103	ϵ-expansion, free	0.6290(25)	0.0360(50)	0.814(18)
103	ϵ-expansion, bc	0.6305(25)	0.0365(50)	
110	3D PT	0.6301(5)	0.0355(9)	
112	3D PT	0.6300(15)	0.032(3)	0.79(3)
103	3D PT	0.6304(13)	0.0335(25)	0.799(11)
115	3D PT	0.6303(8)	0.0335(6)	0.792(3)

The coefficients of this expansion are known up to $O(g^7)$ for $N = 0, 1, 2, 3$,[110] and for arbitrary N up to $O(g^6)$.[111] Here, N refers to the $O(N)$-symmetry of the universality class. In particular, $N = 1$ corresponds to the Ising universality class. These series have to be evaluated at the fixed point value of the four-point coupling constant $g^* \cdot g^*$ can be obtained from the zero of the Callan–Symanzik β-function. The β-function is known up to $O(g^7)$ for all N (g^* can also be computed from high temperature series expansions or Monte Carlo simulations).[111]

In order to obtain a numerical result from these series, a re-summation is needed. Typically, a Borel re-summation is used (see, e.g., Ref. 112). However, the Borel re-summation assumes that corrections are analytic. Nickel[113] pointed out that there should be nonanalytic corrections to the β-function due to sub-leading corrections to scaling. This leads to a slow convergence of the Borel re-summation. For a detailed discussion of this problem, see Refs. 23 and 114.

As examples of results obtained with Borel re-summation, we give in Table 5 the results of Refs. 103 and 112. The authors of Ref. 115 use an alternative re-summation scheme (that also seems to assume that corrections are analytic).

We also give the results of Murray and Nickel,[110] who try to take into account the nonanalytic corrections in their analysis.

The results for the exponent ν all agree with our Monte Carlo results. However, in the case of η, only the results of Ref. 110 nicely agree with the Monte Carlo estimates. The results of Refs. 103 and 115 are very similar, despite the fact that different re-summation schemes have been used. The authors of Ref. 115 seem to have underestimated the error of their estimate of η considerably.

This observation is further supported by the high precision Monte Carlo result $\gamma = 1.1575(6)$ of Ref. 116 for the self-avoiding random walk in three dimensions. Here, Murray and Nickel give $\gamma = 1.1569(4)$, while Refs. 103 and 115 give $\gamma = 1.1596(20)$ and $\gamma = 1.1604(8)$, respectively.

3.7.3. *High temperature expansions*

The analysis of high temperature expansions was the first theoretical method that produced reliable, non-mean-field values for critical exponents of three-dimensional systems. For a review of early work, see Ref. 117. In fact, the most accurate results for critical exponents in the Ising universality class are obtained from high temperature series in Ref. 23. In Ref. 23, the series was computed for the ϕ^4 model, the ϕ^4 model with additional ϕ^6 term and the spin-1 Ising model up to order β^{20} for arbitrary λ and D. In all cases, a simple cubic lattice was studied. These series were analyzed with Padè, Dlog–Padè and integral approximants for $\lambda_{\rm opt}$ and $D_{\rm opt}$, respectively. The values for $\lambda_{\rm opt}$ and $D_{\rm opt}$ were taken from our Monte Carlo simulations (Refs. 38 and 39 and private communication) in the case of the spin-1 Ising model and the ϕ^4 theory. In the case of the ϕ^4 model with additional ϕ^6 term, $\lambda_{\rm opt}$ was taken from a Monte Carlo simulation of the authors of Ref. 23. The results

Table 6. Results for ν, η and ω from high temperature series expansion. η is computed from the scaling relation $\eta = 2 - \gamma/\nu$. For a discussion, see the text.

Ref.	Model	ν	η	ω
23	see text	0.63002(23)	0.0364(4)	
40	DG, Kl, bcc	0.632(1)	0.0388(32)	0.854(80)
41	DG, Kl, bcc	0.6300(15)	0.0365(56)	0.825(50)
100	Ising, sc	0.6315(8)	0.0383(30)	
100	Ising, bcc	0.6308(5)	0.0368(18)	
99	Ising, sc, bcc	0.6302(4)	0.0363(13)	

for the critical exponents ν and η are given in Table 6. The results of Ref. 23 are perfectly consistent with our Monte Carlo results. The accuracy of Ref. 23 is better than ours.

The authors of Ref. 100 have analyzed high temperature series expansions of the Ising model on the simple cubic and body centered cubic lattice up to the order β^{21}. Their result for ν is larger than that of Ref. 23 (and also our Monte Carlo result). The quoted error-bars do not overlap by a small margin. The authors do not quote a value for η in their paper. For the convenience of the reader, we converted $\gamma = 1.2388(10)$ (sc) and $\gamma = 1.2384(6)$ (bcc) given for the exponent of the magnetic susceptibility, using the scaling relation $\eta = 2 - \gamma/\nu$ (converting our numbers, we get $\gamma = 1.2366(15)$). One should note that in this work, ω as well as β_c is taken as external input for the analysis.

Recently, in Ref. 99, the same authors have extended the series up to the order β^{23}. Their new results for ν are consistent with our Monte Carlo results and those of Ref. 23.

We also give results obtained from the series expansion of two parameter models that interpolate between the Gaussian and the Ising model (Double Gaussian, Klauder), similar to the models discussed in this review. While the results of Nickel and Rehr[41] are in perfect agreement with our numbers (with larger error-bars), the value obtained by Chen, Fisher and Nickel[40] for ν is clearly larger than ours. Also, the value $\gamma = 1.237(2)$ obtained by Nickel and Rehr is consistent with ours, while $\gamma = 1.2395(4)$ of Chen, Fisher and Nickel seems too large compared with ours and also that of Ref. 23.

The values obtained by Nickel and Rehr, as well as by Chen, Fisher and Nickel, for the correction to scaling exponent ω are consistent with our result. However, the error-bars are considerably larger than those of Ref. 23.

3.7.4. *Other theoretical methods*

There are a number of other methods to determine critical exponents of three-dimensional spin models. However, they tend to give less accurate results than those discussed above. Therefore, we will just mention these methods without further discussion. Some of these methods are restricted to discrete spin model like

the Ising model.

- Low temperature series expansions
- Transfer-matrix for a $L^2 \times \infty$ system
- Generalizations of mean-field (e.g., coherent anomaly method)
- Low and high temperature series expansions in a Hamiltonian formulation
- "Exact renormalization group"

An interesting result is obtained with the "scaling field method" in Ref. 118. While the results for ν and η are considerably less accurate than those discussed above, the authors are able to give estimates for sub-leading correction exponents. For example for the Ising universality class, they find $\omega_2 = 1.67(11)$.

3.7.5. *Experimental results*

Many experimental results for critical exponents are presented in the literature. A wide variety of systems is studied that is believed to belong to the 3D Ising universality class. They can be divided into four classes:

- Magnetic systems

  Magnets with an uniaxial unisotropy share the Ising universality class. The best experimental results have been obtained with FeF_2 crystals, which become antiferromagnetic below $T \approx 78.3$ K.
- Binary mixtures

  Typically, a mixture of two fluids is considered. One fluid is identified with the 1 of the Ising model and the other with -1. This is a very crude identification. In particular, there is certainly no exact symmetry between the two fluids. Therefore, the Z_2 symmetry has to be "restored" at the transition point. A number of systems have been studied. For example, a mixture of cyclohecane and aniline has a mixing temperature of $\approx 29.632°$C at the critical concentration $x_c \approx 0.4551$ (mole fraction of aniline).
- Liquid–vapor systems

  In the liquid–vapor system, one identifies the liquid with the 1 and the vapor with the -1 of the Ising model. Obviously, the liquid–vapor lacks the Z_2 symmetry of the Ising model. Therefore, one also has to expect corrections related to the restoration of Z_2 symmetry at the transition point. In experiments, the transition of, e.g., SF_6, CO_2 or H_2O has been studied at the end-point of the line of first order phase transitions in the pressure–temperature plane.
- Micellar systems

  Here, one studies emulsions. For example, in Ref. 143, a micro-emulsion of benzene and benzyldimethyl-n-hexadecylammonium chlorid in water was studied.

In experiments, one is faced with the uncertainty in the measurements of the temperature (actually only temperature differences matter) and the observable one

is measuring (information on the correlation function is obtained from scattering with visible light, X-rays or neutrons). In addition, the phase transition can be rounded by external influences like magnetic fields, gravity, etc. (the experiment[119] with a SF_6 system was performed on the German Spacelab D-2 mission to avoid gravitational rounding of the transition). Also, the lack of equilibration leads to a rounding of the transition (note that critical slowing down also affects experiments. As T approaches T_c, equilibration times become larger and larger). Impurities of the samples might even change the fixed point.

Furthermore, systematic errors are introduced by missing correction terms in the fits that are used to extract the critical exponents from the experimental data (in this respect, the analysis of experimental data is quite similar to the analysis of Monte Carlo data).

In Table 7 (taken from Ref. 23), the results of several experiments are summarized. Most of the numbers from experiments agree with the theoretical predictions

Table 7. Table taken from Ref. 23. Experimental estimates of critical exponents. *ms* denotes a magnetic system; *bm* a binary mixture; *lv* a liquid–vapor system; *mi* a micellar system.

	Ref.	γ	ν	η	α	β
lv	119				$0.1105^{+0.0250}_{-0.0270}$	
	120				0.1075(54)	
	121				0.1084(23)	
	122				0.111(1)	0.324(2)
	123					0.341(2)
	124				0.117(3)	
bm	126				0.104(11)	
	125	1.233(10)				0.327(2)
	127	1.09(3)				
	128	1.26(5)	0.64(2)			
	129	1.24(1)	0.606(18)		0.077(44)	0.319(14)
	130				0.105(8)	
	131					0.324(5), 0.329(2)
	132					0.329(4), 0.333(2)
	133		0.610(6)			
	134					0.336(30)
	135	1.228(39)	0.628(8)	0.0300(15)		
ms	136	1.25(2)	0.64(1)			
	137				0.115(4)	0.331(6)
	138				0.11(3)	
	139					0.325(2)
	140				0.11(3)	
	141	1.25(2)				0.315(15)
mi	142					0.34(8)
	143	1.18(3)	0.60(2)			
	144	1.216(13)	0.623(13)	0.039(4)		
	145	1.237(7)	0.630(12)			
	146	1.25(2)	0.63(1)			
	147	1.17(11)	0.65(4)			

for the 3D Ising universality class discussed above. However, the results are by far less precise than those from the theoretical methods discussed above. In a few cases, there are rather large deviations, as for example, the value of γ given in Ref. 127. Here, we shall not try to discuss whether this deviation is indeed a sign of a wrong assignment of the system to the Ising universality class or just an error in the experiment.

Table 7 mostly contains results that have been obtained after 1990. For more exhaustive compilations of results and a more detailed discussion, see Refs. 67, 148 and 149.

4. The Mass Spectrum and the Correlation Length

The correlation length ξ is a measure of the range of correlations in the system. The connected correlation function is defined by:

$$G(x) := \langle s_0 s_x \rangle - \langle s_0 \rangle \langle s_x \rangle \,. \tag{107}$$

The exponential correlation length is then given by the large distance behavior of the correlation function

$$\frac{1}{\xi} := -\lim_{|x|\to\infty} \frac{1}{|x|} \ln G(x) \,. \tag{108}$$

In the context of field theory, the inverse of the correlation length is the mass of the lightest particle in the theory. In fact, the whole mass spectrum can be related to the decay of correlation functions. This relation can be worked out in the framework of the transfer matrix. The transfer matrix can be understood as the discrete version $e^{-\Delta t H}$ of the (quantum) Hamiltonian H of the theory.

4.1. *The transfer matrix*

The transfer matrix formalism goes back to Kramers and Wannier in 1941. In Ref. 16, they also discuss the self-duality of the two-dimensional Ising model. The transfer matrix formalism is the basis for the exact solution of the two-dimensional Ising model. In the transfer matrix formalism, one direction of the lattice is identified as "time" direction (in the below discussion, we take the one-direction). The lattice points at the same "time" (i.e., with the same x_1) are elements of one "time slice". For simplicity, let us discuss the transfer matrix at the example of the standard Ising model.

The Boltzmann factor is written as:

$$B(s_{(1,\ldots,1)}, \ldots, s_{(L_1,\ldots,L_d)}) = T(u_1, u_2) T(u_2, u_3) \cdots T(u_{L_1}, u_1) \,, \tag{109}$$

where u is a spin configuration on a $L_2 \times \cdots \times L_d$ time slice. T is given by:

$$T(u_{x_1}, u_{x_1+1}) = V(u_{x_1}) W(u_{x_1}, u_{x_1+1}) V(u_{x_1+1}) \,, \tag{110}$$

where

$$V(u_{x_1}) = \exp\left(\frac{1}{2}\beta \sum_{x_2,\ldots,x_d} \sum_{\mu=2}^{d} s_x s_{x+\hat{\mu}} + \frac{1}{2} h \sum_{x_2,\ldots,x_d} s_x\right), \tag{111}$$

and

$$W(u_{x_1}, u_{x_1+1}) = \exp\left(\beta \sum_{x_2,\ldots,x_d} s_{(x_1,x_2,\ldots,x_d)} s_{(x_1+1,x_2,\ldots,x_d)}\right). \tag{112}$$

If we interpret $T(u,v)$ as a matrix element, where the slice-configurations u and v are the indices, the partition function can be written as:

$$Z = \operatorname{tr} T^{L_1} = \lambda_0^{L_1} + \lambda_1^{L_1} + \cdots, \tag{113}$$

where λ_i are the eigenvalues of the transfer matrix T. Note that the transfer matrix is positive and symmetric. Therefore, the eigenvalues are positive real numbers and the eigenvectors are orthogonal to each other.

In order to understand the relation of the correlation length with the spectrum of the transfer matrix, we express the correlation function in the transfer matrix formalism. First, let us discuss how a simple observable like the expectation value of the field variable $\langle s_x \rangle$ can be expressed:

$$\begin{aligned}
\langle s_{(1,\ldots,1)} \rangle &= \frac{\sum_s \exp(\beta \sum_{\langle xy \rangle} s_x s_y + h \sum_x s_x) s_{(1,\ldots,1)}}{Z} \\
&= \frac{\sum_s T(u_1,u_2) T(u_2,u_3) \cdots T(u_{L_1},u_1) s_{(1,\ldots,1)}}{\sum_s T(u_1,u_2) T(u_2,u_3) \cdots T(u_{L_1},u_1)} \\
&= \frac{\sum_{s,u_{L_1+1}} T(u_1,u_2) T(u_2,u_3) \cdots T(u_{L_1},u_{L_1+1}) A(u_{L_1+1},u_1)}{\sum_s T(u_1,u_2) T(u_2,u_3) \cdots T(u_{L_1},u_1)},
\end{aligned} \tag{114}$$

with $A(u_{L_1+1}, u_1) = \delta(u_{L_1+1}, u_1) s_{(1,\ldots,1)}$.

Interpreted as a matrix, A is diagonal. For each configuration on the time slice, it takes the value of the observable on the configuration.

We arrive at the expression

$$\langle s_{(1,\ldots,1)} \rangle = \frac{\operatorname{tr} T^{L_1} A}{\operatorname{tr} T^{L_1}} = \frac{\sum_i \lambda_i^{L_1} \langle i|A|i\rangle}{\sum_i \lambda_i^{L_1}}, \tag{115}$$

where the $|i\rangle$ are normalized eigenvectors of T. In the limit $L_1 \to \infty$, we obtain

$$\langle s_{(1,\ldots,1)} \rangle = \langle 0|A|0\rangle, \tag{116}$$

where $|0\rangle$ is the eigenvector of the largest eigenvalue.

In order to compute correlation functions (of zero-momentum operators), we have to insert matrices at two different time-slices.

One obtains

$$\langle a_0 b_t \rangle = \frac{\sum_i \sum_j \sum_k \sum_l \langle k|T^{L_1-t}|i\rangle \langle i|A|j\rangle \langle j|T^t|l\rangle \langle l|B|k\rangle}{\operatorname{tr} T^{L_1}}. \tag{117}$$

A and B are the diagonal matrices corresponding to the observables a and b. In the limit $L_1 \to \infty$, we get

$$\begin{aligned}\langle a_0 b_t \rangle &= \sum_i \left(\frac{\lambda_i}{\lambda_0}\right)^t \langle 0|A|i\rangle\langle i|B|0\rangle \\ &= \sum_i \langle 0|A|i\rangle\langle i|B|0\rangle \exp(-m_i t)\,, \end{aligned} \tag{118}$$

with

$$m_i = -\ln\left(\frac{\lambda_i}{\lambda_0}\right), \tag{119}$$

where m_i is the mass of the state i. $\langle 0|A|i\rangle$ is called the overlap of the observable a with the state i.

The correlation function is decaying exponentially with the distance t. Asymptotically, the decay is determined by the smallest m_i with nonvanishing overlaps $\langle 0|A|i\rangle$ and $\langle i|B|0\rangle$. The inverse of this m_i is the correlation length ξ.

The eigenvectors of the transfer matrix can be classified with respect to their symmetry properties.

Translations of a time-slice can be expressed as matrix

$$P_{\mathbf{x}}(u,v) = \prod_{\mathbf{z}} \delta(u^{(\mathbf{z}+\mathbf{x})}, v^{(\mathbf{z})})\,, \tag{120}$$

with $\mathbf{x} = (x_2, \ldots, x_d)$. Since the transfer matrix T commutes with translations P, the eigenvectors (states) of the transfer matrix are also eigenvectors of P. Translational invariant (zero momentum) states have the P-eigenvalue 1 for all $\mathbf{x}$.

In a similar way, the states can be classified with respect to their angular momentum and parity.

One way to compute the low lying mass-spectrum of the Ising model in three dimensions is to compute the eigenvalues of the transfer matrix with the methods of numerical linear algebra.

However, one has to note that the dimension of the Ising transfer matrix is $2^N \times 2^N$, where N is the number of sites within one time slice. Therefore, in practice, the largest system size that can be handled this way is $5 \times 5 \times \infty$.

In order to deal with larger system sizes, Monte Carlo simulations are needed.

4.2. *Correlation length from Monte Carlo simulation*

In a Monte Carlo simulation, one computes expectation values of observables. However, it is unfavorable to use Eq. (108) to compute the correlation length. In Monte Carlo simulations, the signal to noise ratio for $G(x)$ becomes worse with increasing distance. Therefore, a reliable determination of the correlation length requires a fast convergence with increasing distance x. One way to achieve an improvement is to consider operators, which have well-defined symmetry properties. Mostly, one

uses so-called time slice correlation functions. The magnetization of a time slice is given by:

$$S_{x_1} = \frac{1}{L^2} \sum_{x_2,x_3} s_{(x_1,x_2,x_3)} \,. \tag{121}$$

Note that this operator is invariant under translations. Therefore, it has only nonvanishing overlap with zero-momentum states. Let us define the time slice correlation function

$$G(\tau) = \{\langle S_{x_1} S_{x_1+\tau}\rangle - \langle S_{x_1}\rangle^2\} \,. \tag{122}$$

The large distance behavior of $G(\tau)$ is given by:

$$G(\tau) = c \exp\left(\frac{-\tau}{\xi}\right), \tag{123}$$

where ξ is the (exponential) correlation length, and c is a constant. A common tool to extract the asymptotic ξ is the so-called effective correlation length

$$\xi_{\text{eff}}(\tau) = \frac{-1}{\ln(G(\tau+1)) - \ln(G(\tau))} \,. \tag{124}$$

From Eq. (118), we see that the effective correlation length is a monotonically increasing function of τ. In the limit $\tau \to \infty$, it converges to the exponential correlation length ξ.

For lattices with moderate extension L_1, it is important to take into account the periodicity of the lattice. $\xi_{\text{eff}}(\tau)$ is then computed from the ansatz

$$G(\tau) = \text{const}\left[\exp\left(\frac{-\tau}{\xi}\right) + \exp\left(\frac{-(L_1-\tau)}{\xi}\right)\right], \tag{125}$$

by solving the system of equations for τ and $\tau+1$.

4.2.1. *Second moment correlation length*

This definition of the correlation length is very popular since its numerical evaluation (say in Monte Carlo simulations) and its calculation in series expansions is simpler than that of the exponential correlation length. Moreover, it is the length scale, which is directly observed in scattering experiments. However, it is important to stress that it is not exactly equivalent to the exponential correlation length. The square of the second moment correlation length is defined for a d-dimensional model by:

$$\xi^2_{\text{2nd}} = \frac{\mu_2}{2d\mu_0} \,, \tag{126}$$

where

$$\mu_0 = \lim_{L\to\infty} \frac{1}{V} \sum_{x,y} \langle s_x s_y\rangle_c \,, \tag{127}$$

and

$$\mu_2 = \lim_{L\to\infty} \frac{1}{V} \sum_{x,y} (x-y)^2 \langle s_x s_y \rangle_c \,, \tag{128}$$

where the connected part of the correlation function is defined by:

$$\langle s_x s_y \rangle_c = \langle s_x s_y \rangle - \langle s_x \rangle^2 \tag{129}$$

and V is the lattice volume.

4.2.2. *The $\xi/\xi_{2\mathrm{nd}}$ ratio*

The relation between ξ and $\xi_{2\mathrm{nd}}$ can be obtained as follows:

$$\begin{aligned} \mu_2 &= \frac{1}{V} \sum_{x,y} (x-y)^2 \langle s_x s_y \rangle_c \\ &= \frac{1}{V} \sum_{x,y} \sum_{\mu=1}^{d} (x_\mu - y_\mu)^2 \langle s_x s_y \rangle_c \\ &= \frac{d}{V} \sum_{x,y} (x_1 - y_1)^2 \langle s_x s_y \rangle_c \,. \end{aligned} \tag{130}$$

Due to the exponential decay of the correlation function, this sum is convergent and we can commute the spatial summation with the summation over configurations

$$\mu_2 = dL^2 \sum_{\tau=-\infty}^{\infty} \tau^2 \langle S_0 S_\tau \rangle_c \,, \tag{131}$$

with S_{x_1} given by Eq. (121). Analogously, one obtains

$$\mu_0 = L^2 \sum_{\tau=-\infty}^{\infty} \langle S_0 S_\tau \rangle_c \,. \tag{132}$$

If we now insert these results in Eq. (126), we obtain

$$\xi_{2\mathrm{nd}}^2 = \frac{\sum_{\tau=-\infty}^{\infty} \tau^2 G(\tau)}{2 \sum_{\tau=-\infty}^{\infty} G(\tau)} \,. \tag{133}$$

With Eq. (118),

$$\langle S_0 S_\tau \rangle_c = \sum_i c_i \exp\left(\frac{-|\tau|}{\xi_i}\right), \tag{134}$$

where $c_i = \langle 0|S|i\rangle^2$ and replacing the summation by an integration over τ yields

$$\xi_{2\mathrm{nd}}^2 = \frac{1}{2} \frac{\int_{\tau=0}^{\infty} \mathrm{d}\tau \tau^2 \sum_i c_i \exp(-\tau/\xi_i)}{\int_{\tau=0}^{\infty} \mathrm{d}\tau \sum_i c_i \exp(-\tau/\xi_i)} = \frac{\sum_i c_i \xi_i^3}{\sum_i c_i \xi_i} \,, \tag{135}$$

which is equal to ξ^2 if only one state contributes.

4.2.3. *Variational analysis*

The method of the effective correlation length, Eq. (124), is adequate as long as the correlation function $G(\tau)$ is clearly dominated by the first excited state and one is only interested in this state. Else, one can try to fit with a multi-exponential ansatz like

$$G(\tau) = c_1 \exp\left(\frac{-\tau}{\xi_1}\right) + c_2 \exp\left(\frac{-\tau}{\xi_2}\right) + \cdots . \tag{136}$$

However, fits with many parameters are often delicate and it is hard to obtain reliable results.

It turns out that it is more efficient to compute the cross-correlations of a (large) set of operators. The cross-correlation function is defined by:

$$C_{\alpha\beta}(\tau) := \langle a_\alpha(0) a_\beta(\tau) \rangle \,, \tag{137}$$

where the $a_\alpha(x_1)$ are observables defined on the time slice x_1.

From Eq. (118), we get

$$C_{\alpha\beta}(\tau) = \sum_i c_i^{\alpha\beta} \exp(-m_i \tau) \,, \tag{138}$$

with

$$c_i^{\alpha\beta} = \langle 0|A_\alpha|i\rangle\langle i|A_\beta|0\rangle \,, \tag{139}$$

where A_α is the matrix that corresponds to the observable a_α.

The masses can then be extracted from the cross-correlation matrix by studying the generalized eigenvalue problem[150,151]

$$C(\tau)\psi = \lambda(\tau, \tau_0) C(\tau_0)\psi \,, \tag{140}$$

where τ_0 is small and fixed (say, $\tau_0 = 0$). Then, it can be shown that the various masses m_i are related to the generalized eigenvalues as follows[150,151]:

$$m_{i,\,\mathrm{eff}}(\tau, \tau_0) = \ln\left(\frac{\lambda_i(\tau, \tau_0)}{\lambda_i(\tau + 1, \tau_0)}\right). \tag{141}$$

The $m_{i,\,\mathrm{eff}}(\tau, \tau_0)$ converge to m_i as τ goes infinity (for τ_0 fixed).

This method is clearly discussed in Refs. 150 and 151, to which we refer for further details.

4.2.4. *The operator basis*

While the formalism of the variational approach to compute the spectrum is quite general, a suitable set of operators to compute the correlation functions has to be found for each model separately. Suitable in this context means that the states with small masses are given, to a good approximation, by some linear combination of the operators applied to the ground state.

Let us first discuss the Z_2 gauge theory in $2+1$ dimensions. The excitations of the Z_2 gauge theory are called "glueballs", in analogy with QCD in 3+1 dimensions.

The various glueballs are labeled by their angular momentum and parity. Thus, in order to distinguish the various states of the spectrum, one must construct operators with well-defined angular momentum. The fact that we are working in $2+1$ dimensions makes this construction rather nontrivial, and definitely different from the $(3+1)$-dimensional case. Moreover, since we are working on a cubic lattice, where only rotations of multiples of $\pi/2$ are allowed, we must study the symmetry properties of our operators with respect to a finite subgroup of the two-dimensional rotations. Let us first ignore the effect of the lattice discreteness and deal with the peculiar features, which already in the continuum formulation, the $(2+1)$-dimensional Ising (and SU(2), which is completely equivalent in this respect) spectrum has with respect to the $(3+1)$-dimensional SU(3) spectrum. These features have been discussed for the SU(2) model in Refs. 152 and 153 to which we refer for further details. We shall summarize here only the main results:

(a) For the Ising model, as for the SU(2) model, we cannot define a charge conjugation operator. The glueball states are thus labeled only by their angular momentum J and by their parity eigenvalue $P = \pm 1$. The standard notation is J^P.
(b) In $2+1$ dimensions, it can be shown that all the states with angular momentum different from zero are degenerate in parity. Namely J^+ and J^- (with $J \neq 0$) must have the same mass.

Note that on the lattice, we have no exact rotational symmetry. On the cubic lattice, the group of two-dimensional rotations and reflections becomes the dihedral group D_4. This group is non-Abelian, has eight elements and five irreducible representations. Four of these are one-dimensional irreps, the last one has dimension two. The group structure is completely described by the table of characters,[154] which we have reported in Table 8.

In the top row of Table 8, the invariant classes of the group are listed; and in the first column, the irreducible representations. We have followed the notations of Ref. 154 to label classes and representations (with the exception of the class containing the identity, which we have denoted with **1** instead of the usual E to avoid confusion with the two-dimensional representation). The entries of the table allow to explicitly construct the various representations and hence, also the lattice operators, which we are looking for. The relationship of these operators with the various

Table 8. Character table for the group D_4, the table is taken from Ref. 52.

	1	C_4^2	$C_4(2)$	$C_2(2)$	$C_{2'}(2)$
A_1	1	1	1	1	1
A_2	1	1	1	−1	−1
B_1	1	1	−1	1	−1
B_2	1	1	−1	−1	1
E	2	−2	0	0	0

glueball states immediately follows from the group structure. In particular, one can show that:

(a) Only operators with angular momentum $J(\mathrm{mod}(4))$ can be constructed. This is a common feature of all cubic lattice regularizations. It means that glueball states, which in the continuum have values of J higher than 3, appear on the lattice as secondary states in the family of the corresponding $J(\mathrm{mod}(4))$ lattice operator.

(b) The four one-dimensional irreps are in correspondence with the J even states. More precisely:

$$0^+ \to A_1\,, \quad 0^- \to A_2\,, \quad 2^+ \to B_1\,, \quad 2^- \to B_2\,.$$

This means that the discreteness of the lattice splits the degeneracy between 2^+ and 2^-, which we discussed above. The splitting between these two states gives us a rough estimate of the relevance of the breaking of the full rotational group due to the lattice discretization. As we shall see below, this splitting is essentially zero within the errors, in agreement with our expectation that approaching the continuum limit, the full continuum symmetries should be recovered. Notice, however, that this is a very nontrivial result since the operators associated to 2^+ and 2^- on the lattice turn out to be very different.

(c) All the odd parity states are grouped together in the two-dimensional irreducible representation E. This means that we cannot distinguish them on the basis of the lattice symmetries. We can conventionally assume that the $J = 3$ states have a mass lower than the $J = 1$ (this would agree with the pattern, which emerges from the Isgur–Paton model[155]), and that the $J = 1$ thus appear as secondaries in the $J = 3$ family. However, in the following, we shall avoid this assumption and shall denote the states belonging to this family as $J = 1/3$ states. In agreement with the above discussion, if the full rotational symmetry is recovered, we expect that the states belonging to this family are degenerate in parity and thus that the lowest mass states, which are the ones that we can measure more precisely, appear as a doublet. This prediction will be confirmed by our results.

In order to determine the spectrum, we have measured correlation functions of Wilson-loops. These Wilson-loops differ by their size and shape. The simplest Wilson-loops, constructed according to the character table, are shown in Fig. 5 (taken from Ref. 52). Notice however that these are only a small subset of the operators that we actually measured in our simulations. In particular, we have studied 27 different operators for the 0^+ channel, and 15, 9, 5, 16 for the 2^+, 2^-, 0^- and $1/3$ channels, respectively.

The Ising spin model is related with the Z_2 gauge theory by duality.[16] In Ref. 54, we proof that the same states appear in the spectrum of the spin model in the symmetry broken phase and the gauge model in the confined phase.

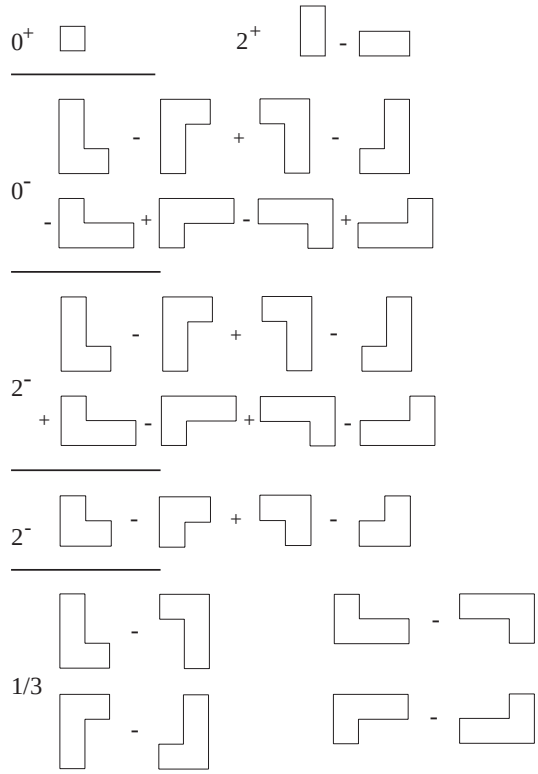

Fig. 5. Wilson loops for different channels.

One could try to construct the dual transforms of the Wilson-loops discussed above to measure the spectrum of the Ising model. However, it turns out that the dual of Wilson-loop correlators are complicated objects. Therefore, we looked in Ref. 53 for a new set of operators for the study of the Ising spin model and also the ϕ^4 theory on the lattice. We kept the basic idea that different operators should correspond to different length scales. We also wanted to include the standard time-slice magnetization in our basis of operators.

We have chosen a recursive definition of the operators. The starting point is the field $\phi^{(0)}_{x_1,x_2,x_3} = \phi_{x_1,x_2,x_3}$ as it is generated by the Monte Carlo. In the case of the Ising model, we similarly start with $\phi^{(0)}_{x_1,x_2,x_3} = s_{x_1,x_2,x_3}$. Then, the field (for each time-slice separately) is transformed according to the following rule:

$$\phi^{(\alpha+1)}_{x_1,x_2,x_3} = \mathrm{sign}(u)((1-w)|u| + wy)\,, \tag{142}$$

with

$$u = r\phi^{(\alpha)}_{x_1,x_2,x_3} + (1-r)\frac{1}{4}\left(\phi^{(\alpha)}_{x_1,x_2-1,x_3} + \phi^{(\alpha)}_{x_1,x_2+1,x_3} + \phi^{(\alpha)}_{x_1,x_2,x_3-1} + \phi^{(\alpha)}_{x_1,x_2,x_3+1}\right), \tag{143}$$

where w, y and r are free parameters of the transformation. The operators are then given by the sum of the $\phi^{(\alpha)}$ over a given time-slice

$$S^{(\alpha)}(x_1) = \sum_{x_2,x_3} \phi^{(\alpha)}_{x_1,x_2,x_3} \,. \tag{144}$$

The correlation matrix is then built by:

$$C_{\alpha\beta}(\tau) = \langle S(x_1)^{(\alpha)} S(x_1+\tau)^{(\beta)} \rangle - \langle |S(x_1)^{(\alpha)}| \rangle \langle |S(x_1+\tau)^{(\beta)}| \rangle \,. \tag{145}$$

We performed test simulations with different choices for the parameters w, y and r for small correlation length both, in the Ising and ϕ^4 models. The quality of the resulting operator basis was judged by looking at the convergence of effective masses towards their asymptotic values. It turned out that $r = 0$ is a good choice for ϕ^4 (for Ising, we have to choose r slightly different from 0 to have a well-defined transformation). There is no sharp constraint on the value of y. Mostly, we have taken y equal to the magnetization. In the case of w, it turned out that values close to 0 are a good choice. Note, however, that taking w exactly equal to 0 would result in all $S^{(\alpha)}$ being equal.

4.3. *The spectrum of the three-dimensional Ising model*

First, let us note that the ratios of masses are universal. That means these ratios converge to finite values as T_c is approached and these values are the same for all systems in a given universality class. This can be understood quite easily from the RG. All masses transform as $m_i' = bm_i$, where b is the blocking scale. Hence, ratios of masses are invariant under RG transformations. In addition, as $T \to T_c$, the thermal scaling field u_t (after sufficiently many RG-transformations) becomes (for $h = 0$) the only nonvanishing variable.

4.3.1. *Monte Carlo results for the Z_2 gauge theory*

In Ref. 52, we have studied the model in the confining phase. This phase corresponds to the symmetry broken, low temperature phase of the Ising spin model. The simulations were performed with a local demon update that has been implemented in multi-spin coding technique. The Z_2 gauge model can also be simulated with a cluster algorithm (see Ref. 156). However, for the moderate ξ that have been reached, we expected the local algorithm with multi-spin coding implementation to be more efficient. Simulations were performed for $\beta = 0.74057$, 0.74883, 0.75202 and 0.75632. These values of β correspond to $\beta_{\rm spin} = 0.23142$, 0.2275, 0.226 and 0.224, respectively. We have simulated on lattices up to a size of 100×70^2. We extracted the mass spectrum with the variational method discussed above. One should note that we have scaled the size of the Wilson-loops that have been used with the correlation length, to keep a good overlap with the glueball states. For the inverse of the lightest mass at these β's, we find $\xi_0 = 1.864(5)$, 2.592(5), 3.135(9) and 4.64(3) in lattice units, respectively.

In addition, we have measured the lightest mass in each of the channels discussed above. We also determined the masses of higher excited states. In particular, we have obtained results for the second and third mass of the 0^+ channel. In Ref. 52, we give the results for all β-values that have been studied. In Table 9, we give the extrapolation to the continuum (critical) limit of the masses. The masses are given in units of the string tension $\sqrt{\sigma}$. The string tension of the Z_2 gauge theory is the same (by duality) as the interface tension of the Ising spin model. For a detailed discussion of the interface tension, see Sec. 6 of this review. The continuum limit is obtained from the extrapolation to $\xi = \infty$, where we assume that corrections are proportional to $\xi^{-\omega}$ with $\omega \approx 0.8$. A first result is that the parity degeneration is indeed recovered in the continuum limit also for the even J sector. Taking into account this degeneration, we end up with eight independent states in the continuum limit. The results are given in Table 9.

In Table 9, we also give the corresponding results for SU(2) obtained in Ref. 157 and with the predictions of the IP model (for details of the IP model, see Ref. 52). Note that we have replaced (compared with the corresponding table in Ref. 52) in Table 9 the numbers of Ref. 152 by those of Ref. 157. Note that in Ref. 157 also results for SU(3) and SU(4) are given. Looking at Table 9, we see the biggest discrepancy in the mass values for the lowest state, which is too light in the IP model, and turns out to be very different in the Ising and SU(2) cases. This is due first to the lack of validity of the adiabatic approximation (in the IP-model) at small scales and second to the fact that in the IP model, an "ideal" picture of a string (without self repulsion terms) is assumed for the flux tube.

Apart from this state, in the remaining part of the spectrum, we immediately see good agreement between the Ising and SU(2) spectra.

We can conclude from these data that the qualitative features of the glueball spectrum are largely independent from the gauge group and well described by a flux tube effective model. While the higher states of the spectrum show a remarkable independence from the gauge group, for the lowest state, the flux tube picture breaks down and the gauge group becomes important. The IP model, which is

Table 9. Comparison between the Ising, SU(2) and IP spectra.

J^P	Ising	SU(2)	IP
0^+	3.08(3)	4.718(43)	2.00
$(0^+)'$	5.80(4)	6.83(10)	5.94
$(0^+)''$	7.97(11)	8.15(15)	8.35
$2^\pm$	7.98(8)	7.84(14)	6.36
$(2^\pm)'$	9.95(20)		8.76
0^-	10.0(5)	9.95(32)	13.82
$(0^-)'$	13.8(6)		15.05
$\left(\frac{1}{3}\right)^\pm$	12.7(5)	11.13(42)	8.04

the simplest possible realization of such a flux tube, seems able to catch (at least at a qualitative level) some of the relevant features of the glueball spectrum.

4.3.2. *Monte Carlo results for the Ising spin model and the ϕ^4 model*

In Ref. 48, we have determined the exponential and the second moment correlation length for various β values in the low and high temperature phase of the Ising spin model at vanishing external field. The results are summarized in Tables 14 and 15.

In the high temperature phase, the correlation function is clearly dominated by the first excited state and one can reliably determine the exponential correlation length with the effective correlation length method. Using the cluster-improved estimator of the correlation function, one can obtain very precise estimates of the exponential correlation length. On the other hand, in the low temperature phase, it turns out that $\tau \approx 3\xi$ is needed to reduce the systematic errors in $\xi_{\rm eff}$ to less than 1%. An additional problem in the low temperature phase is that there is no substantial reduction of the variance of the connected correlation function by cluster estimators.

Therefore, we applied in Ref. 53 the variational method with the operator basis discussed in Sec. 4.2.4 to the Ising model and the ϕ^4 theory at $\lambda = 1.1$ on the lattice in the low temperature phase. The simulation of the ϕ^4 theory can obviously not be implemented with the multi-spin coding technique. Therefore, we used the single cluster algorithm for the simulation. Since we wanted to simulate the Ising model with essentially the same program as the ϕ^4 theory, we also employed the single cluster algorithm in this case. Using the operator basis discussed above, we have only an overlap with the 0^+ channel. The numerical results for the Ising spin model are given in Table 10. The numbers are compatible with the results for the Z_2 gauge theory (at the corresponding values of β).

Corresponding results for the ϕ^4 theory at $\lambda = 1.1$ are given in Table 11.

Table 10. Correlation lengths extracted with the variational approach in 3D Ising model. Below each mass, we report the value of τ at which it has been evaluated. $\tau_0 = 0$ is always assumed. The equation marks denote the fact that the corresponding states are not yet stable within the errors; hence, the values quoted must be better considered as lower bounds. The table is taken from Ref. 53.

β	ξ_1	ξ_2	ξ_3
0.23142	1.870(3)	1.027(7)	0.727(13) (?)
	($\tau = 3$)	($\tau = 3$)	($\tau = 3$)
0.2275	2.593(4)	1.429(8)	1.016(13) (?)
	($\tau = 4$)	($\tau = 4$)	($\tau = 4$)

Table 11. Correlation lengths extracted with the variational approach in the 3D ϕ^4 model at $\lambda = 1.1$. The table is taken from Ref. 53.

β	ξ_1	ξ_2	ξ_3
0.405	1.1130(9)	0.609(2)	0.464(5)
	($\tau = 2$)	($\tau = 2$)	($\tau = 2$)
0.385	2.182(2)	1.182(5)	0.872(9)
	($\tau = 3$)	($\tau = 3$)	($\tau = 3$)
0.3798	3.463(4)	1.827(8) (?)	1.246(19) (?)
	($\tau = 4$)	($\tau = 5$)	($\tau = 4$)

In order to address the issues of scaling and universality, we constructed the ratio of the excited masses with the lowest one.

These dimensional ratios should approach a constant as $\beta \to \beta_c$ and be universal, namely they should have the same value in the Ising and the ϕ^4 model. This is clearly confirmed in Table 12.

4.3.3. *The ratio* $\xi/\xi_{2\mathrm{nd}}$

Since $\xi_{2\mathrm{nd}}$ is accessible in experiments by scattering of light, X-rays or neutrons, and is also easier to access by theoretical methods than the true correlation length ξ, it is important to know the ratio of the two.

In the high temperature phase, it turns out that $\xi/\xi_{2\mathrm{nd}}$ is very close to one. In Ref. 48, we find that $\xi/\xi_{2\mathrm{nd}} < 1.0006$ in the continuum limit. This is clearly confirmed in Ref. 23; they quote $\xi/\xi_{2\mathrm{nd}} = 1.000183(2)$ for the high temperature phase.

Table 12. Mass ratios for Ising model and the ϕ^4 model at $\lambda = 1.1$.

Model	β	ξ_1	ξ_1/ξ_2	ξ_1/ξ_3
ϕ^4	0.405	1.1130(9)	1.828(7)	2.40(3)
Ising	0.23142	1.870(3)	1.821(15)	2.57(5) (?)
ϕ^4	0.385	2.182(2)	1.846(10)	2.50(1)
Ising	0.2275	2.593(4)	1.815(13)	2.55(4) (?)
ϕ^4	0.3798	3.463(4)	1.895(10) (?)	2.78(5) (?)

Table 13. Comparison of our Monte Carlo results for the second moment correlation length with double biased IDA's. The table is taken from Ref. 48.

β	Our MC	Biased IDA
0.2391	1.2335(15)	1.2358(16)
0.23142	1.8045(21)	1.803(5)
0.2275	2.5114(31)	2.509(11)
0.2260	3.0340(32)	3.034(16)
0.2240	4.509(6)	4.493(30)
0.22311	6.093(9)	6.084(46)

The situation is quite different in the low temperature phase. Above, we have seen that there are masses rather close to the lightest mass in the 0^+ channel. Therefore, we expect from Eq. (135) that ξ is considerably larger than $\xi_{2\mathrm{nd}}$. In fact, combining the results of Ref. 48 for $\xi_{2\mathrm{nd}}$ and the results of Ref. 52 for ξ, we find that $\xi/\xi_{2\mathrm{nd}} = 1.031(6)$, Ref. 53, in the critical limit of the low temperature phase. This value is confirmed by the analysis of low temperature series in Ref. 158, who find $\xi/\xi_{2\mathrm{nd}} = 1.037(3)$ and Ref. 159, who find $\xi/\xi_{2\mathrm{nd}} = 1.032(4)$.

The ratio $\xi/\xi_{2\mathrm{nd}}$ in the low temperature phase has also been computed in perturbation theory. At one-loop level, one finds[160,161]:

$$\frac{\xi}{\xi_{2\mathrm{nd}}} = 1 - \frac{u_R}{4\pi}\left(\frac{13}{32} - \frac{3}{8}\log 3\right). \tag{146}$$

Plugging in $u_R^* = 14.3(1)$ (see the next section), we get $\xi/\xi_{2\mathrm{nd}} = 1.00652(3)$. In Ref. 53, we have extended the computation to two-loop. Plugging in the value for u_R^* (without any re-summation), we find $\xi/\xi_{2\mathrm{nd}} \approx 1.01266$.

The explanation for the failure of perturbation theory to predict the right value of $\xi/\xi_{2\mathrm{nd}}$ is that it misses the excited states that we have discussed above. In perturbation theory, the difference of $\xi/\xi_{2\mathrm{nd}}$ from one is only due to the "cut", i.e., contributions of scattering states of two particles. The cut starts at 2 m, which is larger than the second mass that we find.

4.3.4. *Comparison with low temperature series expansions*

For the three-dimensional Ising model on the simple cubic lattice, the exponential correlation length has been computed up to order u^{17} in Ref. 162 and the second moment correlation length up to order u^{23} in Ref. 163, where $u = \exp(-4\beta)$. Pioneering work has been done by Tarko and Fisher.[164] In 1975, they computed the second moment correlation length up to u^{15}.

These series can be analyzed by various methods. Inhomogeneous differential approximants were advertised in Refs. 165 and 166. It is very interesting to directly compare results from the inhomogeneous differential approximants with our Monte Carlo results. In Ref. 48, we used double biased inhomogeneous differential approximants to compute $\xi_{2\mathrm{nd}}$ for the β-values, where Monte Carlo results were available. The approximants were biased with $\nu = 0.631$ and $\beta_c = 0.2216544$, which were the best estimates at the time. The error-bars are dominated by the variation of the result with the parameters K and L of the approximants. The results change only a little, when redoing the analysis with improved estimates for ν and β given in Sec. 3.5 of this review.

Note that the results obtained from Monte Carlo and IDA match very nicely. For $\beta = 0.2391$, the error-bars are roughly of the same size. For larger β-values, the IDA results become less precise than the MC estimates. The larger the β, the more accurate are the results of IDA. Hence, we expect that for $\beta > 0.24$, it is hard to get results from Monte Carlo that are more accurate than that from IDA.

5. Universal Amplitude Ratios

In the previous section, we have seen that the spectrum in the critical limit is universal. This means that ratios of two different correlation lengths have a finite limit as T_c is approached, and that this limit is the same for all models in a given universality class.

The RG predicts that similar combinations of quantities like the magnetization, the magnetic susceptibility, the singular part of the free energy, the energy and the specific heat (for a definition of these quantities, see Sec. 2.1) take universal values.

In addition to critical exponents, these "amplitude ratios" are characteristic for a universality class. Therefore, their determination (calculation/measurement) in various models and experimental systems is an important test of the universality hypothesis.

In the simplest case, the same quantity is considered in the low and the high temperature phase. As an example, let us discuss the magnetic susceptibility. The power laws (ignoring corrections to scaling) are:

$$\begin{aligned} \chi &\simeq C_+ t^{-\gamma} \quad t > 0\,, \\ \chi &\simeq C_- (-t)^{-\gamma} \quad t < 0\,, \end{aligned} \tag{147}$$

with $t = (T - T_c)/T_c$. Here and in the following, we consider a vanishing external field $h = 0$. In this context, the pre-factors $C_\pm$ are called amplitudes. The values of C_+ and C_- depend on the details of the model (or the system that is studied in an experiment). However, the ratio

$$\frac{C_+}{C_-} = \lim_{t \searrow 0} \Gamma_\chi(t)\,, \tag{148}$$

with

$$\Gamma_\chi(t) := \frac{\chi(t)}{\chi(-t)}\,, \tag{149}$$

is universal (universal amplitude ratio). This can be understood in the framework of the renormalization group.

After sufficiently many (n) RG-transformations, all scaling fields except u_t are negligible. Since the RG-transformation is an analytic function, we can write

$$u_t^{(n)} = ct + O(t^2)\,, \tag{150}$$

where the constant c depends on the details of the system that is considered and the number of RG-transformations. Hence, the magnetic susceptibility after n RG-steps can be written as a function of $u_t^{(n)}$ only. Taking into account the transformation of the magnetic susceptibility itself, Eq. (51), we arrive at

$$\chi(t) = b^{-n(2d_\phi + d)} \chi(u_t^{(n)})\,, \tag{151}$$

where we have ignored $O(t^2)$ corrections and corrections due to irrelevant scaling fields. Taking the ratio and blocking n times in both phases yields

$$\frac{\chi(t)}{\chi(-t)} = \frac{b^{-n(2d_\phi+d)}\chi(u_t^{(n)})}{b^{-n(2d_\phi+d)}\chi(-u_t^{(n)})} = \frac{\chi(u_t^{(n)})}{\chi(-u_t^{(n)})}\,. \tag{152}$$

Hence, in the limit $t \to 0$, all model dependence is lost and the ratio is universal.

Similar ratios can be defined for the correlation length (f_+/f_-) and the specific heat (A_+/A_-).

In addition, there are interesting amplitude combinations that relate more than one observable:

$$Q_\pm(t) = -f_s(t)\xi_{2\mathrm{nd}}(t)^d\,, \tag{153}$$

where f_s is the singular part of the free energy density. The second moment correlation length $\xi_{2\mathrm{nd}}$ is considered here, since it can be more precisely determined by various methods than the true correlation length ξ_{exp}. Note that the amplitude combination, Eq. (153), can be defined for both phases $t > 0\,(Q_+)$ and $t < 0\,(Q_-)$.

$$u(t) = \frac{3\chi(t)}{\xi_{2\mathrm{nd}}^3(t)m^2(t)} \quad (t < 0)\,. \tag{154}$$

Note that $u^* = u(0)$ is the expansion parameter of renormalized perturbation theory in the low temperature phase.

$$\Gamma_c(t) = \frac{\chi(t)}{\xi_{2\mathrm{nd}}^3(t)m^2(-t)} \quad (t > 0)\,. \tag{155}$$

(Notice the factor of three between the definitions of Γ_c and u). While Γ_c mixes low and high temperature observables, u only contains quantities evaluated in the low temperature phase. Note that the critical exponent of the combined quantities is always zero.

One can also define universal amplitude combinations that include amplitudes defined by power laws with a magnetic field at the critical temperature $m \sim h^{1/\delta}$. These will not be discussed here. Also, quantities defined by the effective potential in both phases will not be discussed here. For a discussion and numerical results, see, e.g., Ref. 23 (see in particular their Table XIV and their Appendix B).

Furthermore, one can define universal amplitude ratios that are related to interface properties and the dimensional cross-over. These problems will be discussed in detail in Secs. 6 and 7.

Various other cross-over phenomena and their universal properties are discussed in the literature. For the cross-over from mean-field behavior to the Wilson–Fisher fixed point, see, e.g., Refs. 167–170.

5.1. *Monte Carlo results*

In this subsection, we shall briefly discuss the numerical results of Refs. 48 and 49.

In Ref. 48, we have simulated the three-dimensional Ising model at $\beta = 0.2391$, 0.23142, 0.2275, 0.2260, 0.2240 and 0.22311 in the low temperature phase and at $\beta = 0.20421$, 0.21189, 0.21581, 0.21731, 0.21931 and 0.22020 in the high temperature phase. The β-values were chosen such that for each β-value in the low temperature phase, there is a β-value in the high temperature phase with $(\beta_{\text{low}} + \beta_{\text{high}})/2 = 0.221655 \approx \beta_c$. The lattice sizes range from 30^3 to 120^3 in the low temperature phase and from 20^3 to 100^3 in the high temperature phase. In the low temperature phase, we used the canonical demon update with multi-spin coding for the simulation, and in the high temperature phase, we used the single cluster algorithm. The reason for using the local algorithm in the low temperature phase was that there is no advantage from the cluster improved estimator and the correlation length that was reached is still moderate: $\xi_{\text{exp}} \approx 6.2$ for $\beta = 0.22311$ (and therefore the autocorrelation time of the local algorithm is not too large). Hence, we should profit from the fast execution of the multi-spin coding implementation.

We have measured the energy density E, the magnetic susceptibility χ, the second moment correlation length ξ_{2nd} and the exponential correlation length in both phases. In the low temperature phase, we measured, in addition, the magnetization m. Analyzing the low temperature simulation, one has to take into account the problems of finite system versus symmetry breaking as discussed in Sec. 2.1.

In a first step of the study, we determined the ratio L/ξ that is needed to reach the thermodynamic limit with the desired accuracy (i.e., the deviation from the thermodynamic limit is much smaller than the statistical errors of the quantities). It turned out that in the high temperature phase, $L/\xi > 6$ is sufficient, while in the low temperature phase, much larger lattice sizes are needed. We had chosen $L/\xi \approx 20$ in the low temperature phase.

Our numerical results are summarized in Table 14 for the low temperature phase and in Table 15 for the high temperature phase.

These numbers can be directly compared with other Monte Carlo results and also with low and high temperature series expansions.

In Ref. 92, the magnetization of the Ising model on a simple cubic lattice in the low temperature phase was computed by Monte Carlo simulation. The authors find that their data are well described by the following empirical approximation:

$$m(t) = t^{0.32694109}(1.6919045 - 0.34357731\, t^{0.50842026} - 0.42572366\, t)\,, \qquad (156)$$

with $t = (\beta_c - \beta)/\beta$. It turns out that our data are compatible with this formula. Note that our estimates for the magnetization are, in general, more precise than those reported in Ref. 92 (where however a much larger number of β-values was studied).

The authors of Ref. 171 give Monte Carlo results for the second moment correlation length in the low temperature phase. Their β-values match with ours for $\beta = 0.2260$ and 0.2240, where they find $\xi_{\text{2nd}} = 3.22(1)$ and $\xi_{\text{2nd}} = 4.61(6)$, respectively. Note that the results of Ref. 171 were obtained with $L \approx 4.7\xi$ and $L \approx 7.8\xi$ for $\beta = 0.226$ and $\beta = 0.224$, respectively.

Table 14. Results in the low temperature phase. The table is taken from Ref.48.

β	L	m	$E/3$	$\xi_{\rm exp}$	$\xi_{\rm exp}$	χ
0.2391	30	0.667162(20)	0.553732(17)	1.2851(15)	1.2335(15)	4.178(3)
0.23142	40	0.570306(16)	0.478046(12)	1.8637(45)	1.8045(21)	9.394(4)
0.2275	50	0.491676(14)	0.430364(10)	2.578(7)	2.5114(31)	18.706(10)
0.2260	80	0.449984(16)	0.409609(4)	3.103(7)	3.0340(32)	27.596(11)
0.2240	100	0.372490(10)	0.378612(3)	4.606(13)	4.509(6)	61.348(34)
0.22311	120	0.320830(10)	0.362946(2)	6.208(18)	6.093(9)	112.60(7)

Table 15. Results in the high temperature phase. The table is taken from Ref. 48. stat gives the statistics. The first number is the number of measurements and the second, the number of single clusters per measurement.

β	L	stat	$\xi_{\rm exp}$	$\xi_{\rm 2nd}$	$E/3$	χ
0.20421	20	50000×500	2.363(1)	2.346(1)	0.262928(49)	25.255(16)
0.21189	30	50000×500	3.477(2)	3.465(2)	0.284663(35)	52.09(4)
0.21581	40	50000×500	4.864(3)	4.854(3)	0.298366(28)	98.90(10)
0.21731	50	50000×800	5.892(3)	5.885(3)	0.304493(20)	143.04(12)
0.21931	80	50000×1000	8.766(5)	8.760(5)	0.313849(14)	308.58(31)
0.22020	100	50000×1200	11.884(9)	11.877(7)	0.318742(11)	557.57(61)

The results in the high temperature phase can be compared with those of Ref. 172. They report Monte Carlo results for the second moment correlation length and the magnetic susceptibility. Interpolation of their results, using a power law ansatz, to our β-values leads to results consistent with ours. One has to note, however, that our statistical errors are at least three times smaller than those of Ref. 172, in the common β-range.

In the previous section, we have already discussed the comparison of the correlation length with IDA's (inhomogeneous differential approximants) of low temperature series. In Ref. 48, we in addition computed double biased IDA's for the magnetization and the magnetic susceptibility. The IDA was biased with the value of $\beta_c = 0.2216544$ and the value of the exponent. The coefficients of the low temperature series were taken from Ref. 173. We find that for $\beta = 0.2391$, the results from the series is more accurate than our Monte Carlo result for the magnetization as well as the magnetic susceptibility. For the β values closer to β_c, the Monte Carlo results are more accurate. In all cases, the Monte Carlo result and the double biased IDA's of the low temperature series are consistent (for details, see Tables 7 and 8 of Ref. 48).

In Ref. 49, we have measured only the energy density and the specific heat. We performed simulations of the standard Ising model in three dimensions on the simple cubic lattice. At $\beta = 0.2216544$ (which was the best estimate of β_c at the time), we have simulated lattices of size 12^3 up to 112^3. These simulations were performed with the single cluster algorithm, interleaved with a Metropolis sweep. The numerical results are summarized in Table 1 of Ref. 49. Furthermore,

we simulated the model in the low and the high temperature phase on lattices that are sufficiently large to give, with good accuracy, thermodynamic limit results. The numerical results are summarized in Table 4 of Ref. 49.

5.2. *Analysis of the data*

One way to compute the amplitude ratios is to extract first the amplitudes from fitting the data with the power laws (e.g., Eq. (147)) and then just taking the ratio of the resulting numbers. It turns out that the value of the amplitudes depend much on the value of the exponents that is plugging into the power law. Hence, the uncertainty of the estimates of the exponents induce a considerable error in the estimates of the amplitudes (this problem is reduced to some extend now, since the error-bars for the critical exponents became smaller after Ref. 48 was published).

However, the problem can be eliminated completely by computing $\Gamma_\chi(t)$ for finite t first. This way $t^{-\gamma}$ cancels. The remaining problem is to deal with corrections to scaling. In Ref. 48, we used an ansatz with leading nonanalytic and analytic corrections to extract C_+/C_- from our numerical data:

$$\Gamma_\chi(|\beta - \beta_c|) = \frac{C_+}{C_-} + a_0|\beta - \beta_c|^\theta + a_1|\beta - \beta_c| \,. \tag{157}$$

We used $\theta = 0.51(3)$ as numerical value for the correction exponent. We included all data except for the pair $\beta = 0.2391$ and $\beta = 0.20421$ in the fit. The result is shown in Fig. 6. Our final estimate (that includes the error due to the uncertainty of θ) is:

$$\frac{C_+}{C_-} = 4.75(3) \,. \tag{158}$$

We analyzed the second moment correlation length in the same way. The fit is shown in Fig. 7. Our final result for the amplitude ratio is:

$$\frac{f_+}{f_-} = 1.95(2) \,. \tag{159}$$

The coupling constant u is computed only from quantities in the low temperature phase. Therefore, no analytic correction proportional to t appears. We fitted the data with

$$u(t) = u^* + a_0 t^\theta \,. \tag{160}$$

The fit is given in Fig. 8. Our final result for u^* is:

$$u^* = 14.3(1) \,. \tag{161}$$

In addition, we have obtained in Ref. 48,

$$\frac{C_+}{f_{+,\,2\mathrm{nd}}^3 B^2} = 3.05(5) \,. \tag{162}$$

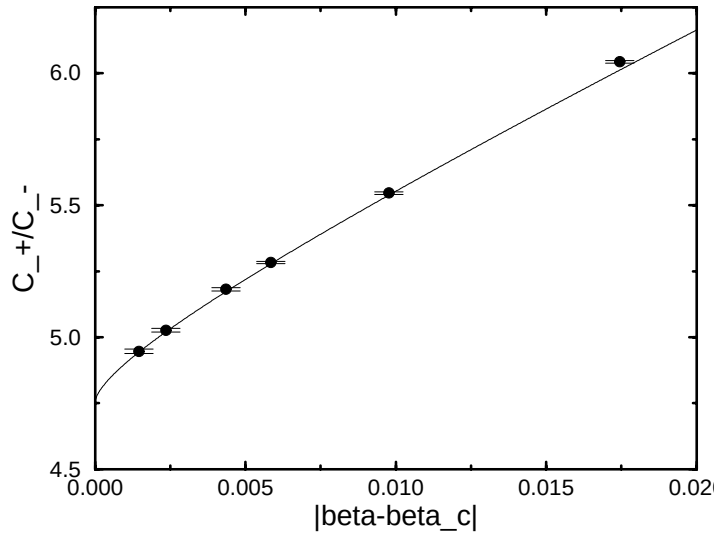

Fig. 6. Fit of Γ_χ with the ansatz (157).

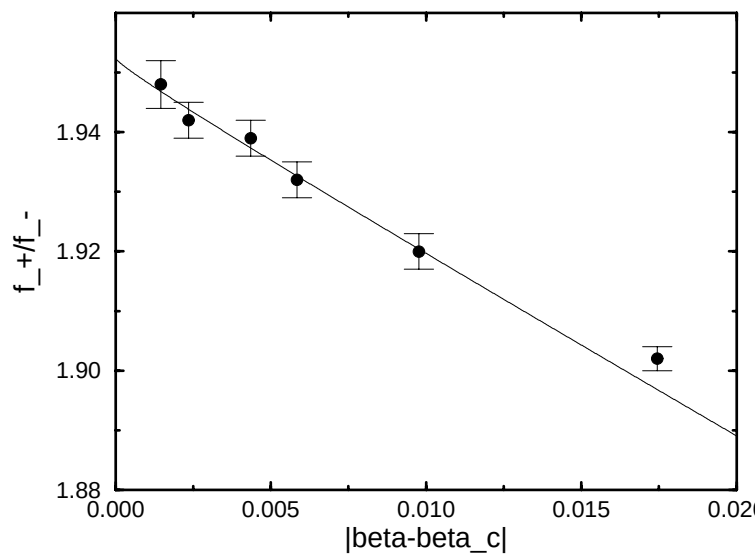

Fig. 7. Fit of $\Gamma_{\xi_{2\mathrm{nd}}}$ with the analogue of ansatz (157).

In Ref. 49, we focussed on quantities related with the energy. The major technical problem is to separate the singular part of the energy density and the specific heat from the analytic background. In the Ising universality class, $\alpha \approx 0.11 > 0$ and therefore the singular part of the specific heat

$$C_s \simeq A_\pm |t|^{-\alpha}\,, \tag{163}$$

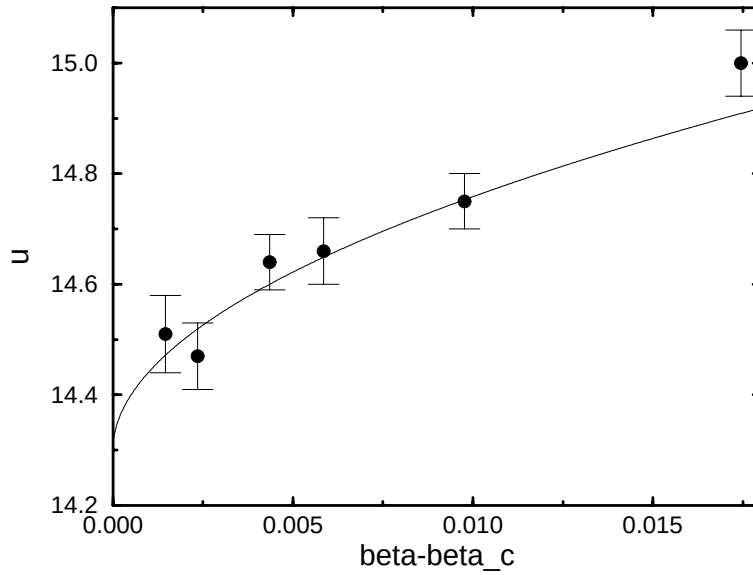

Fig. 8. Fit of $u(\beta - \beta_c)$ with the ansatz (160).

will dominate as T_c is approached and the lattice size is sent to infinity. A_+ and A_- denote the amplitudes of the singular part in the symmetric ($t > 0$) and broken ($t < 0$) phase, respectively. α is the specific heat exponent. However, for the limited lattice sizes that can be accessed in Monte Carlo simulations, it is important to take the analytic part of the specific heat into account.

Let us start the discussion by considering the (reduced) free energy density:

$$f = f_{ns} + f_s \,, \tag{164}$$

where f_{ns} is the analytic, nonsingular part of the free energy density and f_s the singular part (that encodes the critical behavior) of the free energy density. Renormalization group arguments lead to the following finite-size scaling ansatz for the singular part of the free energy density for lattices with periodic boundary conditions[11]

$$f_s \xi^d \sim g_\pm \left(\frac{\xi}{L} \right) , \tag{165}$$

where f_s is taken in the finite volume, while ξ is the correlation length defined in the thermodynamic limit. $g(\xi/L)$ is a universal function. The analytic part f_{ns} is only a function of t and not of L (up to corrections that are exponentially suppressed in L). In the following, we discuss the two extremal cases of the thermodynamic limit and the finite-size scaling exactly at the critical point.

The thermodynamic limit is characterized by $\xi/L = 0$. Inserting the scaling ansatz $\xi \sim t^{-\nu}$ into Eq. (165) for $\xi/L = 0$, we obtain

$$f_s \sim |t|^{d\nu} \,. \tag{166}$$

Here, we use $t = (\beta - \beta_c)/\beta_c$. By differentiation with respect to β, we arrive at:

$$E_s \sim |t|^{d\nu-1}\,, \tag{167}$$

and

$$C_s \sim |t|^{d\nu-2}\,. \tag{168}$$

The last equation implies the hyperscaling relation $\alpha = 2 - d\nu$.

In order to discuss finite-size scaling at the critical point, it is useful to re-parametrize Eq. (165) as:

$$f_s L^d \simeq h_\pm\left(\frac{L}{\xi}\right), \tag{169}$$

with $h(L/\xi) = (L/\xi)^d\, g(\xi/L)$. Inserting the power law $\xi \sim t^{-\nu}$, we obtain

$$f_s \simeq L^{-d}\tilde{h}(L^{1/\nu}t)\,. \tag{170}$$

Note that on a finite lattice, f_s is an analytic function. Therefore, h is, also at $t = 0$, an analytic function.

By differentiation with respect to β,

$$E_s \simeq \frac{L^{-d+1/\nu}\tilde{h}'(L^{1/\nu}t)}{\beta_c}\,, \tag{171}$$

and

$$C_s \simeq \frac{L^{-d+2/\nu}\tilde{h}''(L^{1/\nu}t)}{\beta_c^2}\,. \tag{172}$$

For the critical temperature $t = 0$, this means

$$E_s \sim L^{-d+1/\nu}\,, \tag{173}$$

and

$$C_s \sim L^{-d+2/\nu}\,. \tag{174}$$

In our numerical study, we approximated the analytic (nonsingular) part of the free energy density by its Taylor expansion, truncated at the second order

$$f_{ns} \simeq F_{ns} - E_{ns}(\beta - \beta_c) - \frac{1}{2}\,C_{ns}(\beta - \beta_c)^2\,, \tag{175}$$

where F_{ns}, E_{ns} and C_{ns} are the nonsingular parts of the free energy density, the energy density and the specific heat at the critical point, respectively.

First, we analyzed our data obtained at β_c. We fitted the data for $\beta = 0.2216544$ with the ansatz

$$E = E_{ns} + \mathrm{const}_E\, L^{-d+1/\nu}\,, \tag{176}$$

and

$$C = C_{ns} + \mathrm{const}_C\, L^{-d+2/\nu}\,. \tag{177}$$

A combined fit of the energy and the specific heat, with a minimal lattice size $L_{\min} = 20$ included, gives $\nu = 0.6308(10)$, $\text{const}_E/3 = 0.7431(52)$, $E_{ns}/3 = 0.330209(8)$, $\text{const}_C = 14.58(66)$ and $C_{ns} = -11.12(76)$. In addition, there should be systematical errors since corrections to scaling have not been taken into account. Including a term $L^{-\omega}$ into the ansatz enlarges the statistical errors for the quantities we are interested in considerably. Therefore, we took the pragmatic point of view that the good agreement of the result for ν with the best estimates from the literature indicates that corrections to scaling are small and that one can therefore assume that the systematic errors of E_{ns} and C_{ns} are also small. For details of the fit procedure, see Ref. 49.

Next, we analyzed the data for the thermodynamic limit. Here, we have used the ansatz

$$E = E_{ns} - C_{ns}\beta_c t \mp A_{\pm}\beta_c \frac{|t|^{1-\alpha}}{1-\alpha}\,, \tag{178}$$

which is obtained by integration of the specific heat. Here, we tried various things. In a first attempt, we used E_{ns} and C_{ns} as free parameters. Then, we fixed E_{ns} and C_{ns} by the results obtained at β_c. We also tested the two versions of the reduced temperature $t = (T - T_c)/T_c$ and $t = (\beta_c - \beta)/\beta_c$.

Depending on the precise procedure, we arrive at different results for A_+ and A_-, and also for the universal ratio.

With $t = (T - T_c)/T_c$ and E_{ns} and C_{ns} as free parameters, we arrive at:

$$\frac{A_+}{A_-} = 0.567(16)\,. \tag{179}$$

With $t = (\beta_c - \beta)/\beta_c$ and E_{ns} and C_{ns} as free parameters, we arrive at:

$$\frac{A_+}{A_-} = 0.550(12)\,. \tag{180}$$

Using the results for E_{ns} and C_{ns} from finite-size scaling at T_c, we arrive at:

$$\frac{A_+}{A_-} = 0.560(10)\,. \tag{181}$$

Note that in the last case, the choice of t plays virtually no role, since only data with small t are included into the fit. The scattering of the results gives us an idea of the systematic errors.

We also tried to extract the numerical value of $Q_{\pm} = -f_s\xi^d$ in both phases of the model. The values for the second moment correlation length ξ_{2nd} are taken from Ref. 48.

The estimates for f_s at given β-values were obtained in the following way: we took $E - E_{ns} - C_{ns}(\beta - \beta_c)$ as an approximation of the singular part of the energy. The constants E_{ns} and C_{ns} were taken from the combined energy and specific heat fit at the critical point. Then, we computed f_s as the integral over β of the singular part of the energy. We interpolated the singular part of energy for β-values

not simulated with the scaling ansatz, where we have used $\nu = 0.6308$ and the amplitude was computed from the closest β-value simulated.

In both phases, we just have results for two β-values. Since the results of these two β-values nicely agree, we regard the results

$$Q_+ = 0.1065(45)\,, \tag{182}$$

for the high and

$$Q_- = 0.0255(6)\,, \tag{183}$$

for the low temperature phase as reliable estimates for the critical limits. Note the factor of three compared with Ref. 49. There, the free energy per link is considered, while here, following Eq. (20), the free energy per lattice site is taken.

5.3. *Comparison with other theoretical and experimental results*

In Tables 16 and 17, we have summarized results for universal amplitude ratios and combinations obtained by various theoretical methods and experiments. For further quantities, see Table XIV of Ref. 23.

Table 16. Estimates of the universal amplitude ratios by various approaches. The experimental data are taken from Ref. 149, unless otherwise stated. *ms* denotes a magnetic system; *bm* a binary mixture; *lv* a liquid–vapor transition in a simple fluid. For values marked with an asterisk, the error is not quoted explicitly in the reference. For a discussion of the numbers, see the text.

	A_+/A_-	Ref.	C_+/C_-	Ref.	f_+/f_-	Ref.
MC	0.560(10)	49	4.75(3)	48	1.95(2)	48
	0.550(12)	49	4.72(11)	174	2.06(1)	176
	0.567(16)	49				
IHT–PR	0.530(3)	23	4.77(2)	23	1.961(7)	23
HT, LT	0.523(9)	165	4.762(8)	99	1.963(8)	99
	0.51*	177	4.95(15)	165	1.96(1)	165
			5.01*	164	1.96*	164
ϵ-exp.	0.527(37)	103	4.73(16)	103	1.91*	183
	0.524(10)	181, 182	4.9*	181		
			4.8*	183, 184		
$d = 3$ exp.	0.537(19)	103	4.79(10)	103	2.013(28)	188, 189
	0.540(11)	186	4.77(30)	187		
	0.541(14)	187	4.72(17)	188, 189		
Experiments						
bm	0.56(2)		4.4(4)		1.93(7)	
lv	0.50(3)		4.9(2)			
ms	0.51(3)		5.1(6)		1.92(15)	
lv	0.53^{+8}_{-7}	119				
lv	0.538(17)	120				
ms			4.6(2)	136		

Table 17. Estimates of the universal amplitude combinations by various approaches. The conventions are the same as in Table 16. The universal quantity $R_\pm$ is related to $Q_\pm$ defined in Eq. (153) by $R_\pm = \alpha(1-\alpha)(2-\alpha)Q_\pm$.

	u^*	Ref.	R_+	Ref.	R_-	Ref.
MC	14.3(1)	48	0.0197(8)	49	0.00472(11)	49
IHT–PR			0.01880(8)	23	0.00471(5)	23
HT, LT	14.25(12)	114	0.0202(9)	180	0.00477(20)	158
	14.13(15)	178, 179	0.01880(15)	165		
ϵ-exp.			0.0197*	185, 182		
$d = 3$ exp.	14.2*	188, 189	0.01968(15)	190		
Experiments						
lv			0.0174(32)	121		
lv			0.023(4)	119		

Universal amplitude ratios have been computed with the ϵ-expansion (ϵ-exp.), perturbation theory in three dimensions ($d = 3$ exp.) and by the combination of high and low temperature series expansions of the three-dimensional Ising model on simple cubic, body centered cubic, and face centered cubic lattices (HT, LT). In Ref. 158, a review of low and high temperature series results is given. In Ref. 165, details of the analysis are discussed.

The most accurate results, for many amplitude ratios, come from Ref. 23. Their results are based on high temperature series expansions of the ϕ^4 theory and the spin-1 Ising model. As already discussed in the section on critical exponents, the values of $\lambda_{\rm opt}$ and $D_{\rm opt}$ from Monte Carlo are an important ingredient in their work. Information on the low temperature phase can be obtained from the high temperature phase by the "Griffith's analyticity" of the "equation of state". The equation of state is the function $h(m,t)$, where h is the external field, m the expectation value of the magnetization and t the reduced temperature. Griffith's analyticity means that this function is regular at $m = 0$ for $t > 0$ (high temperature phase) and at $t = 0$ for $m > 0$ fixed. In practice, this is exploited by a parametric representation of the equation of state. Hence, the abbreviation IHT–PR. For the details of the analysis, see Sec. VII of Ref. 23.

There exist also a number of experimental results from systems that are supposed to share the Ising universality class. The experimental results come from different systems such as binary mixtures (bm), liquid–vapor (lv) and uniaxial magnetic systems (ms).

Let us first discuss the Monte Carlo (MC) results of other authors. In Ref. 174, the SU(2) gauge theory at finite temperature was studied. Following the conjecture of Svetitsky and Yaffe,[175] it shares the Ising universality class. The nice agreement of their result for C_+/C_- with our Monte Carlo result for the Ising model and the result of Ref. 23 is the further confirmation of this conjecture.

Ruge, Zhu and Wagner[176] also simulate the standard Ising model on three-dimensional lattice. Their result for f_+/f_- is by 5 standard deviations larger than

our Monte Carlo result. It seems likely that systematical errors in the study of Ref. 176 cause this discrepancy. However, it was not possible to pin-point the problem from the data they provide in their paper.

In general, the results from the different approaches show a reasonable agreement. For most universal quantities that are listed in Tables 16 and 17, the most accurate result is given by Ref. 23. Our Monte Carlo results for C_+/C_- and f_+/f_- are in nice agreement with Ref. 23 and the error-bars are only slightly larger. In the case of u^*, our result is still the most accurate. In contrast, our values for A_+/A_- have considerably larger statistical errors and are too large compared with that of Ref. 23. For A_+/A_-, one would like to redo the simulations with an improved action.

The results for f_-/f_+ from ϵ-expansion and 3D perturbation theory are puzzling. They are considerably too small and too large, respectively.

The results from experiments are less precise than the best theoretical estimates. Still, the good agreement of the experimental results for A_+/A_- and C_+/C_- (which have a reasonable small error), among each other and with the theory, is a nice confirmation of universality.

6. Interfaces

Below the mixing temperature, the two components of a binary mixture separate and an interface between the two components forms.

Interfaces can be studied within the Ising model or the one component ϕ^4 (Landau–Ginzburg) model in the low temperature phase. By suitable boundary conditions, one part of the system is forced into the phase with positive magnetization, while the other part is forced to negative magnetization. An interface forms between the two phases.

Let us consider an interface perpendicular to the three-axis. One possible boundary condition is to set the spins at $x_3 = 1$ to -1 and at $x_3 = L_3$ to $+1$. Another type of boundary conditions are the so-called anti-periodic boundary conditions. Here, $J_{\langle xy\rangle} = -1$ for $x_3 = L_3$, $y_3 = 1$ and $J_{\langle xy\rangle} = 1$ else. For an illustration, see Fig. 9.

Macroscopically, an interface is characterized by the interface tension. The interface tension is the free energy per area that is needed to create the interface.

Interfaces in the Ising model and the ϕ^4 theory have been studied by various theoretical methods, such as low temperature series expansion,[191–193] ϵ-expansion,[194] perturbation theory in three dimensions[195–197] and Monte Carlo simulations. For reviews, see, e.g., Refs. 55 and 56. A large number of articles on the subject can be found in Ref. 198. In the following, we will focus on Monte Carlo simulations.

An interface on a (001)-plane in the standard Ising model on the simple cubic lattice undergoes a so-called roughening transition at $\beta_R = 0.40758(1)$,[199] which is almost twice β_c. At low temperatures, the interface is in the so-called "smooth" phase. This means that the interface is rough only on small (length) scales, but is

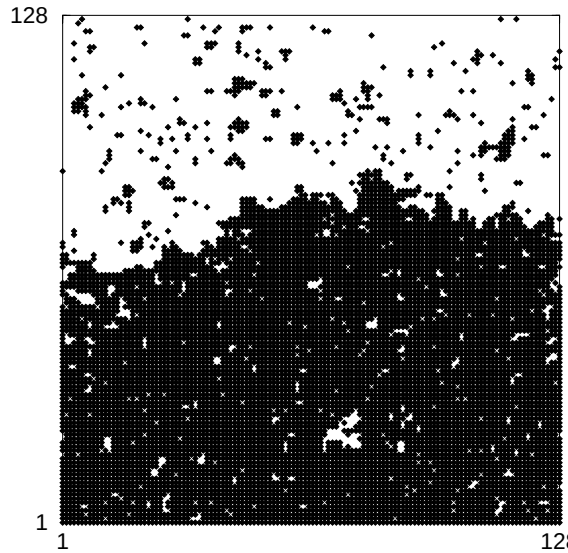

Fig. 9. An equilibrium configuration of the two-dimensional Ising model at $\beta = 0.48$ (low temperature phase) on a 128×128 lattice with anti-periodic boundary conditions in y-direction. $s_x = 1$ is illustrated with black and $s_x = -1$ with white. The upper part of the lattice is dominted by negative magnetization and the lower part by positive magnetization. In-between, an interface is formed.

smooth on large scales. Above the roughening temperature, in the "rough" phase, the interface is rough on all scales. The roughening transition is of the Kosterlitz–Thouless (KT)[200] type.

In order to improve the understanding of interfaces, one considers two-dimensional interface (or surface) models. One assumes that atoms pile up above some reference plane. The interface is then characterized by the height (of the pile) above the reference plane.

Such models are called SOS (solid on solid) models. In the literature, many types of SOS models are discussed. Various SOS models differ in their action. For example, the action of the ASOS (absolute value SOS) model and the DGSOS (Discrete Gaussian SOS) are given by:

$$S_{\mathrm{ASOS}} = K \sum_{\langle xy \rangle} |h_x - h_y| \,, \quad S_{\mathrm{DGSOS}} = K \sum_{\langle xy \rangle} (h_x - h_y)^2 \,, \tag{184}$$

where h_x is integer.

In the sine-Gordon model, the field variable is a real number. This is more suitable for a field-theoretic study of the model. The periodicity perpendicular to the interface is taken into account by a periodic potential. The action of the sine-Gordon model on the square lattice is given by:

$$S_{\mathrm{SG}} = K \sum_{\langle xy \rangle} (\phi_x - \phi_y)^2 + z \sum_x \cos(2\pi\phi_x) \,. \tag{185}$$

SOS models and the sine-Gordon model undergo a roughening transition. The strongest support for the fact that the roughening transition is of the Kosterlitz–Thouless[200] type comes from the exact solution of the so-called body centered solid on solid (BCSOS) model.[19,201,202] Note also that SOS models are related to XY models via the duality transformation.[203]

In this review, we will focus on universal properties of interfaces close to the bulk transition temperature. In the rough phase (and in particular close to the bulk transition temperature), the periodicity of the potential is irrelevant (in the sense of the RG). Therefore, the large scale properties of the interface are well described by a vanishing periodic potential. At the transition temperature, the rotational symmetry is restored. Therefore, the angle between the interface and the lattice planes does not matter.

Below, we will first discuss the RG-behavior of the interface tension. Then, we will summarize results for the capillary wave model (this is an effective interface model). Next, we will review the numerical results for the interface tension obtained in Refs. 58, 60–62. Finally, we briefly discuss the magnetization profile and the width of the interface.

6.1. *The interface tension and the RG*

Above, we have already explained that the interface tension is the difference of the free energy of a system with an interface and a system without an interface, divided by the interface area. Let us be more precise: let us consider a system with anti-periodic boundary conditions in three-direction. Then, the (reduced) interface tension is defined as:

$$\sigma := \lim_{L_3\to\infty} \lim_{L_1=L_2\to\infty} -\frac{\ln Z_a - \ln Z_p}{L_1 L_2}\,. \tag{186}$$

Z_a is the partition function with anti-periodic and Z_p the partition function with periodic boundary conditions (appropriate Dirichlet boundary conditions can also be used in the definition). Note that the limit $L_1 = L_2 \to \infty$ has to be taken, at finite L_3, first, to ensure that only a single interface is present. The transformation of σ under RG-transformations can be seen directly from Eq. (186). The partition functions are conserved under RG-transformations. The area $L_1 L_2$ is trivially rescaled by a factor b^{-2}, where b is the scale factor of the RG-transformation. Therefore, $\sigma' = b^2\sigma$. Since the correlation length transforms as $\xi' = b^{-1}\xi$, the combination

$$R = \sigma\xi^2\,, \tag{187}$$

is RG-invariant and therefore universal in the neighborhood of the transition (this applies to the second moment correlation length $\xi_{\rm 2nd}$ as well as the "true" correlation length $\xi_{\rm exp}$). The determination of R is one of the major tasks of the numerical studies to be discussed below. The interface tension behaves in the neighborhood

of the transition temperature as:

$$\sigma \simeq \sigma_0 t^{\mu}\,, \tag{188}$$

with $t = (T_c - T)/T_c$. From Eq. (187), we read off: $\mu = 2\nu$ (Widoms scaling law, Ref. 204).

6.2. *Finite size effects*

In Monte Carlo studies of interfaces, one is restricted to rather small system sizes. Therefore, accurate knowledge of the finite system behavior of the interface free energy is needed. In the following discussion, we will focus on a lattice with periodic boundary conditions in one and in two-direction and anti-periodic boundary conditions in three-direction.

6.2.1. *Effects of a finite* L_3

Let us first discuss the dependence on L_3 in Eq. (186). Our starting point is the phenomenological picture that the creation of an interface at a fixed location requires the interface free energy F_I (the dependence of F_I on L_1 and L_2 will be discussed below in the section on the capillary wave model). Furthermore, we assume that the interfaces are dilute and that we therefore can ignore interactions among interfaces. In the Ising model with anti-periodic boundary conditions, there can be an odd number of interfaces (at least one is forced into the system by the boundary conditions). With periodic boundary conditions, there can be an even number of interfaces. This leads to the result[58]:

$$\tanh(\exp(-F_I + \ln L_3)) = \frac{Z_a}{Z_p}\,. \tag{189}$$

For large F_I (corresponding to a large area $L_1 L_2$), only one interface is present in the system with anti-periodic boundary conditions and no interface in the system with periodic boundary conditions. Equation (189) reduces to:

$$F_I = \ln Z_p - \ln Z_a + \ln L_3\,. \tag{190}$$

Note that the term $\ln L_3$ stems from the fact that the interface can take any position in three-direction.

An interface has a certain intrinsic width. L_3 has to be larger than this intrinsic width so that Eqs. (189) and (190) hold. Further information on the dependence of Z_a/Z_p on L_3 at fixed L_1, L_2 can be obtained from the transfer matrix T.

The anti-periodic boundary conditions are represented by a spin-flip matrix P, which flips the sign of all spins in a three-slice.

The partition function of the periodic system and the anti-periodic system are given by:

$$Z_p = \mathrm{Tr}\, T^{L_3} \quad \text{and} \quad Z_a = \mathrm{Tr}\, T^{L_3} P\,. \tag{191}$$

Since matrices T and P commute, they have a common set of eigenfunctions. The eigenvalues of T are λ_i and those of P are p_i. The possible values of p_i are 1 and -1. Eigenstates of T that are symmetric in the magnetization have $p_i = 1$ and those that are anti-symmetric have $p_i = -1$. The partition functions take the form

$$Z_p = \sum_i \lambda_i^{L_3} \quad \text{and} \quad Z_a = \sum_i \lambda_i^{L_3} p_i \,. \tag{192}$$

Let us briefly discuss the spectrum of the transfer matrix in the low temperature phase. For sufficiently large L_1 and L_2, we have

$$\lambda_{0s}, \lambda_{0a} \gg \lambda_{1s}, \lambda_{1a}, \ldots \,, \tag{193}$$

where the subscript s indicates that the state is symmetric and a indicates that the state is anti-symmetric.

$$\xi_t = \frac{-1}{\ln(\lambda_{0a}/\lambda_{0s})} \,, \tag{194}$$

is the so-called "tunneling" correlation length. On a cylinder of infinite length regions of positive and negative magnetization interchange. The tunneling correlation length is a measure for the extension of this regions. The "bulk" correlation length is given by:

$$\xi = \lim_{L_1=L_2\to\infty} \frac{-1}{\ln(\lambda_{1s}/\lambda_{0s})} = \lim_{L_1=L_2\to\infty} \frac{-1}{\ln(\lambda_{1a}/\lambda_{0s})} \,. \tag{195}$$

Ignoring terms of $O[(\lambda_{1s}/\lambda_{0s})^{L_3}]$, we find

$$\left(\frac{\lambda_{0a}}{\lambda_{0s}}\right)^{L_3} = \frac{Z_p - Z_a}{Z_p + Z_a} \,. \tag{196}$$

Now, it is easy to make contact with Eq. (189):

$$\begin{aligned} \frac{Z_a}{Z_p} &= \frac{1 - (\lambda_{0a}/\lambda_{0s})^{L_3}}{1 + (\lambda_{0a}/\lambda_{0s})^{L_3}} \\ &= \frac{(\lambda_{0a}/\lambda_{0s})^{-L_3/2} - (\lambda_{0a}/\lambda_{0s})^{L_3/2}}{(\lambda_{0a}/\lambda_{0s})^{-L_3/2} + (\lambda_{0a}/\lambda_{0s})^{L_3/2}} \\ &= \tanh\left(L_3 \frac{-\ln(\lambda_{0a}/\lambda_{0s})}{2}\right) . \end{aligned} \tag{197}$$

Hence, we can identify

$$F_I = -\ln\left(\frac{-\ln(\lambda_{0a}/\lambda_{0s})}{2}\right) = \ln(2\xi_t) \,, \tag{198}$$

which provides an alternative definition of the interface free energy. For a more general discussion of the relation of the spectrum of the transfer-matrix and the interface free energy, see Ref. 205.

We have ignored terms of order $O[(\lambda_{1s}/\lambda_{0s})^{L_3}]$. Hence, the bulk correlation length $\xi = -1/\ln(\lambda_{1s}/\lambda_{0s})$ has to be small compared with L_3.

6.2.2. *Capillary wave model: Effects of a finite interface area $L_1 \times L_2$*

Let us first discuss the constraints that are imposed by the renormalization group on F_I. Let us start from Eq. (198). Under an RG-transformation, $L_1' = b^{-1}L_1$, $L_2' = b^{-1}L_2$ and $\xi_t' = b^{-1}$. *A priori*, F_I is a function of L_1, L_2 and β. β can be traded in for the interface tension σ. Writing F_I as a function of RG-invariant arguments, we obtain

$$F_I = \ln \xi + \tilde{F}_I \left(\sigma\, L_1 L_2, \frac{L_1}{L_2} \right). \tag{199}$$

Note that the term $\ln \xi$ comes from the transformation of ξ_t under RG-transformations.

Information on the functional form of $\tilde{F}_I$ can be obtained, e.g., from perturbation theory in three dimensions, see Refs. 195 and 196. Here, we will summarize the results obtained from an effective model of the interface, the so-called capillary wave model (CWM).[206] In the literature, this model is also known as Drumhead model. For a derivation of this interface model from the three-dimensional ϕ^4 theory using perturbation theory, see Ref. 208.

The capillary wave model assumes that the interface position is given by a unique height ϕ_{x_1,x_2} above some reference plane. This implies that the effective model ignores handles and overhangs of the interface (obviously, also bubbles in the bulk phases are ignored). The action is proportional to the area of the interface:

$$S = \sigma A\,. \tag{200}$$

This particular action is also called Nambu–Goto action. The motivation for this action is that close to the transition, the translational and rotational symmetries are restored. Hence, the effective action should satisfy these symmetries.

Here, σ is a parameter of the effective interface model. In the following, we start with a continuum formulation of the model. This means that the height ϕ_{x_1,x_2} is given for any $(x_1, x_2) \in [0, L_1) \times [0, L_2)$. The interface area is then given by:

$$A = \int_0^{L_1} dx_1 \int_0^{L_2} dx_2 \sqrt{1 + \left(\frac{\partial \phi}{\partial x_1}\right)^2 + \left(\frac{\partial \phi}{\partial x_2}\right)^2}\,. \tag{201}$$

In order to solve the problem, we have to Taylor-expand the action:

$$A = \int_0^{L_1} dx_1 \int_0^{L_2} dx_2 \left[1 + \frac{1}{2}(\nabla\phi)^2 - \frac{1}{8}((\nabla\phi)^2)^2 + \cdots \right]. \tag{202}$$

Note that, to leading order, we obtain the exactly solvable, mass-less Gaussian model:

$$S_G = \sigma \int dx_1 \int dx_2 (\nabla \phi_{x_1,x_2})^2\,, \tag{203}$$

which is the continuous version of the action (185) with $z = 0$. At the Gaussian fixed point, the dimension of an operator is given by naive dimensional analysis.

Higher powers of $(\nabla\phi)^2$ are irrelevant. They just give corrections to the Gaussian results.

Therefore, let us first summarize the results that can be derived from the purely Gaussian action. In order to obtain finite results, a regularization is needed, e.g., a lattice (see Appendix B), or more elegantly, the ζ-function regularization. In addition, the average position of the interface has to be fixed to obtain a finite result. In momentum space, this means that the integration over the zero-mode is omitted. For the discussion of the numerical results, we have to keep this in mind.

For the Monte Carlo simulation, we are most interested in the case of periodic boundary conditions. In the literature,[209–211] the solution for the partition function of the Gaussian model with periodic boundary conditions is given as a function of the ratio L_1/L_2:

$$Z_G(u) = \frac{1}{\sqrt{u}} \left| \frac{\eta(iu)}{\eta(i)} \right|^{-1} , \tag{204}$$

where η is the Dedekind eta-function

$$\eta(\tau) = q^{1/24} \prod_{n=1}^{\infty} (1 - q^n) , \quad q := \exp(2\pi i \tau) , \tag{205}$$

where $\tau = iu$; $u = L_2/L_1$. The normalization is chosen such that $Z_G(1) = 1$.

In the partition function of the interface, we also have to take into account the classical contribution:

$$\exp(F_I) = Z_I = c \exp(\sigma L_1 L_2) Z_G(u) . \tag{206}$$

To have a better understanding of this result, one can compute the partition function of the free field theory on the lattice exactly. For this exercise, see Appendix B.

The dependence on u in Eq. (206) was first numerically studied for an interface in the Ising model in Ref. 211. Further check is provided by Ref. 61.

For a study of an interface with fixed boundary conditions (which corresponds to Wilson-loops of the three-dimensional Z_2 gauge theory), see Ref. 212.

Corrections to the Gaussian behavior:

It is a very interesting question, whether the terms beyond the Gaussian contribution in Eq. (202) encode the physics of an interface. One might have the following arguments against this assertion: in the action (200), no curvature term is present. Also, the bulk correlation length ξ forms a natural cut-off for the effective string model. Therefore, one might expect cut-off effects, that are due to physics beyond the effective model, even in the limit $T \to T_c$.

To answer this question, the contribution to the partition function is computed as a perturbation in the Gaussian model. For this calculation, a regularization scheme is needed. In Ref. 213, the ζ-function regularization is used. In Ref. 61, the result is re-derived with a point-splitting method. For further check of the independence of the result on the regularization method, see Ref. 214.

As result, one obtains

$$\exp(F_I) = Z_I = c\exp(\sigma L_1 L_2) Z_G(u) \left[1 + \frac{f(u)}{\sigma L_1 L_2} + O\left(\frac{1}{(\sigma L_1 L_2)^2}\right)\right], \qquad (207)$$

where

$$f(u) = \frac{1}{8}\left[2 + \left(\frac{\pi}{3} u E_2(iu) - 1\right)^2\right]. \qquad (208)$$

E_2 denotes the first Eisenstein series

$$E_2(\tau) = 1 - 24 \sum_{n=1}^{\infty} \frac{n q^n}{1 - q^n}, \quad q := \exp(2\pi i \tau). \qquad (209)$$

This result was confronted with numerical results for interfaces in the three state Potts model in Ref. 207. A comparison of this result with interfaces in the Ising model can be found in Refs. 61 and 62. It turns out that the numerical data are much better fitted when the perturbative correction is included in the ansatz. Hence, we conclude that Eq. (207) gives (at least) the dominant contribution to $1/\sigma L_1 L_2$ corrections. For a detailed discussion of the numerical results, see Refs. 61 and 62.

6.3. *Numerical methods to study the interface tension*

6.3.1. *The boundary flip*

In Ref. 58, we proposed to use the boundary flip algorithm to determine the ratio of partition functions Z_a/Z_p. For details of the algorithm, see Appendix A. The interface area that is accessible with this method is restricted by the fact that the probability to generate anti-periodic boundary conditions is exponentially suppressed with the area $L_1 \times L_2$. Therefore, the statistical accuracy of Z_a/Z_p rapidly becomes worse with increasing $L_1 \times L_2$. In practice, this means that only areas $\sigma L_1 L_2 < 10$ can be reached with good accuracy. Fortunately, this accessible range of interface areas overlaps with the range of validity of Eqs. (206) and (207). For details, see Refs. 58, 60–62.

The boundary flip method works very well for the three-dimensional Ising model. Unfortunately, this method requires that the model can be simulated with the cluster algorithm and that there exists an exact symmetry between the two phases that are separated by the interface. Therefore, the generalization of the method is restricted to a rather small number of models. The method could be straight forwardly used for the study of interfaces in the ϕ^4 theory. It can also be generalized to the case of an interface between two ordered phases of a q-state Potts model (with $q > 2$). However, it would not work for an interface between the ordered and disordered phase.

6.3.2. *The tunneling correlation length*

A quite general method is to determine the tunneling correlation length from the time-slice correlation function on systems with large L_3. The interface free energy is then obtained from Eq. (198). As an example of a numerical study using this method, see Ref. 215. In Ref. 61, we have used this method in addition to the boundary flip method. The disadvantage of the tunneling correlation length compared with the boundary flip is that much larger L_3 are needed. Also, the tunneling correlation length has to be extracted from the correlation function by some fitting procedure. Also, in the tunneling correlation length method, one can access only a limited range of interface areas. The tunneling correlation length increases exponentially with the interface area. This leads to a similar restriction as for the boundary flip (roughly $\sigma L_1 L_2 < 10$).

6.3.3. *Integration of the interface energy*

In general, it is difficult to access (interface) free energies directly in Monte Carlo simulations. The methods discussed above are suitable only for small interface areas. In contrast, it is quite easy to measure the energy of a system. Since the energy is the derivative of the (reduced) free energy with respect to the inverse temperature, we can compute the free energy as the integral over β of the energy E. In fact, this method was applied in an early Monte Carlo study by Bürkner and Stauffer.[216]

In order to obtain the interface free energy from the integration method, one has to provide the interface free energy at the starting point of the integration.

For $\beta < \beta_c$, the interface free energy vanishes. Therefore, we can start the integration there. Alternatively, one can start at large values of $\beta > \beta_R$ and use the result of the low temperature series for the interface tension as the start value (for a numerical implementation of both choices, see Ref. 60).

Alternatively, one can also use numerical results for F_I as starting point of the integration. The value of F_I can be obtained, e.g., with the boundary flip method in the neighborhood of β_c. The most recent and accurate data on the interface tension of the Ising model near β_c were obtained in Ref. 62 with this approach.

We computed the interface free energy for the cross-sections 32×32, 48×48, 64×64 and 96×96. We computed the interface free energy at $\beta_0 = 0.2230$, 0.2225, 0.2220 and 0.2219 with the boundary flip, respectively. We then integrated the interface energy over β:

$$F_I(\beta) = F_I(\beta_0) + \int_{\beta_0}^{\beta} d\tilde{\beta} E_I(\tilde{\beta}) \,. \tag{210}$$

The integration was performed numerically, using the trapez-rule. For that purpose, we simulated the system with periodic and with anti-periodic boundary conditions for β-values with a step of $\Delta\beta = 0.00005$ or 0.0001.

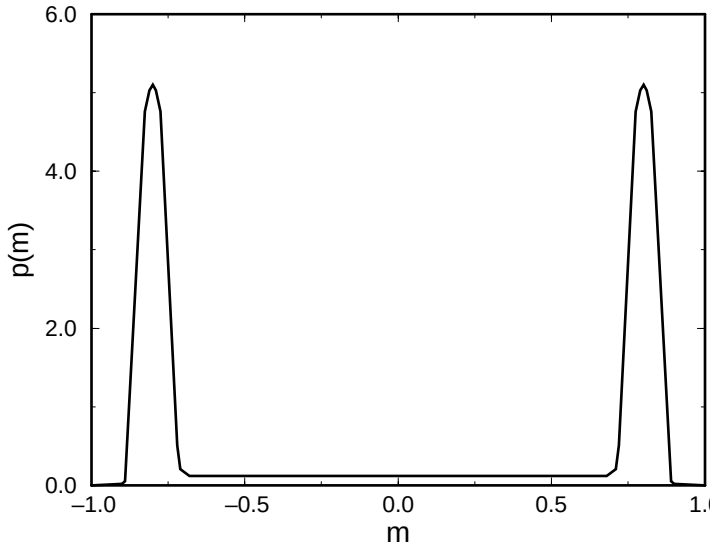

Fig. 10. Sketch of the histogram of the magnetization of the Ising model in the low temperature phase on a cubic lattice with periodic boundary conditions.

6.3.4. *Histogram method*

This method was pioneered by Binder in Refs. 217 and 218. Here, one considers the histogram of the magnetization (in the case of Ising model). For a temperature driven phase transition, one would study the histogram of the energy. In Fig. 10, we give a typical histogram of the magnetization of a cubical system with periodic boundary conditions in the low temperature phase. The histogram is peaked around $\pm\langle m\rangle$. Between these peaks, there is a rather flat minimum.

The phenomenological interpretation is that the peaks correspond to the pure phases, while the flat part in the middle corresponds to configurations, where both phases co-exist. The two phases are separated by two interfaces (because of the periodic boundary conditions).

The interface free energy is now extracted from the histogram as follows.

The probability for the mixed phase case is approximated by:

$$P_{\text{mix}} = 2\langle m\rangle p(0)\,, \tag{211}$$

where $p(0)$ is the probability density of the magnetization at $m = 0$. The interface free energy is then extracted from

$$P_{\text{mix}} \propto L^2 \exp(-2F_s)\,. \tag{212}$$

Note that factor L^2 is due to the fact that both interfaces can take any position on the lattice.

The histogram of the magnetization can be obtained from standard Monte Carlo simulations of the Ising model. However, for the flat part of the histogram, two

interfaces have to be generated and the probability for such configurations becomes small rapidly as L increases. The criterion for the accessible interface areas becomes $\sigma L_1 L_2 < 5$ (here, we just took into account a factor of 2 compared with the boundary flip or the tunneling correlation length method).

The method can be improved considerably by the use of a modified weight in the simulation. The Boltzmann factor is replaced by a weight, where the probability for a magnetization $-\langle m\rangle < m < \langle m\rangle$ is almost constant. For details of this "multimagnetic" simulation method, see e.g., Ref. 219.

6.4. *Numerical results*

After F_I are computed with one of the methods discussed above, the interface tension is extracted by fitting the data with Eq. (206) or Eq. (207) or some similar ansatz. In Table 18, we have summarized the results from Refs. 61, 62, 215 and 219. We have devided σ by t^μ to have numbers of similar size for all β-values. Here, we have used $t = 1 - 0.2216543/\beta$ and $\mu = 2 * 0.6297$. References 58 and 215 use Eq. (206) as fit-ansatz, while Refs. 61 and 62 use Eq. (207). The different fit ansätze are the main reason for the difference in the results of Refs. 58 and 61 for $\beta = 0.2275$ and $\beta = 0.224$. Thanks to the integration method, in Ref. 62, much larger interface areas could be studied than in the previous studies. Therefore, the dependence of the final result for σ on the precise form of corrections is rather small (see Table 3 of Ref. 62 for a comparison of different fit ansätze).

In the next step of the analysis, one can fit the results given above with the power law

$$\sigma = \sigma_0 t^\mu (1 + a t^\theta + bt + \cdots) \,. \tag{213}$$

In Table 19, we summarize results for σ_0 given in the literature. The values for σ_0 and also the error-bars scatter noticeably. This is only partially due to different raw data. The main reason is that the precise form of the fit-ansatz varies. In particular,

Table 18. $\sigma t^{-\mu}$ as a function of β from various authors. $t = 1 - 0.2216543/\beta$ and $\mu = 2 * 0.6297$.

β	Ref. 219	Ref. 215	Ref. 58	Ref. 61	Ref. 62
0.2439	1.511(6)				
0.2391		1.546(5)	1.535(8)		1.501(3)
0.2327		1.523(9)	1.509(9)		
0.232	1.578(7)				
0.23					1.4858(5)
0.2275		1.509(10)	1.530(11)	1.482(4)	1.484(1)
0.227	1.452(19)				
0.2258				1.447(9)	
0.2255			1.524(10)		1.484(1)
0.2246				1.536(16)	
0.224			1.533(12)	1.489(4)	1.490(2)
0.223			1.572(19)		1.482(3)

Table 19. Comparison of a number of estimates for σ_0 taken from the literature. The estimate by Zinn and Fisher is based on data from Ref. 16. The table is taken from Ref. 62.

Year	Author(s)	Ref.	σ_0
1982	Binder	218	1.05(5)
1984	Mon and Jasnow	222	1.2(1)
1988	Mon	220	1.58(5)
1992	Klessinger and Münster	215	1.29–1.64
1993	Berg *et al.*	219	1.52(5)
1993	Ito	221	1.42(4)
1993	Hasenbusch and Pinn	60	1.22–1.49
1993	Hasenbusch	58	1.5(1)
1993	Gausterer *et al.*	223	1.92(15)
1994	Caselle *et al.*	61	1.32–1.55
1996	Zinn and Fisher	224	1.50(1)
1997	Hasenbusch and Pinn	62	1.55(5)

the problem of correction terms has been treated differently by the authors, e.g., the authors of Ref. 219 just average their numbers given in Table 18. On the other hand, Ref. 62 takes into account the corrections given in Eq. (213). Also note that Refs. 220 and 221 just measure the interface energy density e_I and compute σ_0 from the power law $e_I \sim (\sigma_0/\beta_c)t^{\mu-1}$.

Having extracted the value of σ_0, one can compute $R = f_-^2\sigma_0$. However, our point of view is that it is favorable to compute $\xi_{2\mathrm{nd}}^2\sigma$ for each β value separately

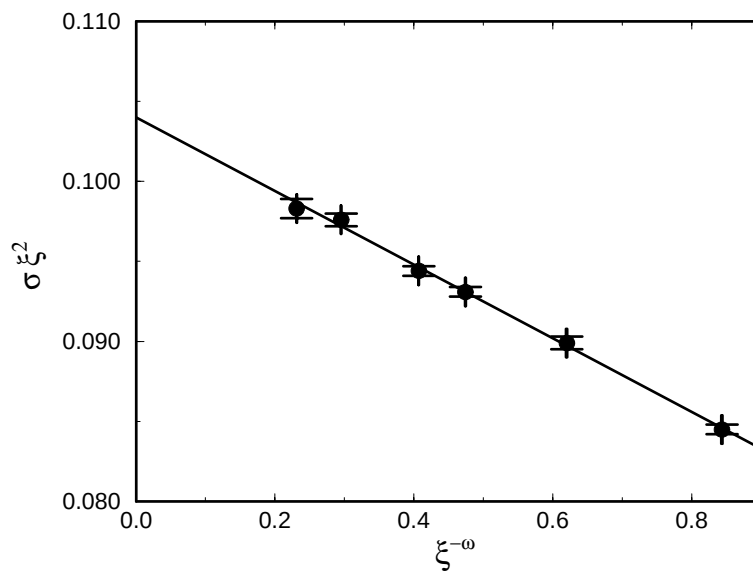

Fig. 11. $R = \sigma\xi_{2\mathrm{nd}}^2$ as a function of $\xi_{2\mathrm{nd}}^{-\omega}$ with $\omega = 0.81$. The solid line is given by $R = 0.1040 - 0.023\xi_{2\mathrm{nd}}^{-\omega}$. The data are taken from Ref. 62.

Table 20. Comparison of a number of estimates for R taken from the literature. The estimate of Zinn and Fisher is based on data of Ref. 60. Agostini *et al.* used the true instead of the second moment correlation length. The table is taken from Ref. 62.

Year	Author(s)	Ref.	R
1992	Klessinger and Münster	215	0.090(3)
1993	Hasenbusch and Pinn	60	0.090(5)
1996	Zinn and Fisher	224	0.096(2)
1996	Agostini *et al.*	52	0.1056(19)
1997	Hasenbusch and Pinn	62	0.1040(8)

and then extract the universal result from a fit with

$$\xi_{\rm 2nd}^2\sigma = R + c\xi_{\rm 2nd}^{-\omega} + \cdots . \tag{214}$$

The advantage of this procedure, compared with ansatz (213), is that we have eliminated analytic corrections and also, the value of ν is not needed in the analysis.

In Fig. 11, we show the results of the fit with the ansatz (214) performed in Ref. 62. We have used as input $\omega = 0.81(5)$. We obtained $R = 0.1040(8)$ and $c = -0.023(1)$. In Table 20, this result is compared with previous Monte Carlo results given in the literature. Note that our new result is more than 10% larger than that of Refs. 60 and 215. This is mainly due to the fact that in these older studies, corrections to scaling were not properly taken into account.

All Monte Carlo studies of the interface tension that we have discussed above deal with the standard Ising model. It would be a valuable check to redo the study with the ϕ^4 model at $\lambda = 1.1$. In particular, it would be a nice check of our work, to see whether in Eq. (214) the correction amplitude vanishes.

6.5. *Results from field theory*

Brézin and Feng[194] computed the universal constant R from ϵ-expansion. They define $(4\pi\omega)^{-1} = R$. Their result is:

$$\omega = \frac{2\pi}{3}\epsilon\left(1 - \epsilon\left(\frac{47}{54} + \frac{1}{2}\ln(4\pi) - \frac{1}{2}\gamma - \frac{5\pi\sqrt{3}}{18}\right)\right) + O(\epsilon^3)\,, \tag{215}$$

with $\gamma = 0.5772\ldots$. Their numerical evaluation for $\epsilon = 1$ gives results for ω that range from 1.39 to 1.57. This corresponds to $R \approx 0.051$ up to $R \approx 0.057$. Note that this is only about half the value obtained from the Monte Carlo simulations of the Ising model.

The study of interfaces using perturbation theory in three dimensions was pioneered by Münster.[195,196] The starting point of this calculation is the classical solution (i.e., configuration with minimal action) of a system with fixed boundary conditions in three-direction. At one boundary, the field is fixed to the negative minimum, and at the other, to the positive minimum of the potential.

Then, fluctuations around this classical solution are studied. In the recent paper,[197] this analysis was extended to two-loop. Their result is given by (note that they use the second moment definition of the correlation length):

$$R = \frac{2}{u_R^*}\left\{1 + \sigma_{1l}\frac{u_R^*}{4\pi} + \left(\sigma_{2l}\frac{u_R^*}{4\pi}\right)^2 + O(u_R^{*3})\right\}, \tag{216}$$

with

$$\sigma_{1l} = \frac{1}{4}\left(3 + \frac{3}{4}\log 3\right) - \frac{37}{32} = -0.2002602\,, \tag{217}$$

and

$$\sigma_{2l} = -0.0076(8)\,. \tag{218}$$

Using Padé and Padé–Borel analysis, with $u_R^* = 14.3(1)$, they obtain as the final result

$$R = 0.1065(9)\,. \tag{219}$$

Note that the error that is quoted is dominated by the error of u_R^*. At this point, one also should note the principle problems related with the definition of u_R^* as discussed in Ref. 53.

6.6. *Experimental results*

A number of experiments on interfaces in binary mixtures can be found in the literature. Since it is difficult to measure the correlation length in the low temperature phase, the universal quantity R_+ is determined. It is defined as:

$$R_+ = \lim_{t\searrow 0} \sigma(-t)\xi_{2\mathrm{nd}}(t)^2\,, \tag{220}$$

with $t = T - T_c$. The correlation length is obtained from the scattering of light. A recent experiment with a cyclohexane–aniline mixture[225] gave $R_+ = 0.41(4)$. Converting our Monte Carlo result, we obtain $R_+ = R(f_+/f_-)^2 = 0.40(1)$, which is in perfect agreement with the experiment.

6.7. *Magnetization profile and width of the interface*

Let us start the discussion with the two-dimensional interface models introduced at the beginning of this section. For these models, the interface width is defined by:

$$W^2 := \frac{1}{L_1 L_2}\sum_x h_x^2 - \left(\frac{1}{L_1 L_2}\sum_x h_x\right)^2 = \frac{1}{L_1 L_2}\sum_x (h_x - \bar{h})^2\,, \tag{221}$$

where $\bar{h} = 1/(L_1 L_2)\sum_x h_x$ is the interface position. The KT-theory predicts that below the roughening transition, in the smooth phase, the interface width stays finite in the thermodynamic limit. Above, in the rough phase, the width diverges as

the system size goes to infinity. For a numerical test of this scenario in the Discrete Gaussian SOS model, see Ref. 226.

In the case of the Ising interface, it is less trivial to define the interface width. Due to overhangs and bubbles in the bulk phases, it is difficult to assign locally (i.e., for each (x_1, x_2)) an interface position. Hence, we cannot directly apply the definition (221) to the Ising interface.

To circumvent this problem, we first define the magnetization profile:

$$\bar{m}(x_3) := \frac{1}{L_1 L_2} \sum_{x_1, x_2} s_x \,. \tag{222}$$

While this definition is straight forward for a given configuration, the problem becomes a little tricky when defining expectation values, e.g., with anti-periodic boundary conditions, the interface is free to move as a whole. Hence, $\langle \bar{m}(x_3) \rangle = 0$, which is a quite boring result. For a discussion of Dirichlet boundary conditions, see e.g., Ref. 57.

In order to learn about the intrinsic profile of the interface, we have to keep the interface position fixed or we have to take the relative distance to the position x_I of the interface as argument.

Following Refs. 191 and 227, we define the normalized magnetization gradient by:

$$\rho(x_3) := \frac{1}{\bar{m}(\infty) - \bar{m}(-\infty)} \left[\bar{m}\left(x_3 + \frac{1}{2}\right) - \bar{m}\left(x_3 - \frac{1}{2}\right) \right], \tag{223}$$

where ∞ stands for $x_3 \gg x_I$ and $-\infty$ for $x_3 \ll x_I$. Effectively, $\rho(x_3)$ counts the number of positions, where the interface is located at x_3. Translated to the SOS models, this means:

$$\rho_{\mathrm{SOS}}(z) := \frac{1}{L_1 L_2} \sum_{x} \delta_{z, h_x} \,, \tag{224}$$

where δ is the Kronecker symbol.

Then, the interface width can be defined as[191,227]:

$$W^2 := \sum_{x_3} \rho(x_3) x_3^2 - \left(\sum_{x_3} \rho(x_3) x_3 \right)^2 . \tag{225}$$

One easily checks that this definition coincides, using Eq. (224), with the definition (221) of the interface width for SOS models.

Above the roughening transition temperature of the three-dimensional Ising model, the periodicity of the lattice is irrelevant. The interface can be described by the capillary wave model (200). In the Gaussian approximation (203), it is rather simple to compute the expectation value of the interface width exactly (see Appendix B):

$$W^2 = \mathrm{const} + \frac{1}{2\pi\sigma} \ln L \,, \tag{226}$$

where $L_1 = L_2 = L$. Equation (226) applies only in the neighborhood of the bulk phase transition. For lower temperatures, still above the roughening transition, σ has to be replaced by the interface stiffness κ. For details, see Ref. 59.

Starting from Eq. (224), we derive the normalized magnetization gradient in the Gaussian approximation of the capillary wave model:

$$\begin{aligned}\langle \rho(z)\rangle &= \frac{1}{L_1 L_2}\sum_x \langle \delta(z-\phi_x)\rangle = \langle \delta(z-\phi_x)\rangle \\ &= \frac{\int d\phi \exp(-\phi^2/2W^2)\delta(z-\phi)}{\int d\phi \exp(-\phi^2/2W^2)} \\ &= \frac{1}{\sqrt{2\pi W^2}} \exp\left(-\frac{z^2}{2W^2}\right), \end{aligned} \tag{227}$$

where we have used translational invariance in the first step. Next, we have exploited the fact that the distribution of ϕ_x is Gaussian for each site x. The width of the distribution is the interface width W^2. Note that the interface position is fixed to 0 here.

Integrating Eq. (227), we obtain a prediction for the magnetization profile

$$\langle \bar{m}(z)\rangle = \frac{1}{\sqrt{2\pi W^2}} \int_0^z du \exp\left(-\frac{u^2}{2W^2}\right) = \frac{1}{2}\operatorname{erf}\left(\frac{z}{\sqrt{2W^2}}\right). \tag{228}$$

This behavior of the profile was already suggested in Ref. 228 and experimentally verified for SF_6 systems. Frequently, in the literature (see e.g., Ref. 57), the mean-field approximation of the interface profile is discussed:

$$\langle \bar{m}(z)\rangle_{\mathrm{MF}} = \tanh\left[\frac{z}{2\xi}\right], \tag{229}$$

where ξ is the bulk correlation length.

The prediction (226) for the interface width has been tested in Monte Carlo simulations of the three-dimensional Ising model on the simple cubic lattice in Refs. 59 and 227. In both studies, the model was simulated at $\beta = \beta_c/0.8$ and anti-periodic boundary conditions were taken in three-direction. In Ref. 227, a local update with multi-spin coding implementation and in Ref. 59, the cluster algorithm of Ref. 229 was used.

In Ref. 59, we studied lattices of the size $L^2 \times 27$ with $L = 32$, 64, 128, 256 and 512. The results are $\langle W^2\rangle = 2.341(42)$, 2.889(42), 3.365(29), 3.829(23) and 4.326(44), respectively. Fitting all data with the ansatz (226) gives the stiffness $\kappa = 0.226(6)$ and $\chi^2/\text{d.o.f.} = 0.48$. In Ref. 227, lattices up to $960^2 \times 26$ were simulated. Also, their data fit well with Eq. (226). However, they cannot exclude $W = \text{const} + c \ln L$, suggested by percolation theory. Fitting all data of Ref. 59 with this ansatz gives $\chi^2/\text{d.o.f.} = 2.41$.

More recently, Moseley[230] has tested the predictions for the interface profile. He used local updates with multi-spin coding implementation. The largest system size was $1000^2 \times 48$. The temperature is 5% below T_c. For the three-dimensional

system, the data clearly favor the capillary wave prediction (227) compared with the mean-field approximation (229). It remains a little puzzling however that, in his Fig. 2, he gives 0.599 as prefactor of erf( ) instead of 1/2.

7. Dimensional Crossover

Thin films of a substance behave effectively like a two-dimensional system. Also, this situation can be studied using lattice models. We consider lattices with $L_3 \ll L_1, L_2$. On scales that are larger than L_3, the system behaves effectively as a two-dimensional system. The cross-over from three-dimensional behavior to two-dimensional behavior with increasing scale can be understood within the framework of the RG.

To mimic an experimental situation, certain Dirichlet boundary conditions in three-direction are most appropriate. For a Monte Carlo study of the XY model with such boundary conditions, see e.g., Ref. 231. For simplicity and conceptual clearness, we will discuss periodic boundary conditions in the following.

In the context of field-theory, the finite extension in one of the three directions can be interpreted as a finite temperature of the associated two-dimensional quantum system. Consider the transfer-matrix of the system. The eigenvalues are labeled by λ_i. Then, the partition function is given by:

$$Z = \sum_i \lambda_i^{L_3} = \sum_i \exp(-L_3 E_i)\,, \tag{230}$$

with the energies of the quantum states $E_i = -\ln \lambda_i$. Hence, $L_3 = 1/kT$ corresponds to the inverse temperature.

This interpretation is in particular interesting for the dual of the three-dimensional Ising spin model, the Ising gauge model. Following the conjecture of Svetitsky and Yaffe,[175] a finite temperature $d+1$ gauge theory belongs to the same universality class as the d-dimensional spin model with the symmetry of the center of the gauge group. In the case of the Z_2 gauge theory in $2+1$ dimensions, this is the two-dimensional Ising model.

The theory of the dimensional cross-over was worked out in Ref. 232 as a special case of finite-size scaling. One important result is the dependence of the shift in the critical temperature as a function of the thickness of the system:

$$\beta_c(L_3) - \beta_c(\infty) \sim L_3^{-1/\nu}\,. \tag{231}$$

This relation can be easily shown in the framework of the RG: assume that the system is blocked to the fixed size $L_3' = b^{-n} L_3$ with $L_3' \gg 1$. Then, there exists a unique transition temperature u_t' of the system with thickness L_3'. Since $L_3' \gg 1$, the RG-flow of the couplings is the flow of the three-dimensional system. Therefore, the scaling field u_t after n block-transformations is given by:

$$u_t' = \frac{t}{t_0}\, b^{n y_t} = \frac{t}{t_0} \left(\frac{L_3}{L_3'}\right)^{y_t}\,, \tag{232}$$

where we have used that $b^n = L_3/L_3'$. Since u_t' and L_3' are constants by construction, we obtain

$$t \sim L_3^{-y_t} \,. \tag{233}$$

As a consequence, there also exist universal combinations with quantities that scale like a length scale: ξ/L_3 and σL_3^2.

In our numerical study,[63] we demonstrated that the system behaves, on scales larger than L_3, like a two-dimensional system and we verified the predictions for the dimensional cross-over.

In our study, we have used the ratio of partition functions Z_a/Z_p. This ratio can be exactly evaluated for the two-dimensional system at the critical point

$$\frac{Z_a}{Z_p} = \frac{\theta_2(0,\tau) + \theta_3(0,\tau) - \theta_4(0,\tau)}{\theta_2(0,\tau) + \theta_3(0,\tau) + \theta_4(0,\tau)} \,, \tag{234}$$

where $\tau = iL_1/L_2$ and $\theta_i(0,\tau)$ denote the Jacobi theta-functions (for the notations, see for instance Ref. 6).

First, we localized the transition temperature by tuning β such that $Z_a/Z_p = 0.37288488\ldots$ for $L_1 = L_2$. The resulting $\beta_c(L_3)$ are given in Table 21.

Fitting with the ansatz

$$(\beta_c(L_3) - \beta_c(\infty)) = cL_3^{-1/\nu} \,, \tag{235}$$

where we fix $\beta_c(\infty) = 0.2216543$, gives for $L_{3,\min} = 10$ the result $\chi^2/\text{d.o.f.} = 1.56$, $c = 0.1267(14)$ and $1/\nu = 1.614(4)$. This result has to be compared with $1/\nu = 1.5881(13)$ obtained in Sec. 3. Taking into account that the fit-ansatz does not include corrections to scaling, this is a clear confirmation of Eq. (231).

As a test of the hypothesis that the systems with fixed L_3 belong to the two-dimensional Ising universality class, we computed for $L_3 = 6$ the ratio of partition

Table 21. Summary of inverse transition temperatures $\beta_c(L_3)$. In the second column, we give our results. For comparision, the results of Refs. 233 and 232 are given in columns three and four, respectively. The table is taken from Ref. 63.

L_3	β_c	Ref. 233	Ref. 232
2	0.27604(3)	0.2758(4)	0.2760(10)
3	0.24607(8)		0.2449(1)
4	0.236025(8)	0.2358(2)	0.2347(1)
5	0.231421(13)		0.2301(2)
6	0.228818(4)		0.2273(3)
7	0.227195(9)		0.2258(3)
8	0.226102(5)	0.2262(2)	0.2248(1)
10	0.224743(5)		
12	0.223951(3)		
14	0.223442(4)		
16	0.223101(2)		
∞	0.2216543(4)		

Table 22. For $L_3 = 6$, we tested the two-dimensional Ising universality hypothesis by comparing Monte Carlo results with Eq. (234). The table is taken from Ref. 63.

L_1	L_2	Z_a/Z_p	Eq. (234)
32	96	0.0858(11)(4)	0.0867
48	96	0.1778(15)(8)	0.1752
64	96	0.2461(18)(12)	0.2491
96	64	0.5279(23)(15)	0.5292
96	48	0.6531(20)(12)	0.6558
96	32	0.8248(20)(7)	0.8269

functions Z_a/Z_p for various ratios L_1/L_2. All simulations were performed at the value of β_c obtained from the simulation with $L_1 = L_2$. The results are summarized in Table 22. For comparison, Eq. (234) is evaluated. For all L_1/L_2 that have been simulated, we find a perfect agreement between the simulation and the exact two-dimensional result.

Finally, let us compute the two universal amplitude combinations that we have discussed above. Let us first discuss

$$\frac{\xi_{\rm 2nd}(\beta_c(L_3))}{L_3}\,. \tag{236}$$

Here, we use as input the data of Ref. 48 for $\xi_{\rm 2nd}$. In order to obtain estimates for $\xi_{\rm 2nd}$ at the $\beta_c(L)$, we define

$$c(\beta) = \ln \xi_{\rm 2nd}(\beta) + \nu(\beta - \beta_c)\,, \tag{237}$$

where we use the most recent estimates $\nu = 0.6296$ (see Sec. 3) and $\beta_c = 0.2216543$.[38] Then, $c(\beta_c(L_3))$ is computed by linear interpolation. In the case of $L_3 = 2$ and $L_3 = 3$, we compute $\xi_{\rm 2nd}$ from the low temperature series expansion[163] using double biased inhomogeneous differential approximants. In Ref. 48, we have shown that this gives up to $\beta = 0.2391$ results that are more precise than our Monte Carlo results (see also Sec. 4).

Next, we study the combination

$$\sigma(\beta_c(L_3))L_3^2\,. \tag{238}$$

In the case of the interface tension, we use a similar interpolation scheme as used above. As input, we take for $0.223 < \beta \le 0.23$ the numbers obtained in Ref. 60 and for $\beta > 0.23$, the numbers of Ref. 62.

In Table 23, we list our result obtained for both quantities for the L_3 studied in our paper.

There is still a variation of the numbers with L_3 visible. Therefore, we tried to extract the continuum limit by fitting the data to the ansatz

$$X = X^* + L_3^{-\omega}\,, \tag{239}$$

Table 23. Universal combinations that relate the dimensional cross-over with the second moment correlation length $\xi_{2\mathrm{nd}}$ and the interface tension σ. In the last line, we give the extrapolation to the critical limit.

L_3	$\xi_{2\mathrm{nd}}/L_3$	σL_3^2
2	0.2875(2)	0.8193(5)
3	0.3301(7)	0.7423(29)
4	0.3505(5)	0.7040(14)
5	0.3609(5)	0.6876(31)
6	0.3674(5)	0.6813(5)
7	0.3713(6)	0.6766(14)
8	0.3737(5)	0.6740(10)
10	0.3781(7)	0.6714(15)
12	0.3808(8)	0.6706(15)
14	0.3823(8)	0.6675(22)
16	0.3823(7)	0.6672(19)
∞	0.396(2)	0.654(3)

where X stands for one of the two quantities discussed above. The result for the $L_3 \to \infty$ limit is given in the last line of Table 23. The error that is quoted takes into account the statistical error of the data and the error of ω.

8. Conclusions and Outlook

In this review, we have discussed the Monte Carlo study of universal properties of the three-dimensional Ising model and similar lattice spin models. Today, Monte Carlo simulations provide more accurate results for critical exponents and amplitude ratios than field theoretic methods (ϵ-expansion and perturbation theory in three dimensions).

Recently, the analysis of high temperature series expansions of lattice models with improved actions (Hamiltonians)[23] yielded even more accurate numbers. Note that in this analysis, the value of the coupling constant (at which the leading corrections to scaling vanish) were taken from Monte Carlo (Refs. 38 and 39 and own simulations of Ref. 23) as input.

The improvement of Monte Carlo results in the recent years was possible because simulation algorithms have improved and the computer time that is available for the simulations rapidly increases. All models discussed in this review can be simulated with cluster algorithms (note also the boundary flip algorithm[58] for the study of the interface tension).[36,90] A PC, today, is as powerful as a supercomputer one decade ago. As a side remark: the easy access to fast computers allows nowadays to integrate simulation techniques in the education of students.

In addition to the technical advance, a good theoretical understanding of finite size effects and of corrections to scaling is needed to extract reliable results. As a

recent progress, we have discussed the use of improved actions in the simulation[37–39] to eliminate leading corrections to scaling.

Also in the case of the XY,[42–44] the Heisenberg and the O(4)-invariant[45] universality classes, improved actions allowed us to obtain high precision results for critical exponents and other universal quantities. Note that in the case of the XY universality class, experiments on the λ-transition of ^{4}He provide results for the exponents α and ν and some critical amplitude ratios that are still more accurate than the theoretical estimates.

Finally, as a test of universality and in order to enhance the accuracy of the results, it would be nice to redo the studies reported in Secs. 5, 6 and 7 with an improved model replacing the standard Ising model. This applies in particular to the interface tension close to T_c, since it cannot be obtained from low temperature series expansions.

Appendix A. Monte Carlo Simulations

In this appendix, we briefly discuss the algorithms that have been used in the studies discussed in this review. In particular, we will explain the new versions of the cluster algorithm, namely the boundary flip algorithm and the wall cluster algorithm that have been introduced in Refs. 38 and 47, respectively. For an introduction to Monte Carlo simulations of spin models and lattice field theories, see, e.g., Refs. 7, 234–240.

To achieve the Boltzmann distribution of the configurations, one employs a so-called Markov chain. A Markov chain (of first order) is characterized by the fact that the probability distribution for the event (configuration in our case) at "time" $t+1$ is completely determined by the event at "time" t.

In order to generate the Boltzmann distribution, the Markov chain has to satisfy the following three conditions (in order to keep the notation simple, we assume a system with a finite number of configurations):

- Normalization:

$$\sum_Y P(Y,X) = 1 \quad \text{for all } X\,, \tag{240}$$

- Ergodicity:

$$P(Y,X) > 0 \quad \text{for all } X, Y\,, \tag{241}$$

- Stability:

$$\sum_X P(Y,X)B(X) = B(Y) \quad \text{for all } X\,, \tag{242}$$

where X, Y are configurations and $P(Y,X)$ is the probability to go from configuration X to Y. $B(X) = \exp(-S(X))$ is the Boltzmann factor. Note that condition (241) is, in practice, mostly realized by a composition of several elementary "updates".

The condition (242) is often proved via the so-called "detailed balance" condition

$$\frac{P(Y,X)}{P(X,Y)} = \frac{B(Y)}{B(X)}\,. \tag{243}$$

It follows that

$$\sum_X P(Y,X)B(X) = \sum_X B(Y)P(X,Y) = B(Y)\,, \tag{244}$$

where we have used the condition (240) in the last step.

A.1. *The Metropolis algorithm*

A simple and very generally adaptable algorithm is the Metropolis (the name goes back to Ref. 28) algorithm. Here, the update probability is split into two parts:

$$P(Y,X) = A(Y,X)V(Y,X) + \delta(Y,X)\left(1 - \sum_Z A(Z,X)V(Z,X)\right), \tag{245}$$

where $V(Y,X)$ is the probability to propose Y for a given X, and $A(Y,X)$ is the probability to accept this proposal. If the proposal is not accepted, the old configuration is kept.

There is much freedom in the choice of $V(Y,X)$ and $A(Y,X)$. Let us discuss the most simple versions:

$$V(Y,X) = V(X,Y)\,, \tag{246}$$

and

$$A(Y,X) = \min[1, \exp(-S(Y) + S(X))]\,. \tag{247}$$

If the update satisfies Eqs. (246) and (247), then the normalization (240) and the stability condition (242) are guaranteed. In order to proof ergodicity, further specification of the proposal $V(X,Y)$ is needed.

Mostly, local updates are performed, i.e., the proposal consists just of a change of the configuration at a single site. In the case of the standard Ising model, this leaves no further choice for the proposal:

$$s'_x = -s_x\,, \tag{248}$$

while all other spins are kept. Obviously, ergodicity cannot be achieved by updating just a single spin. We have to combine elementary updates at all lattice points x. Here, one can use different orders to visit the sites. One choice is to select the site of the spin that should be updated randomly each time. An other choice is to sweep like a type-writer through the lattice.

The local Metropolis, applied to the Ising model, has a critical dynamical exponent $z \approx 2$. The hand-waving argument is that the change of information is spread in a diffusion-like process.

Let us discuss the details of the Metropolis algorithm applied (in combination with the cluster algorithm to be discussed below) in Refs. 38 and 39 for the simulation of the spin-1 Ising model and for the ϕ^4 model.

Again, an elementary update step consists of a change of the field variable at a single site x.

In the case of the spin-1 Ising model, the proposal is to take one of the other two possible values of the spin with probability 1/2.

In the case of the ϕ^4 model, the proposal is generated by:

$$\phi'_x = \phi_x + s\left(r - \frac{1}{2}\right), \tag{249}$$

where r is a random number from a uniform distribution in the interval $[0, 1)$. s is a real number. This parameter should be chosen such that the algorithm performs best (i.e., integrated autocorrelation times $\tau_{\rm int}$ are minimal). A rule of thumb is that s should be chosen such that the acceptance rate is about 1/2. It is easy to see that condition (246) is fulfilled.

In all cases, we sweep through the lattice in type-writer fashion.

A.2. *Demons*

Demons are auxiliary degrees of freedom that are added to the action. These auxiliary degrees do not change the expectation value of observables. However, they enable new updates of the combined demon–spin system. The combined action is given by:

$$S_{\rm comb} = S_{\rm spin} + \beta \sum_\alpha d_\alpha \,, \tag{250}$$

where $S_{\rm spin}$ is any of the actions discussed in Sec. 2. One can use any number of demon degrees of freedom. In the simplest case, there is just one demon degree of freedom. However, often it is useful to have a demon for every site or link of the lattice.

The action of the standard Ising model with a vanishing external field takes values that are even multiples of β. Therefore, one chooses

$$d_\alpha \in \{0, 2, 4, 6, \ldots, d_{\rm max}\} \,, \tag{251}$$

where $d_{\rm max}$ is either an even positive integer or ∞.

Updates of the combined system can now be performed as follows: generate a proposal $s'_x = -s_x$, as in the case of the Metropolis algorithm. Then compute

$$\Delta S_{\rm Ising} = S_{\rm Ising}(s') - S_{\rm Ising}(s) \,, \tag{252}$$

and

$$d' = d - \Delta S_{\rm Ising} \,. \tag{253}$$

If d' is in the allowed range (i.e., $d_{\max} \geq d' \geq 0$), then accept the proposal. The main advantage of the demon method is that no random number is needed for the acceptance step.

The update discussed above keeps the value of S_{comb} fixed. Therefore, the micro-canonical ensemble of the combined system is simulated if only these updates are performed. If there is only one demon, essentially the micro-canonical ensemble of the spin system is generated. On the other hand, for very large number of demons, the canonical ensemble of the spin system is approximated.

This micro-canonical demon algorithm was proposed and tested in Refs. 241–244. For a micro-canonical update of the Ising model without demons, the so-called Q2R-algorithm, see Ref. 245.

In order to obtain the canonical ensemble of the combined system, one has to alternate the spin–demon updates with updates that change the value of the combined action. This can be achieved very efficiently by a global canonical update of the demons that was proposed in Ref. 246.

The spin–demon update can be implemented very efficiently with the multi-spin coding technique. Multi-spin coding means that all bits of a word are used to store an Ising spin (i.e., on a 32-bit computer, 32 spins are stored in one word and on a 64-bit computer, 64 spins are stored in one word). The update is implemented by bit-operations. For details, see e.g., Refs. 242 and 243. Using a different multi-spin coding implementation, Stauffer[247] simulated lattices of world record size, e.g., $10\,000^3$ in three dimensions.

In Refs. 48, 49 and 61, we applied these techniques (demons, canonical update of demons, multi-spin coding) to simulate the standard Ising model. In Ref. 52, we simulated the Z_2 gauge theory with this method.

One expects that the demon algorithm suffers from critical slowing down in the same way as the local Metropolis algorithm does. However, the multi-spin coding implementation and the rare use of random numbers lead to a great reduction of the CPU-time that is needed to update a single spin. We found in Ref. 62 that the update of a single spin with the demon-update takes 21×10^{-9} s on a DEC Alpha 250 workstation. On the same computer, the update of a single spin with the single cluster algorithm (see the subsection below) takes 19×10^{-7} s.

In order to judge the efficiency of the update, we also have to take into account the autocorrelation time. The smaller the CPU-time needed per sweep times the integrated autocorrelation time τ_{int}, the better. Since critical slowing down is almost eliminated by the cluster algorithm, eventually as the lattice size is increased (at β_c), the cluster algorithm will win. The crossover in the efficiency for the three-dimensional Ising model is roughly at a lattice size of $L = 50$ (the precise number depends very much on the computer that is used and the observables one likes to measure).

Demons can also be used in simulations of spin models with continuous field variables, such as the ϕ^4 model. Here, the demon is a real positive number $d \in$

$[0, \infty)$. The advantage is again that updates can be performed without using random numbers. For the details of the implementation, see Sec. 3.2 of Ref. 39.

Demons can also be used to determine RG-flows in Monte Carlo simulations.[248–250]

A.3. *Cluster algorithms*

Most of the studies that are discussed in this review took advantage of the so-called "cluster algorithm". The cluster algorithm was introduced by Swendsen and Wang[36] in 1987 for the standard Ising model (and the Potts models). Brower and Tamayo[251] explained how the cluster algorithm can be used in simulations of the one-component ϕ^4 theory. Wolff[90] proposed the "single cluster algorithm" and has shown how the cluster algorithm can be applied to $O(N)$-invariant nonlinear σ-models.

Below, we will briefly explain the cluster algorithm applied to the standard Ising model. Then, we discuss the variants of the cluster algorithm proposed by us in Refs. 38 and 58.

The critical slowing down of the Metropolis algorithm is due to the fact that only local changes of the configuration are performed at once. In contrast, the cluster algorithm allows for simultaneous updates of large parts ("cluster") of the lattice in one step. Critical slowing down can be eliminated to a large extent.

The cluster algorithm is based on the equivalence of the Ising and the Potts models with so-called "weighted percolation models" shown by Kasteleyn and Fortuin.[252] Let us briefly follow their derivation. Auxiliary variables $\sigma_{\langle xy\rangle} \in \{0, 1\}$ are introduced on the links. These values will also be called 0 = "deleted" and 1 = "frozen".

Let us rewrite the Ising partition function:

$$\begin{aligned} Z &= \sum_{s=\pm 1} \exp\left(\beta \sum_{\langle xy\rangle} s_x s_y\right) = \sum_{s=\pm 1} \prod_{\langle xy\rangle} \exp(\beta\, s_x s_y) \\ &= \exp(-dV\beta) \sum_{s=\pm 1} \prod_{\langle xy\rangle} (1 + \delta_{s_x,s_y}(\exp(2\beta) - 1)) \\ &= \exp(-dV\beta) \sum_{s=\pm 1} \prod_{\langle xy\rangle} \sum_{\sigma_{\langle xy\rangle}=0,1} ((1 - \sigma_{\langle xy\rangle}) + \sigma_{\langle xy\rangle}\delta_{s_x,s_y}(\exp(2\beta) - 1)) \,. \end{aligned} \tag{254}$$

Kasteleyn and Fortuin go on and perform the sum over the spins s_x. At the end, only the new fields $\sigma_{\langle xy\rangle}$ remain. In order to derive the cluster algorithm, it is best to keep both fields as in the last line of Eq. (254).

For fixed spins s_x, the weights of the new variables $\sigma_{\langle xy\rangle}$ factorize. Therefore, we can directly read off the single link distribution from Eq. (254):

$$\begin{aligned} p_d(x, y) &:= p(\sigma_{\langle x,y\rangle} = 0) = \min[1, \exp(-2\beta s_x s_y)] \,, \\ p_f(x, y) &:= p(\sigma_{\langle x,y\rangle} = 1) = 1 - p_d(x, y) \,. \end{aligned} \tag{255}$$

Note that these are the same delete/freeze probabilities proposed by Coniglio and Klein[253] to generate percolating clusters at the phase transition of the Ising model.

For fixed $\sigma_{\langle x,y\rangle}$, the distribution of the spins s_x can be easily understood: only configurations that satisfy the constraint $s_x = s_y$, where $\sigma_{\langle x,y\rangle} = 1$, have a weight larger than 0. All configurations that satisfy the constraint have the same weight.

In order to classify the configurations that satisfy the constraint, we need the concept of a "cluster". A cluster is an equivalence class of lattice points. The equivalence relation between two points is that there exists a path of frozen links (i.e., $\sigma_{\langle x,y\rangle} = 1$) that connects the two points. The constraint implies that all spins within one cluster have to take the same value. Hence, the remaining degrees of freedom are a sign for each of the clusters.

In the cluster algorithm, updates of the auxiliary variables $\sigma_{\langle xy\rangle}$ and the spins s_x alternate:

(I) In the first step, the $\sigma_{\langle xy\rangle}$ are updated for given s_x. The new values of $\sigma_{\langle xy\rangle}$ can be chosen independently from the old values: $\sigma_{\langle xy\rangle} = 0$ with probability p_d and $\sigma_{\langle xy\rangle} = 1$ else.
(II) In the second step, the spins are updated for given $\sigma_{\langle xy\rangle}$. The clusters have to be identified. Efficient methods to identify the clusters are the Hoshen–Kopelman algorithm[254] and spanning tree algorithms (in our studies, we used the "burning" variant). For a detailed discussion of cluster search algorithms, see Ref. 255.

There are many possible ways to update the sign of the clusters:

(i) In the original Swendsen–Wang algorithm,[36] the sign is chosen (independently of the old value) to be either -1 or $+1$ with equal probability. All clusters get a new value in one step.
(ii) In the single cluster algorithm of Wolff,[90] the cluster that contains a randomly chosen site is flipped with probability 1. It is easy to see that this fulfills detailed balance since the probability to choose the same cluster again (with identical $\sigma_{\langle xy\rangle} = 0$) is not changed by the update. The single cluster algorithm can be easily implemented such that only those $\sigma_{\langle xy\rangle}$ that are needed for the single cluster have to be constructed.
(iii) Some more elaborate rules to update the clusters have been proposed by Kerler. For details, see Ref. 256.
(iv) Recently, we have proposed to change the sign of all clusters that intersect with a plane of the lattice ("wall cluster").[38] It turns out that the slowing down is reduced compared with the single cluster. From simulations of the 3D Ising model at β_c, we found that $\tau_{\mathrm{int},E} \sim L^{0.035(7)}$ and $\tau_{\mathrm{int},\chi} \sim L^{-0.044(7)}$.

These numbers have to be compared with $\tau_{\mathrm{int},E} \sim L^{0.28(2)}$ and $\tau_{\mathrm{int},\chi} \sim L^{0.14(2)}$ obtained for the single cluster algorithm.[257]

A.3.1. *Boundary flip algorithm*

Many of the numerical studies discussed in this review make use of the ratio of partition functions Z_a/Z_p. This ratio of partition functions can be used to determine the interface tension in the low temperature phase (see Sec. 6 and Refs. 58, 61 and 62) and the critical temperature and the exponent ν by finite-size scaling (see Sec. 3 and Refs. 38, 39 and 47). Below, we explain how Z_a/Z_p can be obtained from the simulation of a system with "fluctuating boundary" conditions. Fluctuating boundary conditions can be efficiently simulated with the "boundary flip" algorithm introduced in Ref. 58.

Let us first define what fluctuating boundary conditions mean: the partition function of the system with fluctuating boundary conditions is given by:

$$Z_{\rm fluct} = Z_p + Z_a = \sum_{J_b=\pm 1} \sum_{s_x=\pm 1} \exp\left(\beta \sum_{\langle xy\rangle} J_{\langle xy\rangle} s_x s_y\right), \tag{256}$$

where $J_{\langle xy\rangle} = J_b$ at the boundary $x = (L_1, x_2, x_3)$ and $y = (1, x_2, x_3)$ and $J_{\langle xy\rangle} = 1$ else. $J_b = 1$ are periodic boundary conditions and $J_b = -1$ are called anti-periodic boundary conditions.

The ratio of partition functions is given by:

$$\frac{Z_a}{Z_p} = \frac{\langle \delta_{J_b,-1}\rangle}{\langle \delta_{J_b,1}\rangle}, \tag{257}$$

where the expectation value is taken with the fluctuating boundary ensemble.

We can perform the Kasteleyn–Fortuin transformation for the system with fluctuating boundary conditions as above. For given $J_{\langle xy\rangle}$ and s_x, we arrive at the delete probability

$$p_d(x, y) = \min[1, \exp(-2\beta J_{\langle xy\rangle} s_x s_y)]\,. \tag{258}$$

Now, for given $\sigma_{\langle xy\rangle}$, we have to discuss the remaining degrees of freedom of the system. A frozen link $\sigma_{\langle xy\rangle} = 1$ demands $J_{\langle xy\rangle} s_x s_y = 1$. This still allows to simultaneously change the sign of $J_{\langle xy\rangle}$ and one of the two spins s_x or s_y. We are in particular interested in moves that change $J_b = 1$ to $J_b = -1$ and vice versa.

The change J_b requires that for all links in the boundary (i.e., connecting $x = (L_1, x_2, x_3)$ and $y = (1, x_2, x_3)$) with $\sigma_{\langle xy\rangle} = 1$, we have to change exactly one of the spins (e.g., at $y = (1, x_2, x_3)$). We have to check whether this sign-change can be performed without violating the remaining constraints imposed by $\sigma_{\langle xy\rangle} = 1$ in the bulk.

This is accomplished by the following construction:

- We introduce an auxiliary variable $c_x \in \{-1, 1\}$.
- The clusters are constructed with the burning algorithm. All sites $x = (1, x_2, x_3)$ are taken as seeds of the cluster construction. At all these sites, we set $c_x = -s_x$. The auxiliary variable is propagated during the construction of the cluster. When a new site y is taken into the cluster from the old site x via the frozen link

$\langle xy\rangle$, then we set $c_y = c_x$, if $\langle xy\rangle$ is not in the boundary. If the link $\langle xy\rangle$ is in the boundary (i.e., $x = (1, x_2, x_3)$ and $y = (L_1, x_2, x_3)$ or vice versa), we set $c_y = -c_x$.

When the cluster-construction is finished, the J_b will be changed (flipped) if all c_x (that have been assigned) are consistent:

- $c_x = c_y$ for $\sigma_{\langle xy\rangle} = 1$ in the bulk; $c_x = -c_y$ for $\sigma_{\langle xy\rangle} = 1$ in the boundary.
- The boundary flip is given by $J_b' = -J_b$ and $s_x' = c_x s_x$.
- If c_x are not consistent, we have to keep the old J_b.

It is important to note that $J_b = -1$ (anti-periodic) can always be flipped to $J_b = 1$. This can be proven as follows:

- Assume that $\sigma_{\langle xy\rangle} = 1$ for $J_{\langle xy\rangle} s_x s_y = 1$ and $\sigma_{\langle xy\rangle} = 0$ else. Note that this is the maximal constraint allowed by the delete probability, Eq. (258). With this constraint, $c_x = -s_x$ for all x where a c_x is assigned. Here, $J_b = -1$ is crucial: $\sigma_{\langle xy\rangle} = 1$ at the boundary implies $s_x = -s_y$. Note that by construction the s_x are consistent (i.e., $\sigma_{\langle xy\rangle} = 1$ comes with $s_x = s_y$ in the bulk and with $s_x = -s_y$ in the boundary). Therefore, c_x are consistent and J_b can be flipped. Notice that this property of the algorithm implies $Z_a/Z_p \leq 1$.

Gliozzi and Sokal have remarked in private that, actually, the boundary flip needs not to be performed in order to determine Z_a/Z_p. It is sufficient to generate (with the single cluster or the wall cluster) configurations with periodic boundary conditions and check whether a flip to anti-periodic boundary conditions could be performed (i.e., check whether c_x can be assigned consistently). Set $b = 1$ if the boundary can be flipped and $b = 0$ else. Then,

$$\frac{Z_a}{Z_p} = \langle b\rangle\,, \tag{259}$$

where the expectation value is taken with the periodic boundary ensemble. In the recent simulations,[38,39] we have used this approach.

A.3.2. *The Brower–Tamayo method*

The basic idea of Brower and Tamayo is to use the cluster algorithm only to update the sign of the field ϕ. One interprets the sign of the field as Ising spin and absorbs the modulus of the field into an effective $\beta_{\langle xy\rangle} = \beta|\phi_x|\,|\phi_y|$. Inserting $\beta_{\langle xy\rangle}$ into Eq. (255) yields

$$p_d(x, y) = \min[1, \exp(-2\beta_{\langle xy\rangle}\mathrm{sign}(\phi_x)\mathrm{sign}(\phi_y))] = \min[1, \exp(-2\beta\phi_x\phi_y)]\,. \tag{260}$$

For the update, we can use any of the variants of the cluster algorithm discussed above. In Ref. 38, we used the single cluster as well as the wall cluster. In Ref. 39, we used only the wall cluster.

In order to obtain an ergodic algorithm, the updates with the cluster algorithm have to alternate with Metropolis updates. This way also the modulus of the field can be updated.

The number of cluster updates per Metropolis sweep is a free parameter of the algorithm. It should be tuned such that the efficiency of the algorithm is optimal, i.e., the CPU time divided by the square of the statistical error is the smallest.

We have applied this type of update in Ref. 39. In Ref. 38, we have simulated the spin-1 Ising model with a similar method. We alternate the local Metropolis discussed above with cluster updates that change the sign of the spin.

A.4. *Random numbers*

Mostly, so-called pseudo-random number generators are used in computer simulations. Genuine random numbers that are generated by a physical process, like a radioactive decay, take too much time to be efficiently used. In the literature, many types of pseudo-random number generators are discussed. In all studies that are discussed in this review, we have used the G05CAF of the NAG-library. The G05CAF is a so-called linear congruential pseudo-random number generator. The numbers are generated by:

$$I_{t+1} = (aI_t + c) \bmod m\,. \tag{261}$$

The G05CAF uses $m = 2^{59}$, $c = 0$ and $a = 13^{13}$. I_0 has to be an odd number. The output is normalized, $r_t = I_t/m$, such that a pseudo-random number that is (approximately) uniformly distributed in the interval $[0, 1)$ is produced. Note that the period of this generator is by far larger than that of the generators discussed, e.g., in the "Numerical Recipes" in Chapter 7.1.[258] For a test of the related generator $m = 2^{64}$, $c = 0$ and $a = 13^{13}$, see Ref. 259.

It is an important question, how well does the pseudo-random numbers mimic genuine random numbers. There exist many studies in the literature discussing this problem (see, e.g., Ref. 260). It turns out that the question of the quality of a pseudo-random number generator cannot be answered in general. A generator might pass one test and fail in another.

Therefore, one has to check how well does the pseudo-random number generator work in the given problem. Is there any bias (within the accuracy that can be reached) caused by the pseudo-random number generator?

This question can be answered easily when the result for the observables is exactly known. In fact, the authors of Ref. 261 found in simulations with the single cluster algorithm of the two-dimensional Ising model deviations from the exact result for the energy and the specific heat (given in Ref. 262) by many standard deviations. They tested random number generators that were considered as safe, up to their study.

In the case of three-dimensional systems, we like to compute the observables from Monte Carlo simulations. The exact results are not known. A principle method

would be to perform at least two simulations with different pseudo-random number generators. Then, the consistency of results with different generators could be used as a check. However, computer time is mostly short and one cannot afford the luxury to perform two simulations.

A very helpful check are so-called Schwinger–Dyson equations. These equations give exact relations among different observables of the model. Typically, these equations are derived for models with a continuous field variable. For a generalization to the Ising model, see Ref. 263.

In Ref. 39, we have used the demon as check. It is straightforward to compute exactly the expectation value $\langle d \rangle$ of the demon. This value can be compared with the value that is measured in the simulation.

Appendix B. Free Field Theory on the Lattice

The action of the free field theory (or Gaussian model) on the lattice is given by:

$$S_G = \frac{1}{2} \sum_{\langle xy \rangle} (\varphi_x - \varphi_y)^2 + \frac{1}{2} m^2 \sum_x \varphi_x^2 \,. \tag{262}$$

The partition function is given by:

$$\int_{-\infty}^{\infty} d\phi_{1,1} \cdots \int_{-\infty}^{\infty} d\phi_{L_1,L_2} \exp(-S_G) \,. \tag{263}$$

For $m^2 > 0$, the partition function is a well defined, multi-dimensional integral. This integral can be solved by Fourier-transformation:

$$\tilde{\varphi}_p = V^{-1/2} \sum_x \exp(ipx) \varphi_x \,, \tag{264}$$

where $V = L_1 L_2$. With

$$p_i = \frac{2\pi}{L_i} k_i \,; \quad k_i = 0, \ldots, L_i - 1 \,. \tag{265}$$

The back-transformation is given by:

$$\varphi_x = V^{-1/2} \sum_p \exp(-ipx) \tilde{\varphi}_p \,. \tag{266}$$

An important identity is:

$$V^{-1} \sum_x \exp(i(p - p')x) = \delta_{p,p'} \,. \tag{267}$$

The Fourier-transformation factorizes our problem. Let us transform the terms of the action:

$$\sum_x \sum_\mu (\phi_x - \phi_{x+\hat{\mu}})^2$$

$$= V^{-1} \sum_x \sum_\mu \left(\sum_p \exp(-ipx) \tilde{\varphi}_p - \sum_p \exp(-ip(x + \hat{\mu})) \tilde{\varphi}_p \right)^2$$

$$= V^{-1} \sum_x \sum_\mu \left(\sum_p [1 - \exp(-ip_\mu)] \exp(-ipx) \tilde{\varphi}_p \right)^2$$

$$= \sum_\mu \sum_p [1 - \exp(-ip_\mu)][1 - \exp(ip_\mu)] \tilde{\varphi}_p \tilde{\varphi}_p^*$$

$$= \sum_\mu \sum_p [2 - 2\cos(p_\mu)] \tilde{\varphi}_p \tilde{\varphi}_p^* . \tag{268}$$

Indeed, all terms depend on a single momentum (wave vector) k. An analogous calculation yields

$$\sum_x \varphi_x^2 = \sum_p \tilde{\varphi}_p \tilde{\varphi}_p^* . \tag{269}$$

Hence, we get

$$S_G = \frac{1}{2} \sum_p (\hat{p}^2 + m^2) \varphi_p \tilde{\varphi}_p^* , \tag{270}$$

where $\hat{p}^2 = 2 - 2\cos p$.

Expressed in terms of $\tilde{\varphi}_p$, the partition function factorizes and we get

$$Z_G = \prod_p \left[\frac{2\pi}{\hat{p}^2 + m^2} \right]^{1/2} . \tag{271}$$

In order to obtain a finite result for the mass-less case, we have to skip the zero momentum mode $p = (0, 0)$:

$$Z_G(m = 0) := \prod_{p \neq (0,0)} \left[\frac{2\pi}{\hat{p}^2} \right]^{1/2} . \tag{272}$$

Now, it is an interesting exercise to compare the lattice result with Eq. (206). For that purpose, we have evaluated Eq. (272) numerically. We have evaluated $Z_G(m = 0)$ for pairs of lattices with $L_1 = L_2 = L$ and $L_1 = uL_2$ with $L_1 \times L_2 = L^2$. In Tables 24 and 25, we give the ratio of partition functions obtained from such lattice pairs for various L for $u = 1/4$ and $u = 4/9$, respectively. For comparison, we give in the last row of Tables 24 and 25 the $L \to \infty$ result predicted by Eq. (206).

An interesting question is whether one can predict properties of an interface beyond the Gaussian approximation. We studied the effects of the next term of the expansion in perturbation theory

$$-\frac{1}{8} \langle ((\nabla \phi)^2)^2 \rangle_{\text{Gaussian}} . \tag{273}$$

On the lattice, this term becomes

$$R = \frac{3S_1^2 + 3S_2^2 + 2S_1 S_2}{8} , \tag{274}$$

Table 24. $u = 1/4$.

L	R
10	2.4661037
20	2.4117168
40	2.4000261
80	2.3971867
160	2.3964816
∞	2.3962470...

Table 25. $u = 4/9$.

L	R
6	1.3056918
12	1.2837950
24	1.2793856
48	1.2783368
96	1.2780774
192	1.2780127
∞	1.2779911...

with

$$S_i = -\sum_{p\neq(0,0)} \frac{\hat{p}_i^2}{\hat{p}_1^2 + \hat{p}_2^2}\,. \tag{275}$$

R can be rewritten as:

$$R = \frac{1}{8}\left[2(L_1L_2)^2 - 4L_1L_2 + 2 + (S_1 - S_2)^2\right]. \tag{276}$$

We interprete this result in the following way: the terms proportional to $(L_1L_2)^2$ and L_1L_2 have to be reabsorbed in the classical part and in the Gaussian part of the partition function, respectively. Only the part that is independent of L_1L_2 contributes to the physics. This part of R depends on the ratio L_1/L_2 and is given by:

$$F = \frac{1}{8}\left[2 + (S_1 - S_2)^2\right]. \tag{277}$$

The numerical result for F can now be compared with the result of the continuum perturbation theory with ζ-function or point-splitting regularization: in Table 26, we give the numerical result for F for various lattice sizes for $u = 4$. In addition, we give an extrapolated result in the third row. This extrapolation assumes that leading corrections decay like $1/L^2$. In the last row, we give the result from Eq. (207) for comparison. Note that for $u = 1$, we immediately get $F = 1/4$.

For a more detailed discussion of the cutoff independence of Eq. (207), see Ref. 214.

Table 26. $u = 4$.

L_1	F	Extrapolation of F
10	1.5442498927	
20	1.5266099690	1.520729994
40	1.5224253315	1.521030453
80	1.5213914407	1.521046811
160	1.5211337135	1.521047805
320	1.5210693280	1.521047566
∞	1.521047870293047...	

It is also easy to compute the interface width in the massless Gaussian model. For fixed interface position, i.e., $p = (0, 0)$ skipped, we get

$$W^2 = \frac{1}{L_1 L_2} \sum_x \langle \varphi_x^2 \rangle = \frac{1}{L_1 L_2} \sum_{p \neq (0,0)} \langle \tilde{\varphi}_p \tilde{\varphi}_p^* \rangle = \frac{1}{L_1 L_2} \sum_{p \neq (0,0)} \frac{1}{\hat{p}^2} \,. \tag{278}$$

Let us further discuss the result for the special case $L_1 = L_2 = L$.

$$\frac{1}{L^2} \sum_{p \neq (0,0)} \frac{1}{\hat{p}^2} \approx \frac{1}{L^2} \sum_{p \neq (0,0)} \frac{1}{p^2} = \frac{1}{4\pi^2} \sum_{k \neq (0,0)} \frac{1}{k_1^2 + k_2^2} \,, \tag{279}$$

where we have used in the first step that the sum is dominated by small $\hat{p}$ and approximate $\cos(p) \approx 1 - 2p^2$.

The sum over k behaves as:

$$\sum_{k \neq (0,0)} \frac{1}{k_1^2 + k_2^2} \approx \text{const} + 2\pi \ln L \,. \tag{280}$$

This behavior can most easily be understood by replacing the summation by an integration:

$$\sum_{k \neq (0,0)} \frac{1}{k_1^2 + k_2^2} \approx \int_1^L dk_1 \int_1^L dk_2 \frac{1}{k_1^2 + k_2^2} \approx 2\pi \int_1^L dr \frac{1}{r} = 2\pi \ln L \,. \tag{281}$$

Acknowledgments

I like to thank my colleagues V. Agostini, G. Carlino, M. Caselle, R. Fiore, F. Gliozzi, K. Pinn, P. Provero, T. Török and S. Vinti for the fruitful collaboration. In addition, I thank U. Wolff, K. Binder and the editor D. Stauffer for a critical reading of the manuscript.

References

1. L. D. Landau, *Phys. Z. Sowjetunion* **11**, 26 (1937); reprinted in *Collected Papers of L. D. Landau*, ed. D. ter Haar (Pergamon, London, 1965), p. 193; V. L. Ginzburg and L. D. Landau, *Zh. Eksp. Teor. Fiz.* **20**, 1064 (1950).
2. K. G. Wilson and J. Kogut, *Phys. Rep. C* **12**, 75 (1974).
3. K. G. Wilson and M. E. Fisher, *Phys. Rev. Lett.* **28**, 240 (1972).
4. G. Parisi, *Statistical Field Theory* (Addison Wesley, 1987).
5. K. Huang, *Statistical Mechanics*, 2nd edition (John Wiley & Sons, 1987).
6. C. Itzykson and J.-M. Drouffe, *Statistical Field Theory*, Vol. I (Cambridge University Press, 1989).
7. C. Itzykson and J.-M. Drouffe, *Statistical Field Theory*, Vol. II (Cambridge University Press, 1989).
8. J. J. Binney, N. J. Dowrick, A. J. Fisher, and M. E. J. Newman, *The Theory of Critical Phenomena, An Introduction to the Renormalization Group* (Clarendon Press, Oxford, 1992).
9. R. J. Creswick, H. A. Farach, and C. P. Poole, *Introduction to Renormalization Group Methods in Physics* (John Wiley & Sons, 1992).

10. N. Goldenfeld, *Lectures on Phase Transitions and the Renormalization Group* (Addison Wesley, 1992).
11. J. Cardy, *Scaling and Renormalization in Statistical Physics* (Cambridge University Press, 1996).
12. C. Domb, *The Critical Point, A Historical Introduction to the Modern Theory of Critical Phenomena* (Taylor & Francis, 1996).
13. M. E. Fisher, *Rev. Mod. Phys.* **70**, 653 (1998).
14. E. Ising, *Z. Phys.* **31**, 253 (1925).
15. R. Peierls, *Proc. Camb. Philos. Soc.* **32**, 477 (1936).
16. H. A. Kramers and G. H. Wannier, *Phys. Rev.* **60**, 252 (1941); *ibid*, p. 263.
17. L. Onsager, *Phys. Rev.* **65**, 117 (1944).
18. B. M. Mc Coy and T. T. Wu, *The Two Dimensional Ising Model* (Harvard University Press, 1973).
19. R. J. Baxter, *Exactly Solved Models in Statistical Mechanics* (Academic Press, 1982).
20. A. A. Belavin, A. M. Polyakov, and A. B. Zamolodchikov, *Nucl. Phys. B* **241**, 333 (1984); *J. Stat. Phys.* **34**, 763 (1984).
21. M. Henkel, *Conformal Invariance and Critical Phenomena* (Springer, 1999).
22. A. B. Zamolodchikov, in *Advanced Studies in Pure Mathematics* **19**, 641 (1989); *Int. J. Mod. Phys. A* **3**, 743 (1988); A. B. Zamolodchikov and Al. B. Zamolodchikov, *Ann. Phys.* **120**, 253 (1979).
23. M. Campostrini, A. Pelissetto, P. Rossi, and E. Vicari, *Phys. Rev. E* **60**, 3526 (1999), cond-mat/9905078.
24. H. Römer and T. Filk, *Statistische Mechanik* (VCH, 1994).
25. M. Plischke and B. Bergensen, *Equilibrium Statistical Physics*, 2nd edition (World Scientific, 1994).
26. D. A. Lavis and G. M. Bell, *Statistical Mechanics of Lattice Systems 1*: *Closed-Form and Exact Solutions*, 2nd edition (Springer, 1999).
27. D. A. Lavis and G. M. Bell, *Statistical Mechanics of Lattice Systems 2*: *Exact, Series and Renormalization Group Methods* (Springer, 1999).
28. N. Metropolis, A. W. Rosenbluth, M. N. Rosenbluth, A. H. Teller, and E. Teller, *J. Chem. Phys.* **21**, 1087 (1953).
29. S. K. Ma, *Phys. Rev. Lett.* **37**, 471 (1976).
30. R. H. Swendsen, *Phys. Rev. Lett.* **42**, 859 (1979); R. H. Swendsen, *Phys. Rev. B* **27**, 391 (1983).
31. G. S. Pawley, R. H. Swendsen, D. J. Wallace, and K. G. Wilson, *Phys. Rev. B* **29**, 4030 (1984).
32. M. N. Barber, in *Phase Transitions and Critical Phenomena*, Vol. 8, eds. C. Domb and J. L. Lebowitz (Academic Press, 1983).
33. V. Privman (ed.), *Finite Size Scaling and Numerical Simulation of Statistical Systems* (World Scientific, 1990).
34. K. Binder, in *Phase Transitions and Critical Phenomena*, Vol. 5b, eds. C. Domb and M. S. Green (Academic Press, 1976).
35. K. Binder, *Z. Phys. B* **43**, 119 (1981); K. Binder, *Phys. Rev. Lett.* **47**, 693 (1981).
36. R. H. Swendsen and J.-S. Wang, *Phys. Rev. Lett.* **58**, 86 (1987).
37. H. G. Ballesteros, L. A. Fernandez, V. Martin-Mayor, and A. Munoz-Sudupe, *Phys. Lett. B* **441**, 330 (1998), hep-lat/9805022.
38. M. Hasenbusch, K. Pinn, and S. Vinti, *Phys. Rev. B* **59**, 11471 (1999), hep-lat/9806012.
39. M. Hasenbusch, *J. Phys. A*. **32**, 4851 (1999), hep-lat/9902026.
40. J. H. Chen, M. E. Fisher, and B. G. Nickel, *Phys. Rev. Lett.* **48**, 630 (1982); M. E. Fisher and J. H. Chen, *J. Physique (Paris)* **46**, 1645 (1985).

41. B. G. Nickel and J. J. Rehr, *J. Stat. Phys.* **61**, 1 (1990).
42. M. Hasenbusch and T. Török, *J. Phys. A* **32**, 6361 (1999), cond-mat/9904408.
43. M. Campostrini, A. Pelissetto, P. Rossi, and E. Vicari, *Phys. Rev. B* **61**, 5905 (2000), cond-mat/9905395.
44. M. Campostrini, M. Hasenbusch, A. Pelissetto, P. Rossi, and E. Vicari, *Phys. Rev. B* **63**, 214503 (2001), cond-mat/0010360.
45. M. Hasenbusch, cond-mat/0010463.
46. A. Pelissetto and E. Vicari, cond-mat/0012164.
47. M. Hasenbusch, *Physica A*, 423 (1993).
48. M. Caselle and M. Hasenbusch, *J. Phys. A* **30**, 4963 (1997), hep-lat/9701007.
49. M. Hasenbusch and K. Pinn, *J. Phys. A* **31**, 6157 (1998), cond-mat/9706003.
50. F. J. Wegner, *J. Math. Phys.* **10**, 2259 (1971).
51. K. G. Wilson, *Phys. Rev. D* **10**, 2445 (1974).
52. V. Agostini, G. Carlino, M. Caselle, and M. Hasenbusch, *Nucl. Phys. B* **484**, 331 (1997), hep-lat/9607029.
53. M. Caselle, M. Hasenbusch, and P. Provero, *Nucl. Phys. B* **556**, 575 (1999), hep-lat/9903011.
54. M. Caselle, M. Hasenbusch, P. Provero, and K. Zarembo, *Phys. Rev. D* **62**, 017901 (2000), hep-th/0001181.
55. K. Binder, in *Phase Transitions and Critical Phenomena*, Vol. 8, eds. C. Domb and J. L. Lebowitz (Academic Press, 1983).
56. D. B. Abraham, H. W. Diehl, and D. Jasnow, in *Phase Transitions and Critical Phenomena*, Vol. 10, eds. C. Domb and J. L. Lebowitz (Academic Press, 1986).
57. K. Binder and M. Müller, *Int. J. Mod. Phys. C* **11**, 1093 (2000).
58. M. Hasenbusch, *J. Phys. I France* **3**, 753 (1993), hep-lat/9209016.
59. M. Hasenbusch and K. Pinn, *Physica A* **192**, 342 (1993), hep-lat/9209013.
60. M. Hasenbusch and K. Pinn, *Physica A* **203**, 189 (1994), hep-lat/9310013.
61. M. Caselle, R. Fiore, F. Gliozzi, M. Hasenbusch, K. Pinn, and Vinti, *Nucl. Phys. B* **432**, 590 (1994), hep-lat/9407002.
62. M. Hasenbusch and K. Pinn, *Physica A* **245**, 366 (1997), cond-mat/9704075.
63. M. Caselle and M. Hasenbusch, *Nucl. Phys. B* **470**, 435 (1996), hep-lat/9511015.
64. K. Binder and E. Luijten, *Phys. Rep.* **344**, 179 (2001).
65. C. F. Baillie, *Int. J. Mod. Phys. C* **1**, 91 (1990).
66. A. P. Young, *Spin Glasses and Random Fields* (World Scientific, 1998).
67. H. W. J. Blöte, E. Luijten, and J. R. Heringa, *J. Phys. A* **28**, 6289 (1995), cond-mat/9509016.
68. M. Blume, *Phys. Rev.* **141**, 517 (1966).
69. H. W. Capel, *Physica* **32**, 966 (1966).
70. F. Rys, *Helv. Phys. Acta* **42**, 608 (1969).
71. M. Blume, V. J. Emery, and R. B. Griffiths, *Phys. Rev. A* **4**, 1071 (1971).
72. M. Deserno, *Phys. Rev. E* **56**, 5204 (1997).
73. J. R. Heringa and H. W. J. Blöte, *Phys. Rev. E* **57**, 4976 (1998).
74. J. Zinn-Justin, *Quantum Field Theory and Critical Phenomena*, 3rd edition (Clarendon Press, Oxford, 1996).
75. M. Le Bellac, *Quantum and Statistical Field Theory* (Clarendon Press, Oxford, 1991).
76. I. Montvay and G. Münster, *Quantum Fields on a Lattice* (Cambridge University Press, 1993).
77. M. Creutz, *Quarks, Gluons and Lattices* (Cambridge University Press, 1983).
78. K. Binder and H. Rauch, *Z. Phys.* **219**, 201 (1969).
79. M. E. Fisher, "Critical phenomena", in *Proceedings of the 51st Enrico Fermi Summer School*, Vaenna, Italy, ed. M. S. Green (Academic Press, New York, 1971).

80. M. E. Fisher and M. N. Barber, *Phys. Rev. Lett.* **28**, 1516 (1972).
81. M. P. Nightingle, *Physica A* **83**, 561 (1976).
82. H. W. J. Blöte, L. N. Shchur, and A. L. Talapov, *Int. J. Mod. Phys. C* **10**, 1137 (1999), cond-mat/9912005.
83. P. M. C. de Oliveira, *Europhys. Lett.* **20**, 621 (1992).
84. L. P. Kadanoff, *Physics* **2**, 263 (1966).
85. Th. Niemeijer and J. M. J. Van Leeuwen, in *Phase Transitions and Critical Phenomena*, Vol. 6, eds. C. Domb and M. S. Green (Academic Press, 1976).
86. T. L. Bell and K. G. Wilson, *Phys. Rev. B* **10**, 3935 (1975); T. L. Bell and K. G. Wilson, *Phys. Rev. B* **11**, 3431 (1975).
87. A. C. D. Van Enter, R. Fernandez, and A. D. Sokal, *J. Stat. Phys.* **72**, 879 (1994), hep-lat/9210032.
88. A. Rosengren, *J. Phys. A* **28**, 1709 (1986).
89. M. E. Fisher, *J. Phys. A* **28**, 6323 (1995).
90. U. Wolff, *Phys. Rev. Lett.* **62**, 361 (1989).
91. H. G. Ballesteros, L. A. Fernandez, V. Martin-Mayor, G. Parisi, and J. J. Ruiz-Lorenzo, *J. Phys. A* **32**, 1 (1999), cond-mat/9805125.
92. A. L. Talapov and H. W. J. Blöte, *J. Phys. A* **29**, 5727 (1996), cond-mat/9603013.
93. R. Gupta and P. Tamayo, *Int. J. mod. Phys. C* **7**, 305 (1996), cond-mat/9601048.
94. D. P. Landau, *Physica A* **205**, 41 (1994).
95. C. F. Baillie, R. Gupta, K. A. Hawick, and G. S. Pawley, *Phys. Rev. B* **45**, 10438 (1992).
96. N. Ito and M. Suzuki, *J. Phys. Soc. Jpn.* **60**, 1978 (1991).
97. A. M. Ferrenberg and D. P. Landau, *Phys. Rev. B* **44**, 5081 (1991).
98. F. Livet, *Europhys. Lett.* **16**, 139 (1991).
99. P. Butera and M. Comi, *Phys. Rev. B* **62**, 14837 (2000), hep-lat/0006009.
100. P. Butera and M. Comi, *Phys. Rev. B* **56**, 8212 (1997), hep-lat/9703018.
101. Z. Salman and J. Adler, *Int. J. Mod. Phys. C* **9**, 195 (1998).
102. P. Hasenfratz and F. Niedermayer, *Nucl. Phys. B* **214**, 785 (1994).
103. R. Guida and J. Zinn-Justin, *J. Phys. A* **31**, 8103 (1998), cond-mat/9803240.
104. H. W. J. Blöte and G. Kamieniarz, *Physica A* **196**, 455 (1993).
105. N. A. Alves, B. A. Berg, and R. Villanova, *Phys. Rev. B* **41**, 383 (1990).
106. H. W. J. Blöte, J. R. Heringa, A. Hoogland, E. W. Meyer, and T. S. Smit, *Phys. Rev. Lett.* **76**, 2613 (1996), cond-mat/9602020.
107. H. W. J. Blöte, A. Compagner, J. H. Croockewit, Y. T. J. C. Fonk, J. R. Heringa, A. Hoogland, T. S. Smit, and A. L. Van Willingen, *Physica A* **161**, 1 (1989).
108. H. Kleinert, J. Neu, V. Schulte-Frohlinde, K. G. Chetyrkin, and S. A. Larin, *Phys. Lett. B* **272**, 39 (1991), erratum, *Phys. Lett. B* **319**, 545 (1993).
109. G. Parisi, *J. Stat. Phys.* **23**, 49 (1980).
110. D. B. Murray and B. G. Nickel, "Guelph University report", 1991, unpublished.
111. S. A. Antonenko and A. I. Sokolov, *Phys. Rev. E* **51**, 1894 (1995); S. A. Antonenko and A. I. Sokolov, *Phys. Rev. B* **49**, 15901 (1984).
112. J. C. Le Guillou and J. Zinn-Justin, *Phys. Rev. B* **21**, 3976 (1980).
113. B. G. Nickel, *Physica A* **117**, 189 (1991).
114. A. Pelissetto and E. Vicari, *Nucl. Phys. B* **519**, 626 (1998); A. Pelissetto and E. Vicari, *Nucl. Phys. Proc. Suppl.* **73**, 775 (1999), hep-lat/9809041.
115. F. Jasch and H. Kleinert, cond-mat/9906246.
116. S. Caracciolo, M. S. Causo, and A. Pelissetto, *Phys. Rev. E* **57**, 1215 (1998), cond-mat/9703250.
117. M. E. Fisher, *Rep. Prog. Phys.* **30**, 615 (1967).

118. K. E. Newman and E. K. Riedel, *Phys. Rev. B* **30**, 6615 (1984).
119. A. Haupt and J. Straub, *Phys. Rev. E* **59**, 1795 (1999).
120. J. Straub and K. Nitsche, *Fluid Phase Equilibria* **88**, 183 (1993).
121. T. J. Edwards, Thesis, University of Western Australia, 1984, unpublished, cited in Ref. 119.
122. I. M. Abdulagatov, N. G. Polikhsonidi, and R. G. Batyrova, *J. Chem. Therm.* **26**, 1031 (1994).
123. S. Kuwabara, H. Aoyama, H. Sato, and K. Watanabe, *J. Chem. Eng. Data* **40**, 112 (1995).
124. M. A. Anisimov, A. T. Berestov, V. P. Voronov, Yu. F. Kiyachenko, B. A. Koval'chuk, V. M. Malishev, and V. A. Smirnov, *Sov. Phys. JETP* **49**, 844 (1979).
125. M. W. Pestak and H. W. Chan, *Phys. Rev. B* **30**, 274 (1984).
126. P. F. Rebillot and D. T. Jacobs, *J. Chem. Phys.* **109**, 4009 (1998).
127. S. Kawase, K. Maruyama, S. Tamaki, and H. Okazaki, *J. Phys. Condens. Matter* **6**, 10237 (1994).
128. D. T. Jacobs, *Phys. Rev. A* **33**, 2605 (1986).
129. K. Hamano, T. Kawazura, T. Koyama, and N. Kuwahara, *J. Chem. Phys.* **82**, 2718 (1985).
130. U. Würz, M. Grubić, and D. Woermann, *Ber. Bunsenges. Phys. Chem.* **96**, 1460 (1992).
131. X. An and W. Shen, *J. Chem. Therm.* **26**, 461 (1994).
132. X. An, W. Shen, H. Wang, and G. Zheng, *J. Chem. Therm.* **25**, 1373 (1994).
133. W. Schröer, S. Wiegand, and H. Weingärtner, *Ber. Bunsenges. Phys. Chem.* **97**, 975 (1993).
134. V. Balevicius, N. Weiden, and A. Weiss, *Z. Naturforsch. A* **47**, 583 (1992).
135. P. Damay, F. Leclercq, and P. Chieux, *Phys. Rev. B* **40**, 4696 (1989).
136. D. P. Belanger and H. Yoshizawa, *Phys. Rev. B* **35**, 4823 (1987).
137. D. P. Belanger, P. Nordblad, A. R. King, V. Jaccarino, L. Lundgren, and O. Beckman, *J. Magn. Magn. Mater.* **31–34**, 1095 (1983).
138. M. Marinelli, F. Mercuri, and D. P. Belanger, *J. Magn. Magn. Mater.* **140–144**, 1547 (1995).
139. J. Mattsson, C. Djurberg, and P. Nordblab, *J. Magn. Magn. Mater.* **136**, L23 (1994).
140. M. A. Salgueiro, B. G. Almeida, M. M. Amado, J. B. Sousa, B. Chevalier, and Étourneau, *J. Magn. Magn. Mater.* **125**, 103 (1993).
141. A. M. Strydom, P. de V. du Plessis, D. Kaczorowski, and E. Troć, *Physica B* **186–188**, 785 (1993).
142. R. Aschauer and D. Beysens, *J. Chem. Phys.* **98**, 8194 (1993).
143. R. Aschauer and D. Beysens, *Phys. Rev. E* **47**, 1850 (1993).
144. J. Schimtz, L. Belkoura, and D. Woermann, *Ann. Phys. (Leipzig)* **3**, 1 (1994).
145. A. Zielesny, L. Belkoura, and D. Woermann, *Ber. Bunsenges. Phys. Chem.* **98**, 579 (1994).
146. K. Hamano, N. Kuwahara, I. Mitsushima, K. Kubota, and T. Kamura, *J. Chem. Phys.* **94**, 2172 (1991).
147. C. Sinn and D. Woermann, *Ber. Bunsenges. Phys. Chem.* **96**, 913 (1992).
148. M. A. Anisimov, *Critical Phenomena in Liquids and Liquid Crystals* (Gordon and Breach, New York, 1991).
149. V. Privman, P. C. Hohenberg, and A. Aharony, in *Phase Transitions and Critical Phenomena*, Vol. 14, eds. C. Domb and J. L. Lebowitz (Academic Press, 1991).
150. A. S. Kronfeld, *Nucl. Phys. B (Proceeding Supplement)* **17**, 313 (1990).
151. M. Lüscher and U. Wolff, *Nucl. Phys. B* **339**, 222 (1990).

152. M. Teper, *Phys. Lett. B* **289**, 115 (1992).
153. T. Moretto and M. Teper, hep-lat/9312035.
154. M. Hamermesh, *Group Theory and Its Application to Physical Problems* (Addison-Wesley, Reading, Mass., 1962).
155. N. Isgur and J. Paton, *Phys. Rev. D* **31**, 2910 (1985).
156. R. Ben-Av, D. Kandel, E. Katznelson, P. G. Lauwers, and S. Solomon, *J. Stat. Phys.* **58**, 125 (1990).
157. M. Teper, *Phys. Rev. D* **59**, 014512 (1999), hep-lat/9804008.
158. M. E. Fisher and S.-Y. Zinn, *J. Phys. A* **31**, L629 (1998).
159. M. Campostrini, A. Pelissetto, P. Rossi, and E. Vicari, *Europhys. Lett.* **38**, 577 (1997); *Phys. Rev. E* **57**, 184 (1998).
160. J. Heitger, Diploma Thesis, University of Münster (1993).
161. P. Provero, *Phys. Rev. E* **57**, 3861 (1998), cond-mat/9709292.
162. H. Arisue and T. Fujiwara, *Nucl. Phys. B* **285**, 253 (1995); H. Arisue and K. Tabata, *Phys. Lett. B* **322**, 224 (1994).
163. H. Arisue and K. Tabata, *Nucl. Phys. B* **435**, 555 (1995).
164. H. B. Tarko and M. E. Fisher, *Phys. Rev. B* **11**, 1217 (1975); *Phys. Rev. Lett.* **31**, 926 (1973).
165. A. J. Liu and M. E. Fisher, *Physica A* **156**, 35 (1989).
166. S.-Y. Zinn and M. E. Fisher, *Physica A* **226**, 168 (1996).
167. A. Pelissetto, P. Rossi, and E. Vicari, cond-mat/9903410.
168. A. Pelissetto, P. Rossi, and E. Vicari, *Phys. Rev. E* **58**, 7146 (1998), cond-mat/9804264.
169. E. Luijten, *Phys. Rev. E* **59**, 4997 (1999), cond-mat/9811332.
170. E. Luijten and K. Binder, *Phys. Rev. E* **58**, R4060 (1998), cond-mat/9807415; **59**, 7254 (1999).
171. J.-K. Kim and A. Patrascioiu, *Phys. Rev. D* **47**, 2588 (1993).
172. J.-K. Kim, A. J .F. De Souza, and D. P. Landau, *Phys. Rev. E* **54**, 2291 (1996).
173. C. Vohwinkel, *Phys. Lett. B* **301**, 208 (1993); and private communication.
174. J. Engels and T. Scheideler, *Nucl. Phys. B* **539**, 557 (1999).
175. B. Svetitsky and L. Yaffe, *Nucl. Phys. B* **210**, 423 (1982).
176. C. Ruge, P. Zhu, and F. Wagner, *Physica A* **209**, 431 (1994).
177. M. Barmatz, P. C. Hohenberg, and A. Kornblit, *Phys. Rev. B* **12**, 1947 (1975).
178. S.-Y. Zinn, S.-N. Lai, and M. E. Fisher, *Phys. Rev. E* **54**, 1176 (1996).
179. M. E. Fisher, private communications with the authors of Ref. 23.
180. P. Butera and M. Comi, *Phys. Rev. B* **60**, 6749 (1999), hep-lat/9903010.
181. J. F. Nicoll and P. C. Albright, *Phys. Rev. B* **31**, 4576 (1985).
182. C. Bervillier, *Phys. Rev. B* **34**, 8141 (1986).
183. E. Brézin, J. C. Le Guillou, and J. Zinn-Justin, *Phys. Lett. A* **47**, 285 (1974).
184. A. Aharony and P. C. Hohenberg, *Phys. Rev. B* **13**, 3081 (1976).
185. C. Bervillier and C. Godrèche, *Phys. Rev. B* **21**, 5427 (1980).
186. S. A. Larin, M. Mönnigman, M. Strösser, and V. Dohm, *Phys. Rev. B* **58**, 3394 (1998), cond-mat/9805028.
187. C. Bagnuls, C. Bervillier, D. I. Meiron, and B. G. Nickel, *Phys. Rev. B* **35**, 3585 (1987).
188. J. Heitger and G. Münster, *Nucl. Phys. B* **424**, 582 (1994), hep-lat/9402017.
189. C. Gutsfeld, J. Küster, and G. Münster, *Nucl. Phys. B* **479**, 654 (1996), cond-mat/9606091.
190. C. Bagnuls and C. Bervillier, *Phys. Rev. B* **32**, 7209 (1985).
191. J. D. Weeks, G. H. Gilmer, and H. J. Leamy, *Phys. Rev. Lett.* **31**, 549 (1973).

192. L. J. Shaw and M. E. Fisher, *Phys. Rev. A* **39**, 2189 (1989).
193. H. Arisue, *Phys. Lett. B* **313**, 187 (1993).
194. E. Brézin and S. Feng, *Phys. Rev. B* **29**, 472 (1984).
195. G. Münster, *Nucl. Phys. B* **324**, 630 (1989).
196. G. Münster, *Nucl. Phys. B* **340**, 559 (1990).
197. P. Hoppe and G. Münster, *Phys. Lett. A* **238**, 265 (1998), cond-mat/9708212.
198. H. J. Herrmann, W. Janke, and F. Karsch (eds.), *Int. J. Mod. Phys. C* **3**(5): *Workshop on Dynamics of First Order Phase Transitions*, 1–3 June 1992.
199. M. Hasenbusch and K. Pinn, *J. Phys. A* **30**, 63 (1997), cond-mat/9605019.
200. To give only a few references:
J. M. Kosterlitz and D. J. Thouless, *J. Phys. C* **6**, 1181 (1973); J. M. Kosterlitz, *J. Phys. C* **7**, 1046 (1974); S. T. Chui and J. D. Weeks, *Phys. Rev. B* **14**, 4978 (1976); J. V. José, L. P. Kadanoff, S. Kirkpatrick, and D. R. Nelson, *Phys. Rev. B* **16**, 1217 (1977); T. Ohta and K. Kawasaki, *Prog. Theor. Phys.* **60**, 365 (1978); D. J. Amit, Y. Y. Goldschmidt, and G. Grinstein, *J. Phys. A* **13**, 585 (1980).
201. H. Van Beijeren, *Phys. Rev. Lett.* **38**, 993 (1977).
202. E. H. Lieb, *Phys. Rev.* **162**, 162 (1967).
203. R. Savit, *Rev. Mod. Phys.* **52**, 453 (1980), and references therein.
204. B. Widom, *J. Chem. Phys.* **43**, 3892 (1965).
205. V. Privman and M. E. Fisher, *J. Stat. Phys.* **33**, 385 (1983).
206. F. P. Buff, R. A. Lovett, and F. H. Stillinger Jr., *Phys. Rev. Lett.* **15**, 621 (1965).
207. P. Provero and S. Vinti, *Physica A* **211**, 436 (1994).
208. P. Provero and S. Vinti, *Nucl. Phys. B* **441**, 562 (1995), hep-th/9501104.
209. C. Itzykson and J. B. Zuber, *Nucl. Phys. B* **275** [**FS17**], 580 (1986).
210. B. Bunk, *Int. J. Mod. Phys. C* **3**, 889 (1992).
211. M. Caselle, F. Gliozzi, and S. Vinti, *Phys. Lett. B* **302**, 74 (1993), hep-lat/9212013.
212. M. Caselle, R. Fiore, F. Gliozzi, M. Hasenbusch, and P. Provero, *Nucl. Phys. B* **486**, 245 (1997), hep-lat/9609041.
213. K. Dietz and T. Filk, *Phys. Rev. D* **27**, 2944 (1983).
214. M. Caselle and K. Pinn, *Phys. Rev. D* **54**, 5179 (1996), hep-lat/9602026.
215. S. Klessinger and G. Münster, *Nucl. Phys. B* **386**, 701 (1992), hep-lat/9205028.
216. E. Bürkner and D. Stauffer, *Z. Phys. B* **53**, 241 (1983).
217. K. Binder, *Z. Phys. B* **43**, 119 (1981).
218. K. Binder, *Phys. Rev. A* **25**, 1699 (1982).
219. B. A. Berg, U. Hansmann, and T. Neuhaus, *Z. Phys. B* **90**, 229 (1993), hep-lat/9206022.
220. K. K. Mon, *Phys. Rev. Lett.* **60**, 2749 (1988).
221. N. Ito, *Physica A* **196**, 591 (1993).
222. K. K. Mon and D. Jasnow, *Phys. Rev. A* **30**, 670 (1984).
223. H. Gausterer, J. Potvin, C. Rebbi, and S. Sanielevici, *Physica A* **192**, 525 (1993).
224. S. Zinn and M. E. Fisher, *Phys. A* **226**, 168 (1996).
225. T. Mainzer and D. Woermann, *Physica A* **225**, 312 (1996).
226. H. G. Evertz, M. Hasenbusch, M. Marcu, and K. Pinn, *Physica A* **203**, 189 (1994), cond-mat/9305029.
227. K. K. Mon, D. Landau, and D. Stauffer, *Phys. Rev. B* **42**, 545 (1990).
228. J. S. Huang and W. W. Webb, *J. Chem. Phys.* **50**, 3677 (1969).
229. M. Hasenbusch and S. Meyer, *Phys. Rev. Lett.* **66**, 530 (1991).
230. L. L. Moseley, *Int. J. Mod. Phys. C* **8**, 583 (1997).
231. N. Schultka and E. Manousakis, *J. Low Temp. Phys.* **109**, 733 (1997), cond-mat/9702216.

232. T. W. Capehart and M. E. Fisher, *Phys. Rev. B* **13**, 5021 (1976).
233. S. Wansleben and J. Zittarz, *Nucl. Phys. B* **280**, 108 (1987).
234. K. Binder and D. W. Heermann, *Monte Carlo Simulations in Statistical Physics*, 3rd edition (Springer, 1992).
235. A. D. Sokal, *Monte Carlo Methods in Statistical Mechanics: Foundations and New Algorithms* (Cours de Troisieme Cycle de la Physique en Suisse Romande, Lausanne, 1989).
236. A. D. Sokal, in *Quantum Fields on the Computer*, *Chapter 5*: *Bosonic Algorithms* (World Scientific, Singapore, 1992), pp. 221–274.
237. K. Binder, *Rep. Progr. Phys.* **60**, 487 (1997).
238. K. Ohno, K. Esfarjani, and Y. Kawazoe, *From Ab Initio to Monte Carlo Methods* (Springer, 1999).
239. M. E. J. Newman and G. T. Barkema, *Monte Carlo Methods in Statistical Physics* (Oxford University Press, 1999).
240. D. P. Landau and K. Binder, *A Guide to Monte Carlo Simulations in Statistical Physics* (Cambridge University Press, 2000).
241. M. Creutz, *Phys. Rev. Lett.* **50**, 1411 (1983).
242. M. Creutz, G. Bhanot, and H. Neuberger, *Nuc Phys. B* **235** [**FS11**], 417 (1984).
243. M. Creutz, K. J. M. Moriarty, and M. O'Brien, *Comp. Phys. Commun.* **42**, 191 (1986).
244. M. Creutz, *Ann. Phys. (NY)* **167**, 62 (1986).
245. H. J. Herrmann, *J. Stat. Phys.* **45**, 145 (1986).
246. K. Rummukainen, *Nucl. Phys. B* **390**, 621 (1993).
247. D. Stauffer, *Braz. J. Phys.* **30**, 797 (2000).
248. M. Creutz, A. Gocksch, and M. Ogilvie, *Phys. Rev. Lett.* **53**, 875 (1984).
249. M. Hasenbusch, K. Pinn, and C. Wieczerkowski, *Phys. Lett. B* **338**, 308 (1994), hep-lat/9406019.
250. A. P. Gottlob, M. Hasenbusch, and K. Pinn, *Phys. Rev. D* **54**, 1736 (1996), hep-lat/9601014.
251. R. C. Brower and P. Tamayo, *Phys. Rev. Lett.* **62**, 1087 (1989).
252. C. M. Fortuin and P. W. Kasteleyn, *Physica* **57**, 536 (1972).
253. A. Coniglio and W. Klein, *J. Phys. A* **13**, 2775 (1980).
254. J. Hoshen and R. Kopelman, *Phys. Rev. B* **14**, 3438 (1976).
255. F. Babalievski, *Int. J. Mod. Phys. C* **9**, 43 (1998), cond-mat/9711304.
256. W. Kerler, *Phys. Rev. D* **47**, 1285 (1993).
257. U. Wolff, *Phys. Lett. B* **228**, 379 (1989).
258. W. Press, S. A. Teukolsky, W. T. Vetterling, and B. P. Flannery, *Numerical Recipes in C*, *The Art of Scientific Computing*, 2nd edition (Cambridge University Press, 1992).
259. D. Stauffer, *Int. J. Mod. Phys. C* **10**, 807 (1999).
260. I. Vattulainen, K. Kankaala, J. Saarinen, and T. Ala-Nissila, *Comp. Phys. Commun.* **86**, 209 (1995), hep-lat/9304008.
261. A. M. Ferrenberg, D. P. Landau, and Y. J. Wong, *Phys. Rev. Lett.* **69**, 3382 (1992).
262. A. E. Ferdinand and M. E. Fisher, *Phys. Rev.* **185**, 832 (1969).
263. H. G. Ballesteros and V. Martin-Mayor, *Phys. Rev. E* **58**, 6787 (1998), cond-mat/9806059.